

Indian Summer
Monsoon variability under
recent, past and future climate
conditions

DISSERTATION

zur Erlangung des akademischen Grades eines
Doktors der Naturwissenschaften (Dr. rer. nat.)
am Fachbereich Geowissenschaften
der Freien Universität Berlin

vorgelegt von
Daniel Johannes Befort
Berlin, August 2016

- | | |
|--------------------|---|
| 1. Gutachter | Prof. Dr. Ulrich Cubasch
Institut für Meteorologie
Freie Universität Berlin |
| 2. Gutachter | PD Dr. Gregor C. Leckebusch
School of Geography, Earth and
Environmental Sciences
University of Birmingham |
| Disputationstermin | 2. Dezember 2016 |

Selbstständigkeitserklärung

Hiermit erkläre ich an Eides Statt, dass ich die vorliegende Arbeit selbstständig und ohne fremde Hilfe angefertigt, keine anderen als die angegebenen Quellen und Hilfsmittel benutzt und die den benutzten Quellen wörtlich oder inhaltlich entnommenen Stellen als solche kenntlich gemacht habe. Diese Arbeit hat in gleicher oder ähnlicher Form noch keiner Prüfungsbehörde vorgelegen.

Berlin, August 2016

(Daniel Johannes Befort)

Zusammenfassung

Der Indische Sommermonsun (ISM) variiert auf verschiedenen Zeitskalen: von intrasaisonal, dekadisch bis hin zu Zeiträumen von Jahrtausenden. Aktive und passive Phasen des indischen Monsuns innerhalb einer Saison haben starken Einfluss auf die Nahrungsmittelproduktion, wohingegen eine jahrhundert lange trockene Periode vor ca. 4200 Jahren möglicherweise Einfluss auf den Niedergang der Indus Valley Civilization hatte (Dixit et al., 2014a). Da heute bereits mehr als 1 Milliarde Menschen in dieser Region leben und prognostiziert wird, dass die indische Bevölkerung bis zum Ende des Jahrtausends bis auf über 1.6 Milliarden Menschen anwachsen wird (United Nations, 2015), ist ein Verständnis der für trockene und feuchte Phasen auf verschiedenen Zeitskalen verantwortlichen Mechanismen von größter Wichtigkeit.

In einer Studie von Sinha et al. (2011a) wird die Hypothese aufgestellt, dass langfristige abrupte Änderungen des Indischen Monsuns im letzten Jahrtausend mit Veränderungen der Häufigkeit aktiver und passiver Phasen auf der intrasaisonalen Skala in Verbindung stehen. Diese Studie untersucht, inwiefern diese These für Modellsimulationen unter rezenten, paleo und zukünftigen Klimabedingungen bestätigt werden kann. Zur Untersuchung der Variabilität des ISM auf verschiedenen Zeitskalen wird eine Modellkette bestehend aus einem voll-gekoppelten Atmosphäre-Ozean Globalmodell (COSMOS), einem Atmosphären-Globalmodell (ECHAM5) und einem Regionalmodell (COSMO-CLM) verwendet.

Zunächst werden das Atmosphären-Globalmodell und das Regionalmodell bezüglich ihrer Fähigkeit, intrasaisonale Eigenschaften des indischen Monsuns zu simulieren, untersucht. Die Ergebnisse suggerieren, dass trotz einiger Einschränkungen ECHAM5 sowie COSMO-CLM in der Lage sind intrasaisonale Eigenschaften des ISM, wie z.B. die Nordwärtsverlagerung des Niederschlags zu simulieren. Zusätzlich konnte gezeigt werden, dass das mit ERA-Interim Reanalysen angetriebene Regionalmodell COSMO-CLM in der Lage ist, trockene und feuchte Phasen innerhalb einer Saison zu simulieren.

Um zu untersuchen, inwiefern Veränderungen der Häufigkeit trockener und feuchter Phasen innerhalb einer Saison zu langfristigen Änderungen des ISM beitragen, werden saisonale Niederschlagsmengen über Zentral- und Nordostindien verwendet. Dies ist motiviert durch die Studie von Sinha et al. (2011a), in der unterschiedliche Trends im Niederschlag in zwei Proxies über diesen beiden Regionen gefunden wurden.

Untersuchungen der dekadisch bis multi-dekadische Variabilität im letzten Jahrtausend basieren auf Modellsimulationen für drei disjunkte Zeitepochen: Mittelalterliche Warmzeit (800-1000 AD), kleine Eiszeit (1515-1715 AD) sowie rezentes Klima (1800-2000 AD). Die Ergebnisse zeigen, dass die Variabilität auf diesen Zeitskalen teilweise mit veränderten Häufigkeiten von aktiver und passiver Phasen des ISM innerhalb einer Saison verbunden sind. Zur Untersuchung der längerfristigen Variabilität während der letzten 6000 Jahre wurde eine voll-gekoppelte transiente Globalmodellsimulation verwendet. Im Gegensatz zu den Ergebnissen für das vergangene Millennium sind trockene und feuchte Perioden in dieser Simulation nicht mit Veränderungen auf der intrasaisonalen Zeitskala erklärbar.

Sensitivitätsexperimente suggerieren, dass Änderungen der Oberflächentemperaturen im Indo-Pacific Warm Pool (IPWP) sowie im nördlichem Arabischen Meer einen deutlich größeren Einfluss auf die langfristige Variabilität des ISM besitzen. Dies ist einerseits durch eine Verschiebung der großskaligen Monsunzirkulation und andererseits durch lokale Änderungen im Feuchteangebot zu erklären.

Klimaprojektionen unter erhöhten Treibhausgaskonzentrationen suggerieren, dass dekadische bis multi-dekadische Variabilität des ISM im 21. Jahrhundert nur teilweise durch Veränderungen auf der intrasaisonalen Zeitskala erklärbar ist, ähnlich zu den Ergebnissen für das letzte Jahrtausend.

Insgesamt geben die Ergebnisse aus dieser Studie neue Einblicke in die verantwortlichen Mechanismen für die langfristige Variabilität des ISM, im Besonderen für den Beitrag von aktiven und passiven Phasen auf intrasaisonaler Zeitskala. Die Ergebnisse sollten für die Auswahl von Regionen zukünftiger proxy basierter Studien verwendet werden, um die Telekonnektionen des Indischen Monsuns wie z.B. mit den Oberflächentemperaturen im IPWP zu berücksichtigen.

Dixit, Y., Hodell, D. A. and Petrie, C. A. (2014a). Abrupt weakening of the summer monsoon in northwest India ~4100 yr ago. *Geologie*, 42(4):339–342

United Nations (2015). *World population prospects: The 2015 revision, key findings and advance tables*. Department of Economic and Social Affairs, Population Division, United Nations, New York, USA

Sinha, A., Berkelhammer, M., Stott, L., Mudelsee, M., Cheng, H., and Biswas, J. (2011a). The leading mode of Indian Summer Monsoon precipitation variability during the last millennium. *Geophysical Research Letters*, 38(15)

Abstract

The Indian Summer Monsoon is known to vary on intraseasonal, decadal, centennial and up to millennial time-scales during the past. Whereas shorter-term variability on subseasonal time-scales influences agricultural outcomes due to drought or flood conditions, longer-term dry conditions on centennial scale might be related to the downfall of the Indus Valley civilization around 4200 years ago (Dixit et al., 2014a). As nowadays more than 1 billion people live in India and the population is expected to increase throughout the 21st century to over 1.6 billion in 2100 (United Nations, 2015) knowledge about the drivers of dry and wet conditions on different timescales are of crucial importance.

In a recent study Sinha et al. (2011a) hypothesized that abrupt changes in rainfall over India on centennial time-scales during the last Millennium are associated with active and break spells on the intraseasonal timescale. This thesis investigates in how far this hypothesis can be supported by analysing the Indian Summer Monsoon variability under past, recent and future climate conditions. A model chain consisting of a fully coupled Atmosphere-Ocean General Circulation Model (COSMOS), an Atmosphere-only General Circulation Model (ECHAM5) and a Regional Climate Model (COSMO-CLM) is used to analyse dry and wet periods of the on different time-scales.

Before testing the hypothesis the models skill in representing observed intraseasonal features of the ISM¹ is assessed. Even though with some limitations, results suggest that the RCM² as well as the AGCM³ are able to capture main intraseasonal features of the ISM, e.g. the northward propagation. Additionally, COSMO-CLM is found to have positive skill in simulating observed dry and wet spells if driven by ERA-Interim at its lateral boundaries. Seasonal mean rainfall amounts over northeastern and central India are used to analyse in how far changes on the intraseasonal time scale contribute to longer-term variability of the ISM. This approach is motivated by the study from Sinha et al. (2011a) who found changes in rainfall with different signs in two proxies over northeastern and central India.

¹Indian Summer Monsoon

²Regional Climate Model

³Atmosphere-only General Circulation Model

Decadal to multi-decadal scale variability of the ISM is analysed in three time periods of the last Millennium: Medieval Climate Anomaly (800–1000), Little Ice Age (1515–1715) and Recent Climate (1800–2000). Results suggest that some part of the decadal to multi-decadal scale variability of the ISM can be attributed to changes on the intraseasonal time scale. Centennial scale variability during the Holocene is analysed using a transient simulation covering the past 6000 years. In contrast to results for the last Millennium, ISM variability in this simulation could not be linked to rainfall trends with different signs over northeastern and central India. Instead results suggest the importance of SST⁴s over the Indo-Pacific Warm Pool and northern Arabian Sea in steering long-term dry and wet conditions over India. Atmosphere-only climate model sensitivity experiments indicate that the ocean temperatures over the IPWP⁵ cause a shift in the large-scale monsoonal circulation, whereas SSTs over the northern Arabian Sea are important in determining the moisture supply over this region.

Results obtained by analysing future climate simulations suggest that only a part of the decadal-scale variability of the ISM could be related to changes in breaks and active spells, similar to results obtained for the last Millennium.

Overall, the work undertaken in this thesis gives greater insight into the steering mechanisms of ISM variability on longer-time scales, especially the role of changes of active and break spells on intraseasonal time scales. Furthermore, results should be considered for further proxy-based studies analysing long-term changes of the ISM for the proxy site selection to take into account teleconnections important for steering rainfall over India.

Dixit, Y., Hodell, D. A. and Petrie, C. A. (2014a). Abrupt weakening of the summer monsoon in northwest India ~4100 yr ago. *Geologie*, 42(4):339–342

United Nations (2015). *World population prospects: The 2015 revision, key findings and advance tables*. Department of Economic and Social Affairs, Population Division, United Nations, New York, USA

Sinha, A., Berkelhammer, M., Stott, L., Mudelsee, M., Cheng, H., and Biswas, J. (2011a). The leading mode of Indian Summer Monsoon precipitation variability during the last millennium. *Geophysical Research Letters*, 38(15)

⁴Sea Surface Temperatures

⁵Indo-Pacific Warm Pool

Contents

1	Preface	13
1.1	Introduction	13
1.1.1	General Monsoon Circulation	13
1.1.2	Variability of the Indian Summer Monsoon on different time-scales . .	15
1.2	Motivation, Aim and Structure of this study	20
2	Overview to Model Setups & Simulations	25
2.1	Models and their Setups used in this Study	25
2.2	Model Simulations	27
3	Recent climate	31
3.1	Intraseasonal Variability of the Indian Summer Monsoon in COSMO-CLM . .	32
3.1.1	Introduction	32
3.1.2	Data	34
3.1.3	Model	35
3.1.4	Method	36
3.1.5	Results	37
3.1.6	Daily rainfall	37
3.1.7	Boreal Summer Intraseasonal Oscillation (BSISO) and Monsoon In- traseasonal Oscillation (MISO)	39
3.1.8	Dry and Wet events	42
3.2	Conclusion	53
3.3	Intraseasonal Variability of the Indian Summer Monsoon under Recent Cli- mate Conditions	55
3.3.1	BSISO	55
3.3.2	MISO	56
3.4	Conclusion	59

4	Variability of the Indian Summer Monsoon during the Holocene	61
4.1	Introduction	62
4.2	The Last Millennium	65
4.2.1	Data & Methods	65
4.2.2	Relationship between AIMR and Active/Break spells in COSMO-CLM	67
4.2.3	Relationship between AIMR and Active/Break spells in ECHAM5 . . .	74
4.3	The Past 6000 years	82
4.3.1	Data & Methodology	82
4.3.2	Rainfall over AIMR during the past 6000 years in COSMOS	83
4.3.3	Variability of Active and Break spells	86
4.3.4	Changes of dry and wet events on the intraseasonal time-scale between 2ka BP and 1.7 ka BP	87
4.3.5	Mechanisms steering ISM rainfall variability between 2ka BP ⁶ and 1.7ka BP	89
4.3.6	Mechanisms influencing the ISM on inter-annual to centennial time scales	99
4.4	Conclusion & Discussion	105
5	Future Changes of the ISM	109
5.1	Introduction	109
5.2	Data & Methodology	111
5.3	Future changes of Active and Break spells in CLM ⁷ simulations	112
5.4	Future changes of Active and Break Spells in ECHAM5 simulations	116
5.5	Conclusion & Discussion	118
6	Summary, Discussion & Outlook	119
6.1	Summary	119
6.2	Discussion	124
6.3	Outlook	130
	Bibliography	133
	List of Figures	151
	List of Tables	158
	Acronyms	161

⁶Before Present

⁷COSMO-CLM

Preface

1.1 Introduction

1.1.1 General Monsoon Circulation

The climate over India is heavily influenced by seasonal variations of surface winds. During boreal summer southwesterly winds prevail over southern Asia transporting huge amounts of moisture into India, leading to high rainfall rates. In contrast, during wintertime mean wind blows from the northeast advecting usually drier and colder air into India, which leads to only little rainfall over most of the country except the southeastern part of India, which receives most of its annual rainfall (cf. Kripalani and Kumar, 2004 and reference within) during this time of the year. Despite the southeastern part of the country, India receives about 80% of its annual rainfall during the summer months between June and September (Basu, 2007). As explained, the marked change in precipitation over India is caused by changes in the prevailing wind direction between summer and winter, which is called monsoon. The word monsoon itself originated from the Arabic word for season called *mausim* (Rao, 2008). With respect to India it can be distinguished between the southwest summer and north-

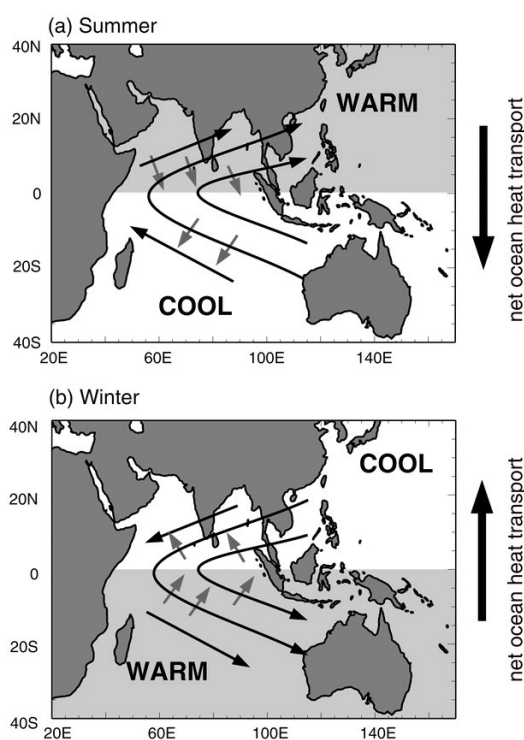


Figure 1.1: Schematic model of the a) boreal summer and b) winter monsoon system and mean surface winds (black arrows) and their associated Ekman transports (gray arrow). (taken from Loschnigg and Webster (2000), their Figure 13)

east winter monsoon season. Besides the Indian or south Asian monsoon, regions characterized by a reversal of the mean wind direction are found over parts of Africa and America, eastern Asia and northern Australia. All these monsoon systems have the same physical origin, which is the seasonal march of the solar insolation, which in turn modifies the position of the Hadley Cell. During boreal winter increased solar radiation over the southern latitudes and smaller solar incoming radiation rates over the northern latitudes lead to a horizontal north-south temperature gradient, which leads to a cross-equatorial flow from the northern to the Southern Hemisphere. This cross-equatorial flow reverses during boreal summer due to higher incoming solar radiation over the northern compared to southern latitudes (see Figure 1.1). This general monsoonal flow on hemispherical scales which is largely associated with changes in the position of the ITCZ¹, is modified by land-sea distribution or high orography on regional scales. For the Indian subcontinent an important factor modifying the general monsoonal flow is the Himalayan and the Tibetan Plateau (Hahn and Manabe, 1975). However, it is still discussed in how far the "thermal effect" due to the high elevation of the Tibetan Plateau or the "barrier effect", which prevents warm, moist air to penetrate further north is more important (Chen et al., 2014 and references therein). Besides the Tibetan Plateau, the Western Ghats mountain range at the western coast of India is an influencing factor for the spatial distribution of rainfall over the Indian subcontinent (Sijikumar et al., 2013).

Overall, the general monsoon circulation over India during summer is driven by differences in incoming solar radiation over the higher latitudes compared to the tropical latitudes. This, in combination with the differential heating of the Indian land-masses as well as the Tibetan Plateau compared to the tropical oceans lead to the formation of a surface low-pressure system over India and a near surface high pressure system over the tropical oceans during boreal summer. This is accompanied by near-surface southerly winds, which are redirected to the west by the Coriolis force and leading to the south-westerly monsoon flow. The lifting of air over the Indian continent is accompanied by high rainfall amounts and a divergent upper-level anti-cyclonic flow (Figure 1.2). In the upper-troposphere the main wind direction reverses to northerlies and a

Summer Broad-Scale Circulations

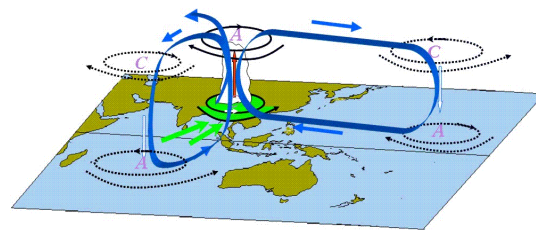


Figure 1.2: Mean summer circulation and its associated atmospheric flow (taken from Clivar, 2016)

¹inter-tropical convergence zone

convergent cyclonic upper-level flow is found over the tropical oceans. Besides topography, the presence of the Arabian Sea and the Bay of Bengal heavily influence the ISM² (Ghosh et al., 1978; Levine and Turner, 2012; Polanski et al., 2014).

1.1.2 Variability of the Indian Summer Monsoon on different time-scales

Intraseasonal Variability

Within the summer season (JJAS³) the ISM shows significant spatial and temporal variations. The occurrence of dry and wet periods, called break and active spells, have a major impact on food production (Rao, 2008) and thus on the society of India. Furthermore, prolonged dry events affect seasonal mean rainfall (Krishnamurti and Bhalme, 1976). One example for a prolonged break was observed during 2002 lasting for about 36 days associated with a rainfall deficit of 56% below normal in the month of July and a seasonal rainfall deficit of about 21% (Bhat, 2006).

Active and break phases differ significantly in terms of their associated atmospheric circulation. During break days the monsoon trough is significantly shifted northward (Blanford, 1886 cited from Gadgil, 2003), leading to reduced rainfall over central India and enhanced rainfall over the Himalayan foothills and northeastern India (Figure 1.3 left panel, taken from Rajeevan et al., 2010). During active days opposite characteristics in rainfall over India are found (Figure 1.3 right panel, taken from Rajeevan et al., 2010). The dominant periodicities of the ISO⁴ of the Indian monsoon are the eastward-northward propagating 30-60 day mode and the westward-propagating 10-20 day mode (Kulkarni et al., 2009, Goswami, 2005 and references therein). Recently, Suhas et al. (2013) developed an index to identify these MISO⁵ in gridded climate data. This study revealed that observed dry events on the intraseasonal timescale as the prolonged break during 2002 are associated with a reduced northward propagation of rainfall (Suhas et al., 2013). In fact, changes in atmospheric conditions influence the formation of synoptic weather systems, e.g. the formation of TC⁶s over the surrounding oceans of India is significantly increased during wet spells compared to dry spells (Goswami et al., 2003).

²Indian Summer Monsoon

³June-September

⁴intra-seasonal oscillation

⁵Monsoon Intra-seasonal Oscillations

⁶Tropical Cyclone

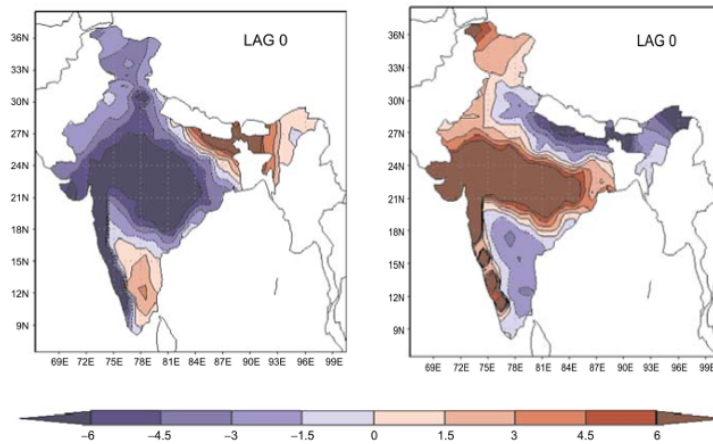


Figure 1.3: Rainfall composite anomaly (mm) during dry spells (left panel) and wet spells (right panel). Figures are taken and adapted from Rajeevan et al. (2010).

However, the ISV⁷ of the ISM is also influenced by interactions between tropics and extra-tropics (Ramaswamy, 1962; Krishnan et al., 2000; Ding and Wang, 2007; Krishnan et al., 2009). Krishnan et al. (2009) showed that anomalous mid- to upper-level westerlies over the Indo-Pakistan region caused by mid-latitude troughs over western Asia are associated with breaks over the Indian subcontinent. This is caused as cold-air convection reduces the north-south temperature gradient and drier winds over northwestern India leading to suppressed convection. Furthermore, Ding and Wang (2007) suggests that rainfall over northwestern India and Pakistan on intraseasonal time scales is linked to a Rossby wave-train over the Eurasian continent. As a substantial part of this study focuses on the ISV of the ISM, a more detailed background about current research is given later in Chapter 3, Section 3.1.1.

Interannual to inter-decadal Variability

Variations on the interannual timescale are comparably small with a standard deviation of about 10% of the mean for the last century (Gadgil, 2003). However, even though the ISM can be regarded as quite stable on interannual time-scales, these small fluctuations have a huge impact on the agricultural sector of India, e.g. rice production (Gadgil, 1995). It is observed that drought and flood years are related to the occurrence of ENSO⁸ (Figure 1.4). In general, decreased monsoon rainfall rates over India are associated with anomalous warm surface waters in the Pacific Ocean and a positive SOI⁹, which is characteristic of El Niño events. In contrast, increased rainfall rates over India are related to colder SST¹⁰s over the Pacific Ocean, which is characteristic of La Niña events respectively. This can be

⁷intraseasonal variability

⁸El Niño Southern Oscillation

⁹Southern Oscillation Index

¹⁰Sea Surface Temperatures

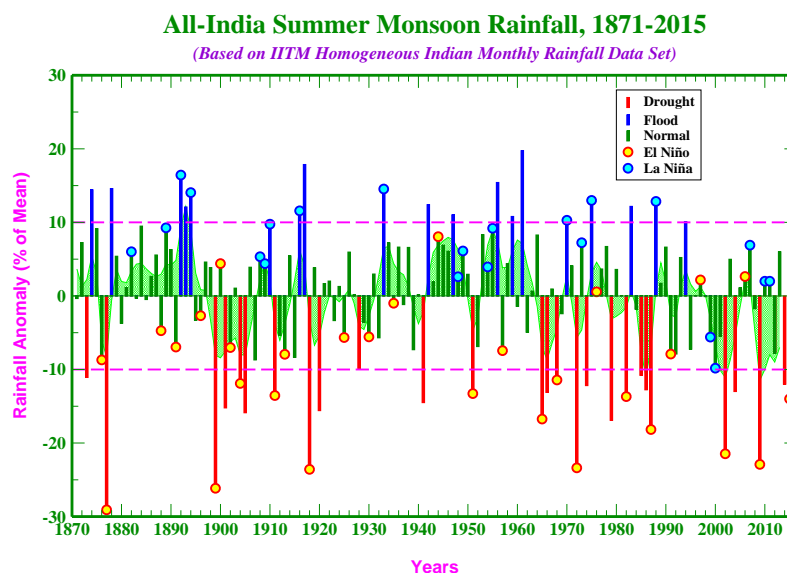


Figure 1.4: All-India Summer Monsoon (June-September) Rainfall (AISMR) Anomalies during 1871-2015. Rainfall anomalies are given relative to its long-term mean (taken from IITM, 2016).

explained as warmer eastern and equatorial Pacific SSTs during El Niño years lead to an anomalous easterly shift of the Walker circulation and, hence, suppressing convection over the Indian subcontinent. Thus, dry and wet conditions over India can in general be related to ENSO (Shukla and Paolino, 1983, see Table 2 from Webster et al., 1998, Figure 1.4), but the ENSO monsoon relationship cannot explain the whole rainfall variability on these time-scales. A good example is the El Niño event in 1997, which was the strongest event ever recorded but ISM rainfall was 2% above normal in this season (Slingo and Annamalai, 2000). Slingo and Annamalai (2000) attributed this to changes in the local Hadley Cell driven by changes in the Walker circulation and an anomalous northerly position of the TCZ¹¹. Despite ENSO, the IOD¹² plays an important role on interannual timescales (Ashok et al., 2001). Furthermore, extra-tropical interactions have shown to be important in influencing summer monsoon rainfall over India via a CGT¹³ (Ding and Wang, 2005).

The ISM also exhibits a strong biennial oscillation. This biennial oscillation of the ISM described by Mooley and Parthasarathy (1984) is also prominent in other monsoonal areas (Tian and Yasunari, 1992; Webster et al., 1998 and references therein) and often referred to as the TBO¹⁴. The mechanisms controlling the TBO can be potentially explained by positive atmosphere-ocean-land feedbacks. A good overview about the processes involved in the TBO is given in Meehl (1997). Furthermore, results from Yasunari (1990) indicate that the

¹¹Tropical Convergence Zone

¹²Indian Ocean Dipole

¹³circumglobal teleconnection

¹⁴Tropical Biennial Oscillation

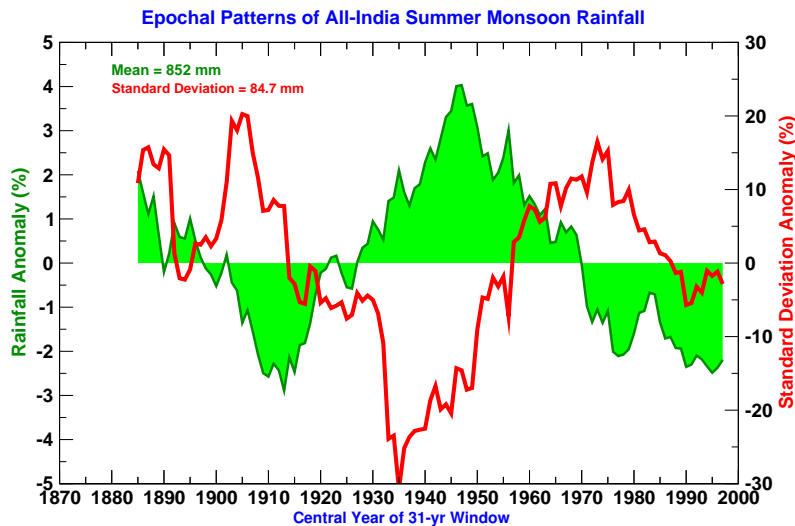


Figure 1.5: All-India Summer Monsoon (June-September) Rainfall (AISMR) Anomalies during 1871-2015 smoothed using a 31 year running mean (taken from IITM, 2016).

Asian monsoon itself plays an active role in the TBO. This mechanism suggests that changes in monsoon intensity influence Pacific SSTs in the following winter (Yasunari, 1990, their Figure 1). The above is further supported by model-based studies (e.g. Masumoto and Yamagata, 1991).

On longer time-scales the Indian monsoon is known to show an epochal behavior (Parthasarathy et al. (1994), Figure 1.5). This inter-decadal variability is thought to be related to ENSO (Krishnamurthy and Goswami, 2000), also affected by the IOD (Ashok et al., 2001). Furthermore, it is found that the ENSO-Indian monsoon relationship is not stable in time and underwent some fluctuations during the past decades (Kumar et al., 1999; Ashok et al., 2001). Kumar et al. (1999) showed that the relationship between ISM rainfall and ENSO weakened during the last decades of the past Millennium. They propose that a southward shift of the Walker circulation or increased surface temperatures over the Eurasian continent lead to a more intense monsoon circulation during El-Niño years during the recent past (Kumar et al., 1999). Additionally, the character of the ENSO itself is of major importance as it is found that drought conditions over India are more affected by SST anomalies in the central equatorial Pacific compared to SST anomalies over the eastern equatorial Pacific (Kumar et al., 2006).

Centennial to millennial-scale Variability

Variability of the ISM on longer time-scales can only be assessed by pure model or pure proxy based studies. In general, a decreasing rainfall trend over India is found from the mid Holocene (around 6000 years BP¹⁵) to present (Fleitmann et al., 2003; Schneider et al., 2014; Dallmeyer et al., 2015), which is in line with decreasing summer solar insolation over the northern latitudes from the mid towards the end of the Holocene. Differences in orbital parameters lead to a reduced northward propagation of the ITCZ during the Holocene, caused by decreasing solar insolation over the Northern Hemisphere and thus changes in the northern-southern Hemisphere temperature contrast (Figure 1.6). As described before, this thermal contrast is one of the major drivers of the monsoonal circulation (see Figure 1.1)

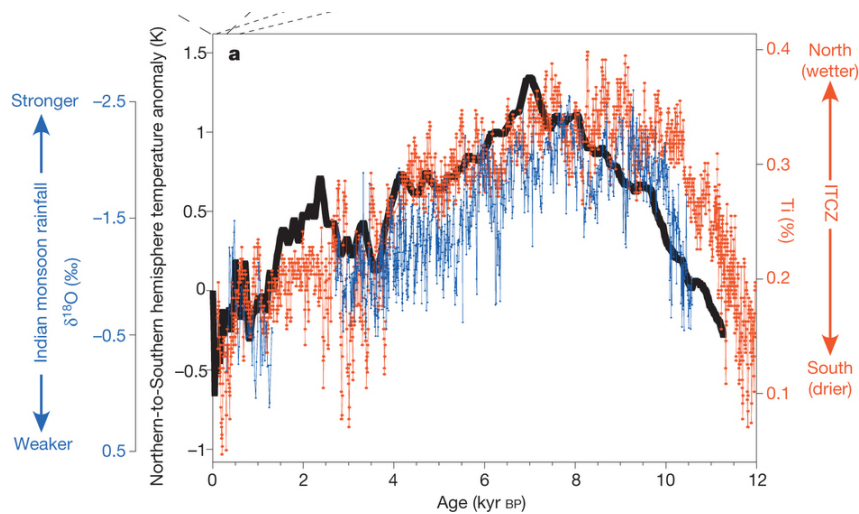


Figure 1.6: Temporal evolution of the temperature contrast between the extra-tropics of the Northern and Southern hemispheres (black lines) a proxy for runoff into Cariaco (red line) and a proxy of Indian monsoon rainfall (blue line) (adapted from Schneider et al. (2014)). For further information about the proxies and derived indices please refer to Schneider et al. (2014).

However, long-lasting dry and wet epochs are also found in model and proxy based studies (Prasad et al., 2014; Dallmeyer et al., 2015), which cannot be attributed to changes in solar insolation. Prasad et al. (2014) linked those dry events over India to anomalous warm conditions over the Indo-Pacific Warm Pool region. An additional proxy-based study by Sinha et al. (2011a), analysing ISM variability during the past Millennium found contrasting trends of rainfall over central and northeastern India, which they suggest to be linked to active and break spells on the intraseasonal time scale. Sinha et al. (2011a) hypothesize that shifts in the A-B¹⁶ regime trigger abrupt changes in ISM rainfall during the last Millennium on centennial time-scales.

A more detailed current state of research of longer-term variability of the ISM with an emphasis on the time-period of the Holocene is given in Chapter 4.

¹⁵Before Present

¹⁶active-break

1.2 Motivation, Aim and Structure of this study

Motivation

The hypothesis by Sinha et al. (2011a) suggesting that abrupt changes of the Indian Summer Monsoon during the last Millennium are caused by changes on the intraseasonal timescale challenges the current understanding of the importance of intraseasonal variability on longer time-scales. Recently several studies pointed out the impact of the occurrence of active and break periods onto seasonal rainfall averages (e.g. Goswami and Mohan, 2001; Goswami et al., 2006b). In contrast, other studies suggest that most of the seasonal anomalies arise from seasonal persisting patterns, rather than a shift of A-B periods (Krishnamurthy and Shukla, 2000, 2007, 2008). However, all these studies focus on the impact of intraseasonal changes on seasonal mean rainfall rates and thus interannual variability, rather than centennial-scale variability. Thus, even though interannual variability might be governed by seasonal persisting patterns, this might be different for abrupt changes on centennial timescales.

The hypothesis from Sinha et al. (2011a) that changes on the intraseasonal time-scale drive centennial scale variability is based on the analyses of rainfall proxy timeseries over central and northeastern India. Both time series show an abrupt change in rainfall around the late 17th century, however with opposite signs (Figure 1.7). The proxy sites coincide with the two centres of the first Empirical Orthogonal Function of seasonal and daily summer rainfall anomalies, which both show a sharp dipole pattern over central and northeastern India (Figure 1.8). This dipole pattern is also present in the active and break composite anomalies (Figure 1.3). In their study, Sinha et al. (2011a) hypothesize that centennial scale variability is associated with the dipole mode in rainfall over northeastern and central India, which is in turn associated with intraseasonal oscillations. If this hypothesis stays true it would have vast impact on both: model and proxy based studies. On the observational, proxy side it would lead to recommended regions to derive proxy archives as the A-B signal is reflected by different signs in rainfall anomaly over northeastern and southern compared to central and western India (Figure 1.3). If long-term dry and wet periods would organize in such a break/active rainfall pattern it would mean that different rainfall behaviour over different regions of India have to be considered, e.g. over southern and central India.

On the model side, this would mean that investigations analysing ISM variability on longer time-scales must use atmospheric models capable of representing observed intraseasonal features of the Indian summer monsoon to obtain meaningful results. As shown by Sperber and Annamalai (2008) this is not the case for all CMIP3¹⁷ models, and even though improved for several models the simulation of the intraseasonal variability is still problematic in CMIP5¹⁸ models (Sperber et al., 2013).

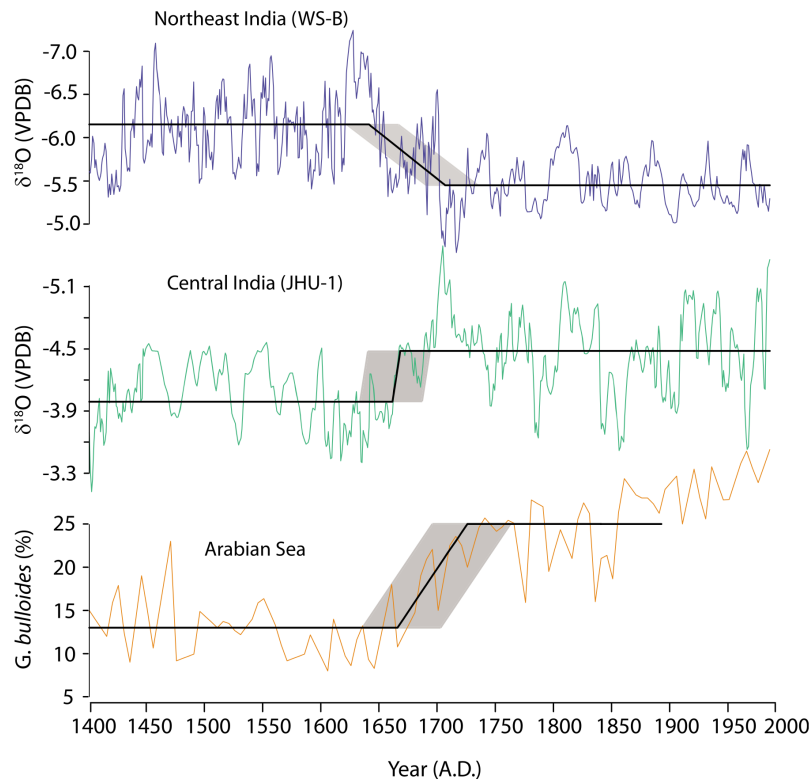


Figure 1.7: $\delta^{18}\text{O}$ timeseries for proxy located in northeastern India (blue), proxy located in central India (green) and in the Arabian Sea (orange) (Figure from Sinha et al. (2011a), their Figure 3). For further information about proxy locations and methods used please refer to Sinha et al. (2011a).

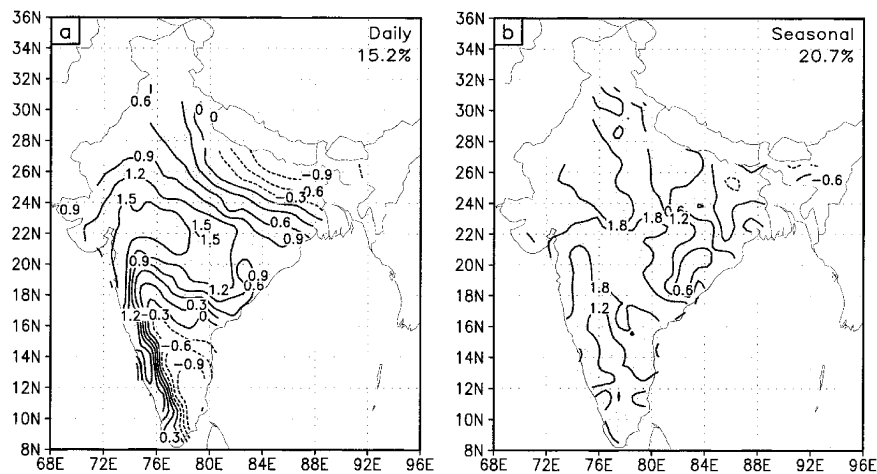


Figure 1.8: "EOF 1 of (a) standardised daily anomalies (5-day running means) and (b) standardised seasonal anomalies of rainfall for JJAS of the 1901–70 period. Positive contours are shaded." (Krishnamurthy and Shukla, 2000; their Figure 6)

¹⁷Coupled Model Intercomparison Project 3

¹⁸Coupled Model Intercomparison Project 5

Aim

The aim of this study is to analyse in how far long-term variability of the ISM can be attributed to changed on the intraseasonal time-scale via the occurrence of active and break periods. The main research question:

ARE CHANGES OF THE ISM RELATED TO A DOMINANT RAINFALL ANOMALY PATTERN, WITH A DIPOLE STRUCTURE OVER NORTHEASTERN AND CENTRAL INDIA, WHICH IN TURN IS ASSOCIATED WITH A SHIFT TO A MORE ACTIVE/BREAK PHASE OF THE MONSOONAL SYSTEM?

is answered by addressing three research tasks:

Task 1 Validation	Are climate models (GCM/RCM) used in this study able to represent observed features of the intraseasonal variability of the ISM (active and break spells, northward propagation)?
Task 2 Paleoclimate	In how far are extreme phases of the ISM related to a dominant rainfall anomaly pattern during the Holocene. Is this associated with more active/break spells on the intraseasonal time scale?
Task 3 Future Climate	Are possible future changes of the ISM related to the same rainfall anomaly pattern and changes on the intraseasonal time scale?

Methodology - Model Chain

The research question is tackled with a purely model-based approach. This is due to the availability of proxy data over the Indian subcontinent and also due to the nature of proxy records. Proxy data do allow to assess climate variability, but they lack the possibility to explain this variability as they do not give any insight into the reasons for these changes, e.g. changes in atmospheric or oceanic circulations. Here, global climate model simulations provide a tool to understand observed climate variability found in proxy archives. However, as this thesis is undertaken in the HIMPAC¹⁹ project, in which new multi-archive proxies have been carried out, findings based on these proxies are also reflected and taken into account in this study.

¹⁹HIMPAC - Himalaya: Modern and Past Climates

To analyse the variability of the ISM during the Holocene a model chain including coarse resolved fully-coupled global climate model simulations (AOGCM²⁰), atmosphere-only global climate model simulations (AGCM²¹) and higher-resolved regional climate model simulations (RCM²²) are used in this study (Figure 1.9). AOGCM simulations are used to simulate long time-periods, e.g. the past 6000 years, however, these simulations only provide coarse resolution (approx. 400 km). Thus, higher-resolved AGCM simulations, forced by SST and SIC²³ fields for the coarse AOGCM simulations, are carried out to obtain deeper insight into the atmospheric circulation. Due to computational resources this is not possible for the whole time periods, but is rather done for selected shorter time periods. Eventually, high-resolved RCM simulations over the Indian subcontinent are carried out. Again, due to computational resources, this is not possible for the whole time period covered by the AGCM simulations, but rather for specified shorter epochs. The intention to use regional climate models is to provide high-resolved spatial information about climate variability over India, which is not possible with coarse resolved AGCM simulations.

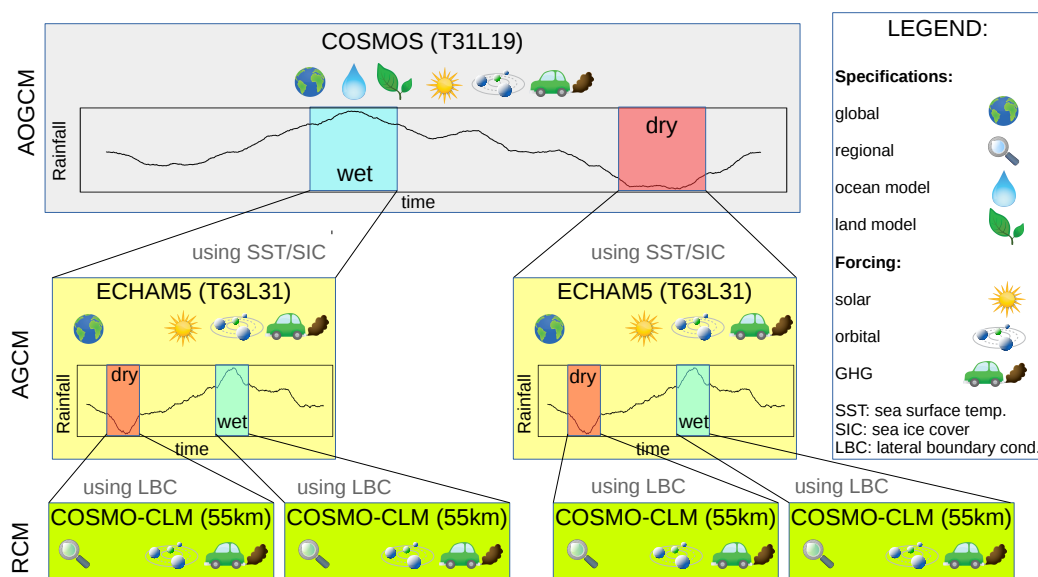


Figure 1.9: Schematic overview of model chain used in this study.

The thesis is structured as following: In Chapter 2 an overview to the climate models, their respective setups and simulations is given, Chapter 3 is dedicated to the validation of the climate models used in the model chain (*Task 1*), Chapter 4 analyses changes of the ISM during the Holocene with an emphasis on extreme phases (*Task 2*), Chapter 5 investigates the contribution on intraseasonal time-scales on longer-term future changes of the ISM under enhanced greenhouse gas concentrations (*Task 3*) and Chapter 6 summarises and discusses the results carried out within this study.

²⁰ Atmosphere-Ocean General Circulation Model

²¹ Atmosphere-only General Circulation Model

²² Regional Climate Model

²³ Sea Ice Concentrations

Overview to Model Setups & Simulations

2.1 Models and their Setups used in this Study

COSMOS

The fully coupled model system COSMOS (Community Earth System Models), consists of three different models: the atmospheric component ECHAM5 (Roeckner et al., 2003), the ocean model MPI-OM (Marsland et al., 2003) and the land surface model JSBACH (Radatz et al., 2007). Additionally, a biogeochemistry module named HAMMOC (Wetzel et al., 2006) is implemented. The coupling between the ocean and atmosphere is performed via the OASIS coupler (Valcke, 2013).

COSMOS is designed to include or exclude certain model components, e.g. running atmosphere-only simulation excluding ocean or land processes. This makes the model itself flexible to be used to address different research questions. Despite different model components included, the horizontal and spatial resolution can be adjusted to the users needs. In this study model simulations with two different resolutions are analysed. The coarse model simulations with a spectral resolution of T31 and 19 vertical levels is used for longer simulations, including atmosphere and ocean processes (AOGCM¹, see Figure 1.9). The spatial resolution of T31 corresponds to a grid spacing of 3.75° x 3.75° (approx. 400 km). Atmosphere-only simulations (AGCM², see Figure 1.9) are carried out with a resolution of T63 and 31 vertical levels, where T63 corresponds to a grid spacing of 1.875° x 1.875° (approx. 200 km).

COSMO-CLM

The COSMO (CONsortium for SMall scale MOdeling) model in Climate Mode (COSMO-CLM) is the community model of the German regional climate research. The model is based on the COSMO model which is used by several weather services across Europe for numerical weather prediction (NWP) and is also part of CORDEX (Coordinated Regional Climate Downscaling Experiment). In this study the version 4.8 subversion 17 is used for dynamical

¹Atmosphere-Ocean General Circulation Model

²Atmosphere-only General Circulation Model

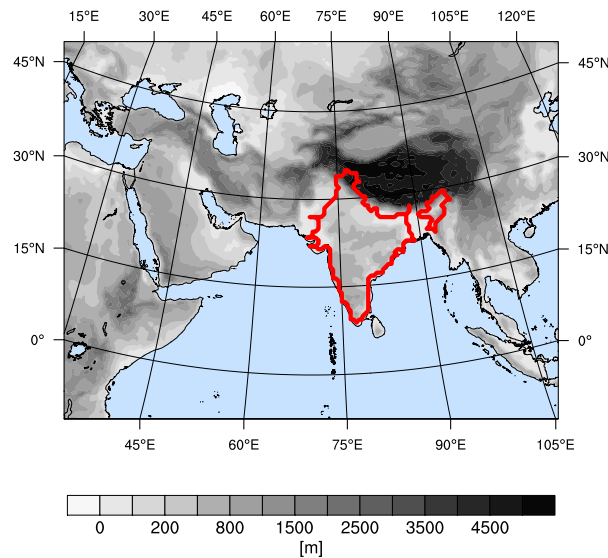


Figure 2.1: Domain of COSMO-CLM simulations used in this study + height of topography (shaded). Red line indicates boundaries of AIMR⁴ region.

downscaling of global climate model (GCM) output as well as reanalysis data. The model is run on a rotated pole grid with a resolution of 0.5° ($\approx 55\text{km}$) over the domain shown in Figure 2.1. The domain covers the area from the eastern African coast to the western Vietnamese coast in east-west and from about 10° south to 50° north in south-north direction with a total of 170×130 grid cells. The internal time step is 150 seconds and the temporal discretization is performed using a leap-frog scheme. The parameterizations used for the model integration include a radiation scheme following Ritter and Geleyn (1992), a microphysics scheme including cloud water, rain and snow (Kessler, 1969) and the Tiedtke mass flux convection scheme (Tiedtke, 1989).

The model configuration for an older COSMO-CLM version used in several studies (Dobler and Ahrens, 2010) has been the basis for the setup used in this study. The horizontal resolution of about 55 km is similar to the simulations provided by CORDEX (mostly about 50 km) and warrants for deeper insights of the regional structures of the ISM³. Furthermore, this resolution is still feasible for long-term simulations of about 30 years under paleo and future conditions. Several changes to the model's source code have been necessary to enable varying orbital parameters (Prömmel et al., 2013) as well as greenhouse gas concentrations.

³Indian Summer Monsoon

2.2 Model Simulations

In total 25 climate model simulations (CLM⁵ & COSMOS⁶) are used in this study from which 60% have been carried out within HIMPAC (15 out of 25). 13 out of these 15 (87%) have been carried out within this thesis itself, adding up to a total of nearly 400 years of atmosphere-only global climate model simulations, as well as over 200 years of regional climate model simulation data. All simulations are listed in Table 2.2.

Present Day Climate

A CLM simulation from 1979 until 2011 forced by ERA-Interim at its lateral boundaries is carried out within this study. The setup of this simulation is described in Section 2.1 and results are presented in Chapter 3 and published in Befort et al. (2016).

Last Millennium

In this thesis, a five member ensemble for the last Millennium in a spatial resolution of T31 with 19 vertical levels is analysed. These simulations are performed using all components of COSMOS. Additionally, varying orbital parameters, solar variability land-cover changes and volcanic eruptions have been considered (Jungclaus et al., 2010). Three 200 year time slices from the mil0014 ensemble-member have been selected and used to force three ECHAM5 simulations at its lower boundaries: MCA⁷ (900-1100 AD), LIA⁸ (1515-1715 AD) and the REC⁹ (1800-2000 AD). Due to the coarse spatial resolution of the coupled COSMOS simulations (T31L19), sea surface temperature and sea ice cover fields have to be interpolated to the grid resolution of the ECHAM5 simulations (T63). Several different methods of interpolation have been tested within this study to conserve the sea surface temperatures in the coupled COSMOS simulations within the higher resolved ECHAM5 simulations. Regarding the three ECHAM5 experiments MCA and LIA results have been published in Polanski et al. (2014). Eventually, CLM simulations for selected 31 year time periods (one wet and one dry phase) are carried out for the three GCM¹⁰ timeslice experiments (*EH5-MCA*, *EH5-LIA*, *EH5-REC*). The setup of these simulations is described in Section 2.1. Orbital parameters as well as Greenhouse Gas Concentrations (GHG) concentrations are set according to the respective time period.

All model experiments are used for investigation in Chapter 4, whereas the GCM experiment for the recent climate (REC) is further used to validate ECHAM5 under recent climate conditions in Chapter 3. Thus, to analyse the variability of the ISM during the past 1000 years the complete model chain as described in Section 1.2 is used.

⁵COSMO-CLM

⁶Community Earth System Models

⁷Medieval Climate Anomaly

⁸Little Ice Age

⁹Recent Climate

¹⁰General Circulation Model

Past 6000 years

Another fully-coupled COSMOS simulation covering the past 6000 years is used to analyse the ISM variability beyond the past 1000 years (Fischer and Jungclauss, 2011). This simulation is performed with varying orbital parameters but using constant (pre-industrial) greenhouse gas conditions. In this study a dry and wet period are selected and simulated using ECHAM5 with a resolution of T63L31. Similar to all three experiments during the last Millennium (*EH5-MCA*, *EH5-LIA*, *EH5-REC*) sea surface temperature and sea-ice cover fields are interpolated to match the ECHAM5 grid (T63). The ECHAM5 run-script are adapted to include changing orbital parameters. These orbital parameters are updated each year and are calculated according to Berger and Loutre (1991). As the dry event is found around 2ka BP and the wet event around 1.7ka BP, the ECHAM5 experiments are from now on called *EH5-2ka* and *EH5-1.7ka* experiment, respectively. Furthermore, three sensitivity experiments are carried out for the *EH5-2ka* experiment. Here SST¹¹/SIC¹² fields for only one ocean basin (North Atlantic, Pacific Ocean, Indian Ocean) are taken from the 1.7ka period and all other ocean grid points are set to 2ka conditions. These simulations will be further called *EH5-1.7ka-NA* (North Atlantic), *EH5-1.7ka-PO* (Pacific Ocean) and *EH5-1.7ka-IO* (Indian Ocean). A more detailed description how these simulations are carried out can be found in Chapter 4, Section 4.3.

CMIP3

COSMOS simulations carried out within the CMIP3 project are used to analyse future changes of ISM variability under enhanced greenhouse gas concentrations. Here, the COSMOS simulations following the A1b, A2 and B1 emission scenarios (Nakicenovic et al., 2000) as well as the commitment simulation forced by observed GHG concentrations until the year 2000 and fixed concentrations thereafter are used (*COSMOS-A1B (run1)*, *COSMOS-A2 (run1)*, *COSMOS-B1 (run1)*, *COSMOS-COM (run1)*). In this study only the first ensemble member of all simulations is analysed, as these simulations have been used to force CLM at its lateral boundaries (Dobler and Ahrens, 2011). It must be noted that CLM simulations under future climate conditions (*CLM-A1B*, *CLM-A2*, *CLM-B1*) as well as under recent conditions and fixed GHG¹³ concentrations after the year 2000 (*CLM-COM*) forced by CMIP3 ECHAM5 simulations are not carried out within this project. Here, existing simulations using a previous model version (2.4.11) described in Dobler and Ahrens (2011) are used. The setup and domain are not identical to the setup used for the other CLM simulations, thus the recent climate CLM simulation is also validated regarding observed intraseasonal features of the ISM (see Chapter 3). All these future climate simulations (RCM¹⁴ & GCM) are analysed in Chapter 5.

¹¹Sea Surface Temperatures

¹²Sea Ice Concentrations

¹³Greenhouse Gas Concentrations

¹⁴Regional Climate Model

Identifier	Model	Resolution	Time period	Forcing	Reference
<i>COSMOS-mil0014</i>	AOGCM	T31L19	1000 AD – 2000 AD	fully-coupled	Jungclaus et al. (2010)
<i>COSMOS-Holocene</i>	AOGCM	T31L19	6000 BP – 0 BP	fully-coupled	Fischer and Jungclaus (2011)
<i>COSMOS-COM (run1)</i>	AOGCM	T63L31	1960 AD – 2100 AD	fully-coupled	Roeckner et al. (2006a)
<i>COSMOS-A1B (run1)</i>	AOGCM	T63L31	2001 AD – 2100 AD	fully-coupled	Roeckner et al. (2006b)
<i>COSMOS-B1 (run1)</i>	AOGCM	T63L31	2001 AD – 2100 AD	fully-coupled	Roeckner et al. (2006d)
<i>COSMOS-A2 (run1)</i>	AOGCM	T63L31	2001 AD – 2100 AD	fully-coupled	Roeckner et al. (2006c)
<i>EH5-MCA</i>	AGCM	T63L31	900 AD – 1100 AD	COSMOS-mil0014	Polanski et al. (2014)
<i>EH5-LIA *</i>	AGCM	T63L39	1515 AD – 1715 AD	COSMOS-mil0014	Polanski et al. (2014)
<i>EH5-REC</i>	AGCM	T63L31	1800 AD – 2000 AD	COSMOS-mil0014	Polanski et al. (2014)
<i>EH5-2ka *</i>	AGCM	T63L31	2008 BP – 1958 BP	COSMOS-Holocene	N/A
<i>EH5-1.7ka *</i>	AGCM	T63L31	1662 BP – 1612 BP	COSMOS-Holocene	N/A
<i>EH5-1.7ka-NA *</i>	AGCM	T63L31	sensitivity experiment	COSMOS-Holocene	N/A
<i>EH5-1.7ka-PO *</i>	AGCM	T63L31	sensitivity experiment	COSMOS-Holocene	N/A
<i>EH5-1.7ka-IO *</i>	AGCM	T63L31	sensitivity experiment	COSMOS-Holocene	N/A
<i>CCLM-ERAint *</i>	RCM	≈ 55km	1979 AD – 2011 AD	ERA-Interim	Befort et al. (2016)
<i>CCLM-MCA-wet *</i>	RCM	≈ 55km	956 AD – 987 AD	EH5-MCA	N/A
<i>CCLM-MCA-dry *</i>	RCM	≈ 55km	1041 AD – 1071 AD	EH5-MCA	N/A
<i>CCLM-LIA-wet *</i>	RCM	≈ 55km	1562 AD – 1592 AD	EH5-LIA	N/A
<i>CCLM-LIA-dry *</i>	RCM	≈ 55km	1597 AD – 1627 AD	EH5-LIA	N/A
<i>CCLM-REC-wet *</i>	RCM	≈ 55km	1943 AD – 1973 AD	EH5-REC	N/A
<i>CCLM-REC-dry *</i>	RCM	≈ 55km	1895 AD – 1925 AD	EH5-REC	N/A
<i>CLM-COM</i>	RCM	≈ 50km	1960 AD – 2100 AD	COSMOS-20C	Dobler and Ahrens (2011)
<i>CLM-A1B</i>	RCM	≈ 50km	2001 AD – 2100 AD	COSMOS-A1B	Dobler and Ahrens (2011)
<i>CLM-B1</i>	RCM	≈ 50km	2001 AD – 2100 AD	COSMOS-B1	Dobler and Ahrens (2011)
<i>CLM-A2</i>	RCM	≈ 50km	2001 AD – 2100 AD	COSMOS-A2	Dobler and Ahrens (2011)

Table 2.1: AOGCM, AGCM and RCM simulations used in this study. Experiments marked with * have been carried out within this thesis.

Recent climate

Large parts of this chapter are published in

Befort, D. J., Leckebusch, G. C., and Cubasch, U. (2016). Intraseasonal variability of the Indian summer monsoon: wet and dry events in COSMO-CLM. *Climate Dynamics*, pages 1–17, doi:10.1007/s00382-016-2989-7.

All scientific approaches and analyses presented in the published paper were developed and performed by the author of this thesis. The co-authors, Prof. Dr. Ulrich Cubasch and PD Dr. Gregor Leckebusch, were involved in the discussion of the scientific results as well as in reviewing preliminary versions of the manuscripts.

This chapter focuses on the validation of models used in the model-chain (COSMOS-ECHAM5-CCLM). Special focus is put on a CLM¹ simulations forced by ERA-Interim data at its lateral boundaries under recent climate conditions. Besides evaluating CLM simulations carried out in this project, it is analysed in how far CLM model simulations described in Dobler and Ahrens (2011) are able to simulate observed features of the ISM² on intraseasonal time-scales. This is necessary as a different model version and setup has been used in comparison to simulations carried out in this study. Eventually, the performance of in simulating intraseasonal variability of the ISM is analysed.

Overall, this chapter answers the first research question:

ARE CLIMATE MODELS (GCM/RCM) USED IN THIS STUDY ABLE TO REPRESENT OBSERVED FEATURES OF THE INTRASEASONAL VARIABILITY OF THE ISM (ACTIVE AND BREAK SPELLS, NORTHWARD PROPAGATION)?

¹COSMO-CLM

²Indian Summer Monsoon

3.1 Intraseasonal Variability of the Indian Summer Monsoon in COSMO-CLM

3.1.1 Introduction

The Indian summer monsoon (ISM) is a fundamental part of the climate of the Indian sub-continent, as India receives about 80% of its annual rainfall amount during the months of June until September (Basu, 2007). The ISM is influenced by external factors, e.g. sea surface temperatures over the Indian Ocean, ENSO³, northern hemisphere snow cover or by teleconnections with the mid-latitudes (Hahn and Shukla, 1976; Ashok et al., 2001; Wang et al., 2003; Krishnan et al., 2009) and is in parallel characterized by a high internal variability (Ajayamohan, 2007). The spatial rainfall distribution over India is heavily influenced by steep orography at the western coast (Western Ghats) and in the north of the country at the Himalayan foothills. This study investigates the ability of the regional climate model COSMO-CLM to simulate subseasonal rainfall characteristics of the ISM system, as well as the models skill to represent observed wet and dry events within the monsoon season.

Several studies investigated the Indian monsoon using global climate models (GCM) under present, paleo and future climate conditions (Gadgil and Sajani, 1998; May, 2003; Wang et al., 2004; May, 2004; Dallmeyer et al., 2010; May, 2011). The main characteristics of the large-scale monsoon system, e.g. the atmospheric circulation are in good agreement with observations. However, these models lack a realistic representation of the spatial rainfall distribution, mainly due to the coarse resolved orography. As this study concentrates on results based on a limited area model, we refer to Wang (2006) (and references therein) for an extensive overview of the Indian summer monsoon system in GCM simulations.

Models with a higher spatial resolution and hence orography, such as regional climate models (RCM), show in general an improved representation of spatial rainfall patterns (Nguyen and McGregor, 2009; Dobler and Ahrens, 2010, 2011; Lucas-Picher et al., 2011; Asharaf et al., 2012; Asharaf and Ahrens, 2013; Srinivas et al., 2013). The majority of these studies investigated seasonal and climatological rainfall distributions over India. Dobler and Ahrens (2010) used the model COSMO-CLM driven by ERA-40 reanalysis data (Uppala et al., 2005) to simulate the Indian summer monsoon under recent climate conditions. They found that the model is able to capture the spatial distribution of rainfall, but also noticed too wet conditions over the west coast of India, which they explain with enhanced convective activity over the warm tropical oceans surrounding India. Lucas-Picher et al. (2011) investigated the representation of the summer monsoon in four different regional climate models. The spatial distribution of mean rainfall is well captured by the models, but large differences on the regional scale were found.

³El Niño Southern Oscillation

Differences of model results compared to observations are mainly caused by insufficient parametrization schemes or deficits in soil conditions: Both, Srinivas et al. (2013) and Dash et al. (2006) showed that rainfall amounts over India in the regional climate models WRF (Srinivas et al., 2013) and RegCM3 (Dash et al., 2006) show high sensitivity to the choice of the convection scheme. Furthermore, previous studies (Saeed et al., 2009; Lucas-Picher et al., 2011) revealed positive surface temperature biases over the northwestern part of India. Saeed et al. (2009) suggested that this overestimation is due to the fact that irrigation over Pakistan is not taken into account in these model simulations. Asharaf et al. (2012) showed that wetter initial soil conditions in the model COSMO-CLM increases rainfall over northwestern India, mainly due to recycling of soil-moisture. Additionally, Saeed et al. (2009) showed that cyclones from the Bay of Bengal enter farer west into India, if soil moisture is increased.

Despite all these differences regarding soil conditions and parametrization of convection, these studies indicate that current RCMs are able to depict seasonal characteristics of the Indian summer monsoon. However, there is only a limited number of studies analyzing rainfall over India on a time scale from days to weeks, although the ISM reveals a high intraseasonal variability. Active and break cycles with a length of several days until several weeks influence the seasonal rainfall pattern significantly (Sperber et al., 2000; Goswami and Mohan, 2001). Long lasting dry spells affect seasonal rainfall over India and have been investigated by Bhat (2006) and Gadgil (2003) (and references within). For example, in the year 2002 the annual rainfall deficit was about 21%, which was mainly due to a dry event lasting for 36 days around July in which rainfall was 56% below normal ((Bhat, 2006; Suhas et al., 2013) showed that this is linked to a reduced northward propagation of rainfall during July.

This study focuses on the intra-seasonal variability of the Indian summer monsoon and is therefore intended to extend the analyses carried out by Dobler and Ahrens (2010) using an earlier model version driven by ERA-40 reanalysis data at its lateral boundaries. Our results regarding the mean spatial rainfall distribution show only slight differences compared to results from Dobler and Ahrens (2010), with a general underestimation of rainfall over most parts of India (Figure 3.1). Here, we will focus on the model's capability to simulate observed daily rainfall variability over the Indian subcontinent, the northern propagation of monsoon intraseasonal oscillations as well as the representation of wet and dry events and their related atmospheric circulation. We use COSMO-CLM with a horizontal resolution of about 55 km, driven by ERA-Interim reanalysis at its lateral boundaries. The choice of the resolution is motivated by the set up of the current CORDEX simulations, which mainly have been running with a similar resolution. Thus, the model configuration offers detailed structures of the Indian summer monsoon simulation compared to GCM simulations and is also suitable for simulations of about 30 years due to the need of reasonable computational resources.

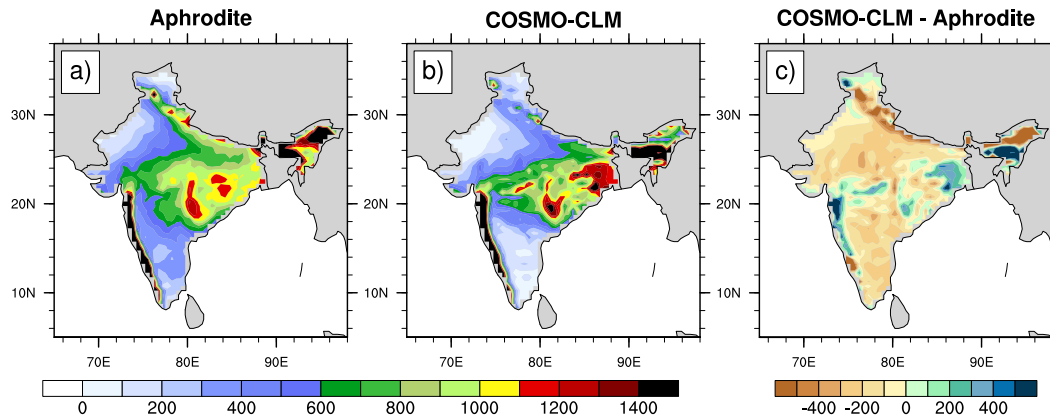


Figure 3.1: Mean rainfall during JJAS [mm/d] (1979-2007) for a) Aphrodite, b) COSMO-CLM and c) difference between COSMO-CLM and Aphrodite.

3.1.2 Data

In this study we use the rainfall dataset carried out within the Aphrodite (*Asian Precipitation - Highly-Resolved Observational Data Integration Towards Evaluation of Water Resources*) project (Yatagai et al., 2012). For this study the Aphrodite (version: V1003R1) for the region "Monsoon Asia" with a horizontal resolution of 0.5° is used (Yatagai et al. (2012)).

We use additionally TRMM (*Tropical Rainfall Measuring Mission*) (Huffman et al., 2007) as well as GPCP (*Global Precipitation Climatology Project*) (Huffman et al., 2001) satellite based rainfall estimates to investigate the uncertainty of rainfall measurements. Similar to Aphrodite, these two datasets are available on a daily time scale and are used to validate model results on a sub-monthly time scale (c.f. Table 3.1 for a detailed overview).

To investigate the performance of the model in comparison to its forcing model, we use ERA-Interim reanalysis data (Dee et al., 2011) over the Indian region. To calculate daily precipitation sums for ERA-Interim reanalysis data we use the forecast simulation starting at 00 UTC and 12 UTC. Using the accumulated rainfall amount after 12 hours from both forecasts we obtain the daily precipitation sum.

For the investigation of the atmospheric circulation ERA-Interim reanalysis data of zonal and meridional wind components in 500 hPa is used.

Dataset	temporal coverage	hor. resolution	temp. resolution	gauge based	satellite based
Aphrodite ¹	1951-2007	0.5°	daily	yes	no
TRMM ¹	1998-2007	0.25°	daily	no	yes
GPCP ¹	1997-2012	1.0°	daily	no	yes
ERA-Interim ^{1,2}	1979-2011	T255	daily		

Table 3.1: Datasets used in this study as well as the temporal coverage, horizontal resolution, temporal resolution and the database used to derive this product (only given for precipitation datasets). For some datasets other horizontal/temporal resolutions are available and the value given here indicates the resolution used within this study. The superscript indicates the parameter used in this study: 1) precipitation, 2) zonal + meridional wind speed components in 500hPa

3.1.3 Model

The COSMO (*C*Onsortium for *S*Small scale *M*ODEling) model in *C*limate *M*ode (COSMO-CLM) is the community model of the German regional climate research. The model is based on the COSMO model which is used by several weather services across Europe for numerical weather prediction (NWP). The main differences between the climate version and the NWP version are given in Böhm et al. (2006). In this study, we use the model version 4.8, subversion 17 for the period from 1979 to 2011 over the domain shown in figure 2.1. The lateral boundary conditions are provided by the ECMWF ERA-Interim (Dee et al., 2011) reanalysis dataset. The simulation is performed on a rotated pole grid with a horizontal resolution of 0.5°x0.5° ($\approx 55\text{km}$) and 32 vertical levels. The parameterizations used for the model integration include a radiation scheme following Ritter and Geleyn (1992), a micro-physics scheme including cloud water, rain and snow (Kessler, 1969) and the Tiedtke mass flux convection scheme (Tiedtke, 1989). The temporal discretization is performed with a leapfrog scheme at a integration time step of 150 seconds.

Soil moisture and soil temperature profiles at the start of the simulation are taken from a previous COSMO-CLM simulation which is integrated for the same model domain, also driven by ERA-Interim reanalysis data at its lateral boundaries but only from 1989 until 2001. We average soil moisture and temperature from this simulation for the 1st of January over all years and take these values to initialize the model simulation presented in this paper. This should reduce the models spin up as the average soil conditions from the earlier simulation are closer to the models climatology compared to the initialized values taken from reanalysis data. Similar to our approach Jaeger et al. (2009) used climatological values from a long-term simulation to initialize the model to validate the land-atmosphere interactions in the model COSMO-CLM.

3.1.4 Method

Daily and weekly unfiltered rainfall amounts are calculated for the All-Indian Monsoon Rainfall (AIMR) region covering all India (Figure 2.1). We applied the method used by Turner and Slingo (2009a) to evaluate the model's capability to capture the northern propagation of the Indian summer monsoon. Therefore, May to October 30-60 day bandpass-filtered precipitation is used. Originally, Turner and Slingo (2009a) used the region from 70°-100° east and 20° south to 20° north. Due to the limited domain of the RCM, this investigation is only carried out from the equator to 20° north. Additionally, the monsoon intraseasonal oscillation index (MISO) developed by Suhas et al. (2013) is applied to the RCM data. Daily anomalies for this analysis are derived by removing the annual cycle (mean and first three harmonics) as done by Suhas et al. (2013). Zonally averaged daily precipitation anomalies derived from the GPCP dataset for the region 60.5°-95.5° east and 12.5° south to 30° north have originally been used by Suhas et al. (2013) for an Extended Empirical Orthogonal Functions (EEOF) analysis. These first two EEOF's are projected on simulated daily precipitation anomalies and the first two PC's are called MISO1 (PC1) and MISO2 (PC2). Due to the limited domain of the RCM simulation we project the EEOF's, derived from GPCP data for the original domain, only on the region ranging from 60.5° – 95.5° east and 0° – 30° north for the model data. The PC's calculated by projecting the EEOF's on the limited domain will be called LMISO1 and LMISO2 (for observation data) and LMISO1-C and LMISO2-C (for COSMO-CLM model data), subsequently. The intensity is defined as $\sqrt{(\text{MISO1}^2 + \text{MISO2}^2)}$ and will be referred as MISO-Int, LMISO-Int and LMISO-C-Int, subsequently.

We use weekly rainfall amounts over the AIMR region as a basis to identify wet and dry events in model, observation and reanalysis data. This approach prevents investigating short lasting extreme events of e.g. one day, which have a smaller impact on the society of the Indian country. As modelled absolute rainfall amounts can show high biases compared to observations, which complicates the comparison between both datasets, we calculated the Standardised Precipitation Index (SPI) based on weekly rainfall sums to detect wet and dry events. To calculate SPI values a gamma distribution is fitted to the weekly rainfall sums. This distribution is afterwards transformed to a normal distribution with a standard deviation of 1 using a quantile-quantile mapping (Lloyd-Hughes and Saunders, 2002). Hence, each precipitation amount can be converted to a SPI value, respecting the local climatological rainfall distribution. Thus, SPI values can be compared between different regions and different times as well as the relative changes in rain amount can be evaluated.

To identify dry and wet events in model and observation data, SPI values are divided into five bins of discrete values (Table 3.2). To assess the skill of COSMO-CLM in simulating dry and wet events we calculate the Gerrity Skill Score (GSS) which is based on the Gandin-Murphy Skill Score (Gerrity, 1992). The GSS gives an objective measurement of the model skill to simulate a multi-category variable with natural ordering. It ranges between mi-

nus infinity and +1, with +1 indicating a perfect agreement between model and reference dataset and values below zero indicating results less skillful compared to climatology. The scoring weight is higher if the model represents rare events correctly (e.g. severe droughts) in comparison to regular occurring events. Additionally, the penalty is lower if the model simulates an event similar to the observed one (e.g. severe drought is observed, but model shows a moderate drought) in comparison to the case when the model simulates a complete different event (e.g. observed is a severe drought and model predicts a flood).

To investigate the spatial variability on a weekly time scale we calculate SPI time series for 34 meteorological subdivisions of India (provided by the Indian Institute of Tropical Meteorology). These time series from model, reanalysis and observation data are further used for a single component analysis.

SPI value	Interpretation
$SPI \leq -2$	severely dry
$-2 < SPI \leq -1$	moderately dry
$-1 < SPI \leq 1$	near normal
$1 < SPI \leq 2$	moderately wet
$SPI \geq 2$	severely wet

Table 3.2: Definition of SPI classes

3.1.5 Results

3.1.6 Daily rainfall

To evaluate the simulated seasonal precipitation of COSMO-CLM compared to reanalysis and observation data we calculate the mean daily rainfall amounts over the AIMR region. Furthermore, we apply a 10-day running mean to smooth day-to-day variability in the datasets (Figure 3.2). COSMO-CLM as well as ERA-Interim are able to capture the observed seasonal cycle over the AIMR region with correlations of 0.95 for COSMO-CLM and 0.99 for ERA-Interim (Figure 3.2). This well marked seasonal cycle is characterised by lower rainfall amounts during June and September and a maximum during the peak monsoon season in July and August. It is found that the overall underestimation of rainfall during JJAS is mainly due to reduced rainfall during July, August and September in COSMO-CLM compared to observations.

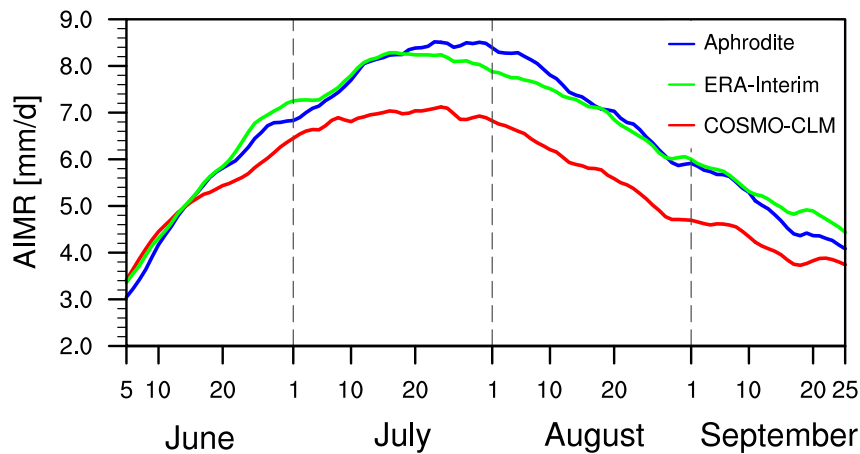


Figure 3.2: Climatological daily precipitation (1979-2009) over India (AIMR) for Aphrodite, ERA-Interim reanalysis data as well as COSMO-CLM simulation data. Rainfall amounts are smoothed with a 10-day running mean filter.

To analyse anomalies of daily rainfall amounts, we calculate correlation coefficients, RMSE and standard deviation for ERA-Interim and COSMO-CLM model output over the AIMR region (Figure 3.3), illustrated in a Taylor diagram. The diagram is normalised to the standard deviation of the reference dataset (Aphrodite).

The temporal correlation of daily rainfall anomalies is similar in COSMO-CLM (≈ 0.65) compared to ERA-Interim data (≈ 0.7) regarding the AIMR region. RMSE is higher for COSMO-CLM but the variability of daily rainfall in the model is in better agreement with observations than for ERA-Interim data.

As gridded precipitation products can differ significantly, even if having the same source of data, we added the satellite based rainfall products TRMM and GPCP to compare with daily rainfall anomalies of COSMO-CLM. As these datasets are only available since 1998 (1997, respectively for GPCP) RMSE, correlation and standard deviation are computed for all four datasets over the period 1998 until 2007. Correlations of ERA-Interim and COSMO-CLM data are nearly the same for the period 1998 until 2007 compared to 1979 until 2007, which indicates a fairly constant skill of COSMO-CLM with increased integration time. TRMM and GPCP show both lower correlation coefficients compared to COSMO-CLM and ERA-Interim, which is consistent with rain gauge data from Thailand and TRMM data (Chokngamwong and Chiu, 2008).

Overall, COSMO-CLM is in good agreement regarding the mean seasonal cycle as well as the day-to-day variability of daily rainfall over the Indian subcontinent.

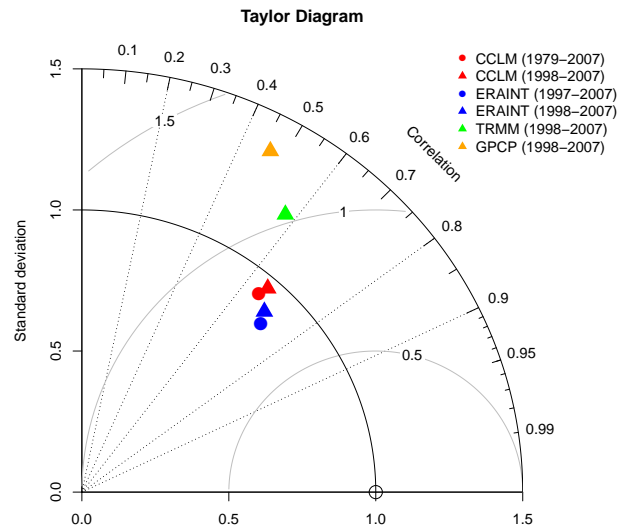


Figure 3.3: Taylor diagram for precipitation anomalies for: COSMO-CLM, ERA-Interim, TRMM and GPCP. Analysis are performed for AIMR for 1979 until 2007 (ERA-Interim and COSMO-CLM only) as well as 1998 until 2007 (all datasets) with Aphrodite as reference dataset. The filled dot gives the results for precipitation over whole India (AIMR)

3.1.7 Boreal Summer Intraseasonal Oscillation (BSISO) and Monsoon Intraseasonal Oscillation (MISO)

We calculate lag correlations of 30-60 day bandpass-filtered precipitation zonally averaged over the region 70° - 100° east against a reference point at 85° east and 12.5° north (see Section 3.1.4) to evaluate the model's capability to simulate observed features of the BSISO (Figure 3.4). Figure 3.4c shows that COSMO-CLM is capable to simulate the observed northward propagation (Figure 3.4a). However, lead-lag correlation coefficients are somehow smaller than observed. ERA-Interim shows a higher ability to capture the observed northward propagation (Figure 3.4b).

As these analyses clearly show the general ability of the model to simulate this feature of the Indian summer monsoon, it does not give any conclusion about the model's ability to simulate the observed northward propagation in specific years. We apply the method developed by Suhas et al. (2013) to the model data. As pointed out in Section 3.1.4, it is not possible to apply the originally proposed method to the RCM data, as the southern boundary is located at around 5° south of the equator. Thus, before carrying out model based results we analysed in how far results using the original domain (12.5° south – 30° north) and the smaller domain (0° – 30° north) vary if using GPCP observations. Therefore, we performed the EEOF analysis for the original domain and projected the first two EEOFs on the GPCP data to obtain the MISO1 and MISO2 indices. In another step, we use the same EEOFs (from the original domain) but used only the values from 0° to 30° north, which are then projected to the GPCP precipitation from 0° to 30° north. We find high correlations for

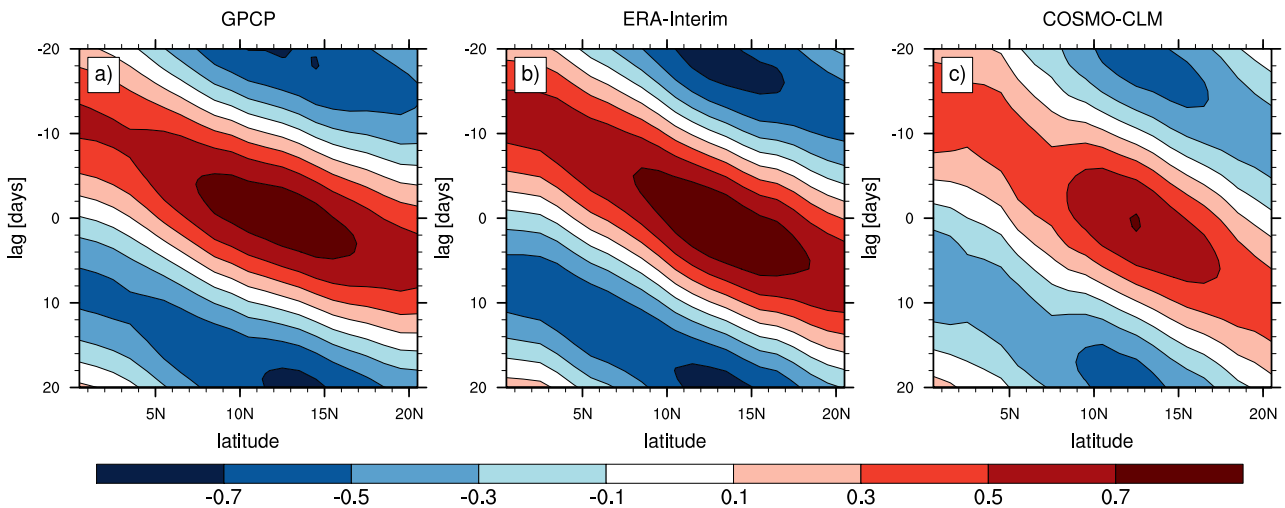


Figure 3.4: Cross-Correlation of zonally average precipitation (for longitudinal section between 70° - 100°) against a reference point near 85° east and 12.5° north for a) GPCP, b) ERA-Interim and c) COSMO-CLM.

MISO1 and LMISO1 (0.94) and MISO2 and LMISO2 (0.97), respectively. Additionally the correlation of the intensity between MISO-Int and LMISO-Int of the original and the small domain yields a correlation of (0.90), which confirms the general usability of this method on the smaller domain.

Finally, we project the EEOF (derived from GPCP data) on COSMO-CLM simulated precipitation anomalies to derive the corresponding LMISO1-C and LMISO2-C indices for COSMO-CLM. We find strong correlation between LMISO1-C and LMISO1 (0.76) and LMISO2-C and LMISO2 (0.71), respectively, suggesting that the temporal development of the northward propagation is well captured by the model. However, the intensities (LMISO-Int and LMISO-C-Int) show a weaker linear relation of only 0.50. Figures 3.5 and 3.6 shows the observed northward propagation (derived from GPCP data), as well as the northward propagation as found in COSMO-CLM and in ERA-Interim reanalysis data in a MISO phase diagram for the years 2005 and 2002. The MISO phase diagram shows the approximate location of anomalous high precipitation. In general, phases 1-4 are characterised by lower than average rainfall amounts over central India, whereas phases 5-8 are characterised by higher amounts over central and northern India (see Suhas et al. 2013).

2002 was marked by a intense MISO event during June, followed by a minor MISO event in July. This minor event during July led to a huge drought affecting all India. ERA-Interim is in good agreement with observations (Figure 3.5a), but it underestimates the MISO intensity during June (Figure 3.5b), which is also seen for COSMO-CLM (Figure 3.5c). For both, reanalysis and COSMO-CLM only a minor event during July is identified, as no activity in phase 5-8 is found. However, COSMO simulates a MISO event with too high values especially in phase 1 and phase 2. During 2005 COSMO-CLM depicts the observed MISO events (Figure 3.6a) quite well, with a strong event taking place during September (Figure 3.6c).

Overall, COSMO-CLM is capable in simulating the observed northward propagation of rainfall during the summer monsoon season. Temporal Variability of these MISO's are in good agreement with observations, even though the model has some problems in simulating the observed strength of observed MISO's.

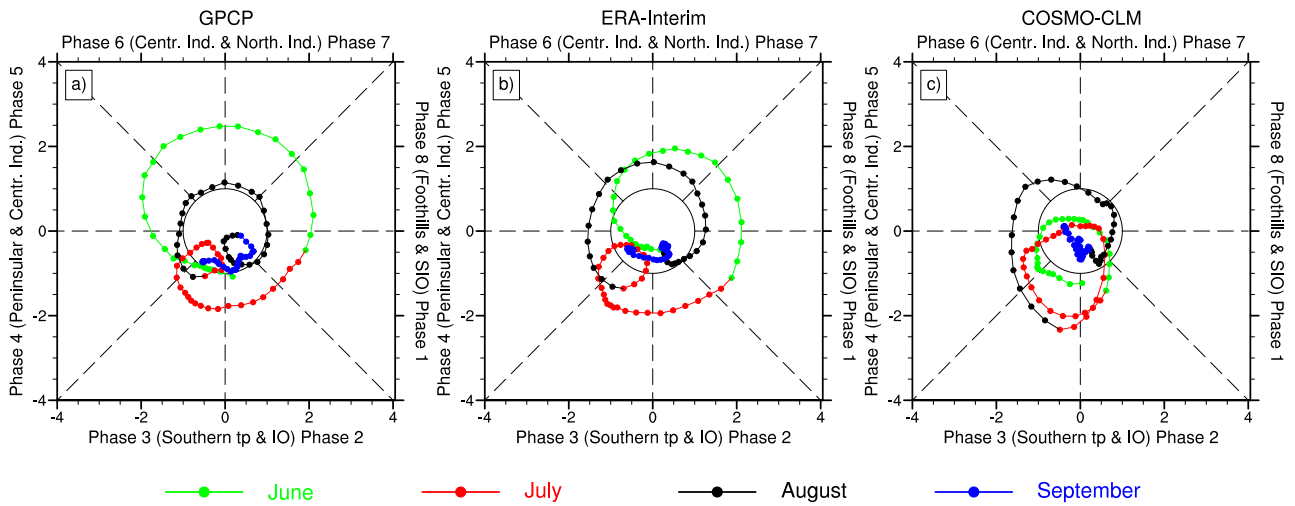


Figure 3.5: Summer season 2002 LMISO phase diagram for a) GPCP, b)ERA-Interim and c) COSMO-CLM.

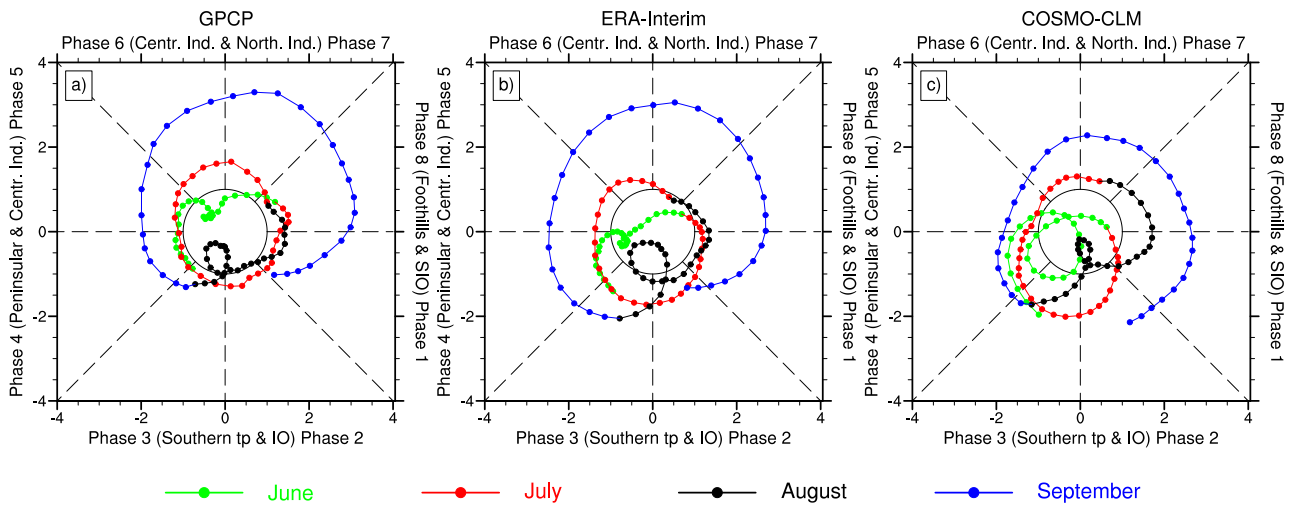


Figure 3.6: Summer season 2005 LMISO phase diagram for a) GPCP, b)ERA-Interim and c) COSMO-CLM.

3.1.8 Dry and Wet events

Dry and wet events are identified using the SPI, derived from weekly rainfall amounts (see Section 3.1.4).

Identification of dry and wet events

The skill of COSMO-CLM and ERA-Interim to represent dry and wet conditions is measured using the Gandin-Murphy Skill Score with the extension from Gerrity (GSS) (see Section 3.1.4). Generally, during observed normal conditions ($-1 \leq \text{SPI} \leq 1$), ERA-Interim and COSMO-CLM simulate normal conditions as well. Only for a small number of these observed events with normal conditions, the model simulates moderate dry or wet events. COSMO-CLM is not able to simulate the observed extreme wet events ($\text{SPI} > 2$) with the same magnitude at the same time. Here, ERA-Interim is also only able to depict a small number of these observed events. The ability of both models simulating moderate to extreme dry events ($-2 < \text{SPI} < -1$) is better compared to wet events.

GSS values (Table 3.3) of 0.52 for ERA-Interim indicate a higher ability of this dataset to detect wet and dry events at the same time with the same intensity than COSMO-CLM (GSS: 0.31). Additionally, we calculate GSS based on the three SPI classes: dry ($\text{SPI} \leq -1$), normal ($-1 \leq \text{SPI} \leq 1$) and wet conditions ($\text{SPI} > 1$). GSS values for both ERA-Interim and COSMO-CLM are increased compared to five SPI categories. The higher skill of ERA-Interim is due to the higher probability to detect observed extreme wet events, whereas COSMO-CLM is not able to simulate these events at the same time with the observed intensity.

To investigate whether the GSS of this COSMO-CLM model simulation is representative, we calculate GSS also for other precipitation datasets which are available on a daily resolution. As discussed in section 3.1.6, TRMM and GPCP satellite based daily rainfall estimates have a lower temporal correlation with Aphrodite observation data compared to COSMO-CLM. Chokngamwong and Chiu (2008) found that the relation between gauge measurements over Thailand and TRMM strengthens when averaging TRMM data over five days or longer time periods. We find a similar behaviour for both: TRMM and GPCP compared to Aphrodite observations (not shown). Thus, it is reasonable to calculate wet and dry spells on a weekly timescale. Unfortunately, both datasets, TRMM and GPCP, are only available since 1997 or 1998, respectively. Thus, when calculating weekly sums of precipitation only 180 weekly rainfall amounts values are left for the summer monsoon season (JJAS) from 1998 until 2007. Concerning the statistical representativeness of this sample we use only three SPI categories (Table 3.3).

GSS is highest for ERA-Interim data (0.62), followed by TRMM (0.59), GPCP (0.52) and COSMO-CLM (0.49). For the shorter period (1998-2007) the GSS of COSMO-CLM is nearly the same as for the whole period (1979-2007), indicating a stable skill in time. As discussed in section 3.1.6 correlation of daily rainfall anomalies with Aphrodite observations is higher for COSMO-CLM than for TRMM and GPCP. Furthermore, temporal correlation of weekly precipitation is similar for COSMO-CLM compared to both satellite products. The reason for higher GSS values for TRMM and GPCP is due to the higher probability of capturing dry events. Normal and wet condition are captured nearly equal in COSMO-CLM compared to TRMM and GPCP. As the scoring weight of rare events (e.g. dry events) is higher compared to regular events (see section 3.1.4), GSS is higher in TRMM and GPCP data. These results have to be interpreted carefully as the gamma distribution fit to derive the SPI values is performed using only 10 years, which is obviously not as robust as fitting a gamma distribution to a 30 year long dataset. Nevertheless, these results can be viewed as an estimate of the value of the COSMO-CLM simulation.

Overall, the ability of COSMO-CLM to simulate extreme precipitation events is comparable to those represented in observation or ERA-Interim data. Thus, COSMO-CLM is useful to investigate those extreme events over India. GSS for different subregions are smaller compared to All-Indian GSS, which reflects the models ability to simulate the observed temporal evolution of events but not their spatial occurrence.

Dataset	CCLM	ERA-Interim	TRMM	GPCP
GSS 1979-2007 (5 bins)	0.31	0.52	-	-
GSS 1979-2007 (3 bins)	0.48	0.65	-	-
GSS 1998-2007 (3 bins)	0.49	0.62	0.59	0.52

Table 3.3: Gerrity skill scores (GSS) for COSMO-CLM, ERA-Interim, TRMM and GPCP compared to Aphrodite observation dataset based on SPI values derived from weekly rainfall over AIMR region.

Spatial variability

Based on weekly SPI values for 34 subregions, we perform an EOF (*empirical orthogonal function*) analysis. As pointed out by Wu et al. (2007) SPI values on short timescales and especially in dry climates can be misleading as the SPI values are not normal distributed due to too many zero rainfall events. In the beginning of June and end of September some subregions in northwestern India receive very little rainfall amounts which might lead to misleading SPI values. To address this fact, we compute EOF analysis using data for the whole summer monsoon season (JJAS) and for the peak monsoon season (July-August), only. As the results from both time periods indicate similar results in general, we discuss EOF patterns for the complete season.

In principle, the first EOF shows a variability pattern with a sharp contrast between north-eastern/southern India and the rest of the subcontinent (Figure 3.7a-c), which is more pronounced in Aphrodite than in ERA-Interim (correlation: 0.92) or COSMO-CLM (correlation: 0.86) data. As we perform an EOF analysis based on SPI values for 34 subregions, we count every subregion only once when computing the correlation. The second EOF (Figure 3.7d-f) shows a strong north-south contrast of the loadings in observation data, which is also present in both: reanalysis (correlation: 0.98) and model data (correlation: -0.89). The third EOF (Figure 3.7g-i) indicates a variability pattern associated with positive loadings over southern/northeastern India and negative loadings over northwestern India, which is well captured by ERA-Interim (correlation: 0.81). EOF 3 and 4 are in reversed order comparing COSMO-CLM to Aphrodite and ERA-Interim. Nevertheless, explained variances of both patterns are similar and comparing EOF 4 of COSMO-CLM with EOF 3 of Aphrodite indicates a high agreement (correlation: -0.73). EOF 4 (Figure 3.7j-l) in Aphrodite data shows positive values over the core monsoon region and negative values over northwestern and southern India. This pattern is well captured by both ERA-Interim (correlation: 0.80) and by the third EOF pattern of COSMO-CLM (correlation: -0.71). The first EOF pattern in COSMO-CLM accounts less explained variance (28.4%) than in Aphrodite (32.8%). For the following three EOF's explained variances have similar magnitudes.

As this study focuses on the validation of the models spatial variability on a weekly time scale, the complete physical explanation of these EOF patterns are beyond the scope of this paper. It is worth mentioning that the first EOF pattern is similar to earlier studies from Krishnamurthy and Shukla (2000) and Sontakke and Singh (1996) even though there are some differences which might be caused by the relatively large regions used in our study. Overall, COSMO-CLM shows high correlations for the first four EOF patterns. As these four EOFs explain over 60% of the natural variability, we conclude that spatial variability on a weekly timescale is well captured by the model.

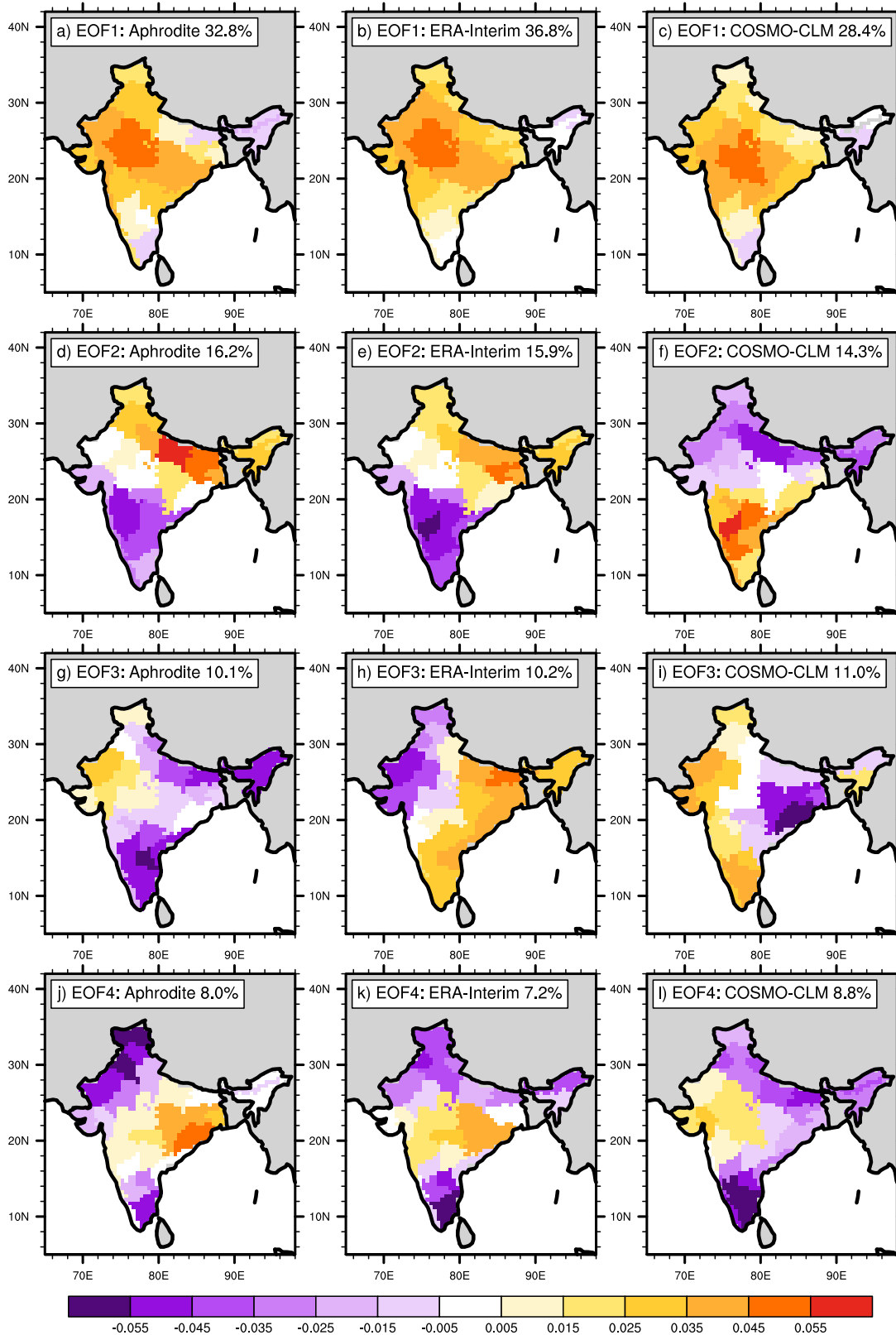


Figure 3.7: SPI EOF loading patterns, based on weekly JJAS precipitation amount from 1979 until 2009, derived for Aphrodite, ERA-Interim and COSMO-CLM. The values within the square brackets represent the explained variance of each loading pattern.

Coupling between rainfall anomalies and the large-scale circulation anomalies on intraseasonal time scales

Rainfall variability on the intraseasonal time scale over India is predominately determined by changes in the large-scale atmospheric circulation. Thus, it is important for the model to capture the coupling between large-scale anomalies in atmospheric conditions and rainfall anomalies over India. We investigate in how far differences in dry and wet events between observations and COSMO-CLM can be attributed to differences in the large-scale atmospheric circulation between both datasets. For this reason composite analysis for three different categories are carried out: 1) events, which are observed **and** simulated with a similar magnitude by COSMO-CLM, 2) events, which are observed and simulated by ERA-Interim **but not** simulated with a similar magnitude by COSMO-CLM and 3) events, which are **not** observed **nor** simulated by ERA-Interim **but** simulated by COSMO-CLM.

As shown in section 3.1.8, the first EOF pattern shows a strong contrast between northeastern India and the rest of the subcontinent, indicating an antisymmetric behaviour of SPI between these regions. As mechanisms leading to extreme events might be different between northeastern India and the rest, we only use SPI information from the region covering all India without the northeastern area for the following investigation. To ensure a reasonable large number of extreme events, we classify events into normal conditions ($-1 < \text{SPI} < 1$), dry conditions ($\text{SPI} < -1$) and wet conditions ($\text{SPI} > 1$). As the SPI is normal distributed with a standard deviation of one, 66% of SPI values are between -1 and +1. Thus, there are 82 dry and 81 wet weeks in the observational dataset (about 31% of the whole dataset).

Dry Events

Out of the observed 82 dry events, COSMO-CLM simulates 49 ($\approx 60\%$) dry events at the same time with a similar magnitude, whereas ERA-Interim captures 64 ($\approx 78\%$) dry events at the same time with a similar magnitude, showing the higher ability of ERA-Interim in depicting these events. 21 ($\approx 26\%$) observed dry events are not simulated by COSMO-CLM but found in ERA-Interim. Thus, 12 ($\approx 15\%$ of all 82) observed dry events are not found in ERA-Interim and COSMO-CLM, indicating that the boundary conditions are the main reason for the mismatch of these events. Figures 3.8, 3.9, 3.10 show composite anomalies of vorticity in 200 hPa, 500 hPa and 850 hPa for the three defined categories of events.

Dry events, which are simulated by COSMO-CLM (category 1) are associated with significant positive vorticity anomalies north of Pakistan and negative anomalies over Bangladesh in 200 hPa (Figure 3.10b). In 500 hPa the positive anomaly is again found over Pakistan region and a negative vorticity anomaly over central India is found (Figure 3.9b). In 850 hPa the positive anomaly over Pakistan is not present, but the negative anomaly over central India is much more pronounced and stretches over large parts of the Arabian Sea (Figure 3.8b). These results compare well with those found by Krishnan et al. (2009). All these

features are captured by COSMO-CLM, meaning that the mechanisms are well represented in the model (Figure 3.10a,3.9a,3.8a). Thus, an observed dry event on the intraseasonal time scale, which is captured by COSMO-CLM is associated with an enhanced low to mid-tropospheric cyclonic activity over central India, which leads to a decreased moisture flow into the Indian subcontinent. Additionally, these events are associated with a mid to upper-tropospheric anti-cyclonic vorticity anomaly over Pakistan, which leads to an increased inflow of dry air from the mid-latitudes into northwestern India (Krishnan et al. (2009)).

For observed dry events, which are not simulated by COSMO-CLM (category 2), changes in the upper-tropospheric circulation are not significant over most of the region, however, signs of a cyclonic anomaly are found over Pakistan again (Figure 3.10d), which is also captured by COSMO-CLM (Figure 3.10c). In line with this, no significant cyclonic vorticity anomaly is found over Pakistan in 500 hPa for ERA-Interim and COSMO-CLM (Figure 3.9c,d). However, ERA-Interim reveals a significant anti-cyclonic vorticity anomaly over central India, which is not found in COSMO-CLM (Figure 3.9c,d). Additionally, COSMO-CLM shows no significant vorticity anomalies over most of India in the lower troposphere, whereas a significant anti-cyclonic vorticity over large parts of India is found in ERA-Interim (Figure 3.8c,d). Thus, the reason why COSMO-CLM does not simulate these events is due to differences in the lower troposphere as the model does not simulate a anti-cyclonic circulation anomaly over India in these cases, which does coherently not lead to an extreme deficit in rainfall. However, it is worth mentioning that for all these 21 events COSMO-CLM simulates drier conditions ($SPI < 0$), however not as dry as observed ($SPI < -1$).

For dry events, which are only simulated by COSMO-CLM but neither observed nor simulated by ERA-Interim (category 3), upper- and mid-tropospheric circulation anomalies do not reveal significant cyclonic anomalies over Pakistan in ERA-Interim and COSMO-CLM (Figure 3.10e,f; Figure 3.9e,f). In contrast, COSMO-CLM shows a significant low-level anti-cyclonic vorticity anomaly over India, which is not found in ERA-Interim (Figure 3.8e,f). Thus, differences in SPI values for these events are caused by a lower-tropospheric anti-cyclonic vorticity anomaly in COSMO-CLM, which is not present in ERA-Interim.

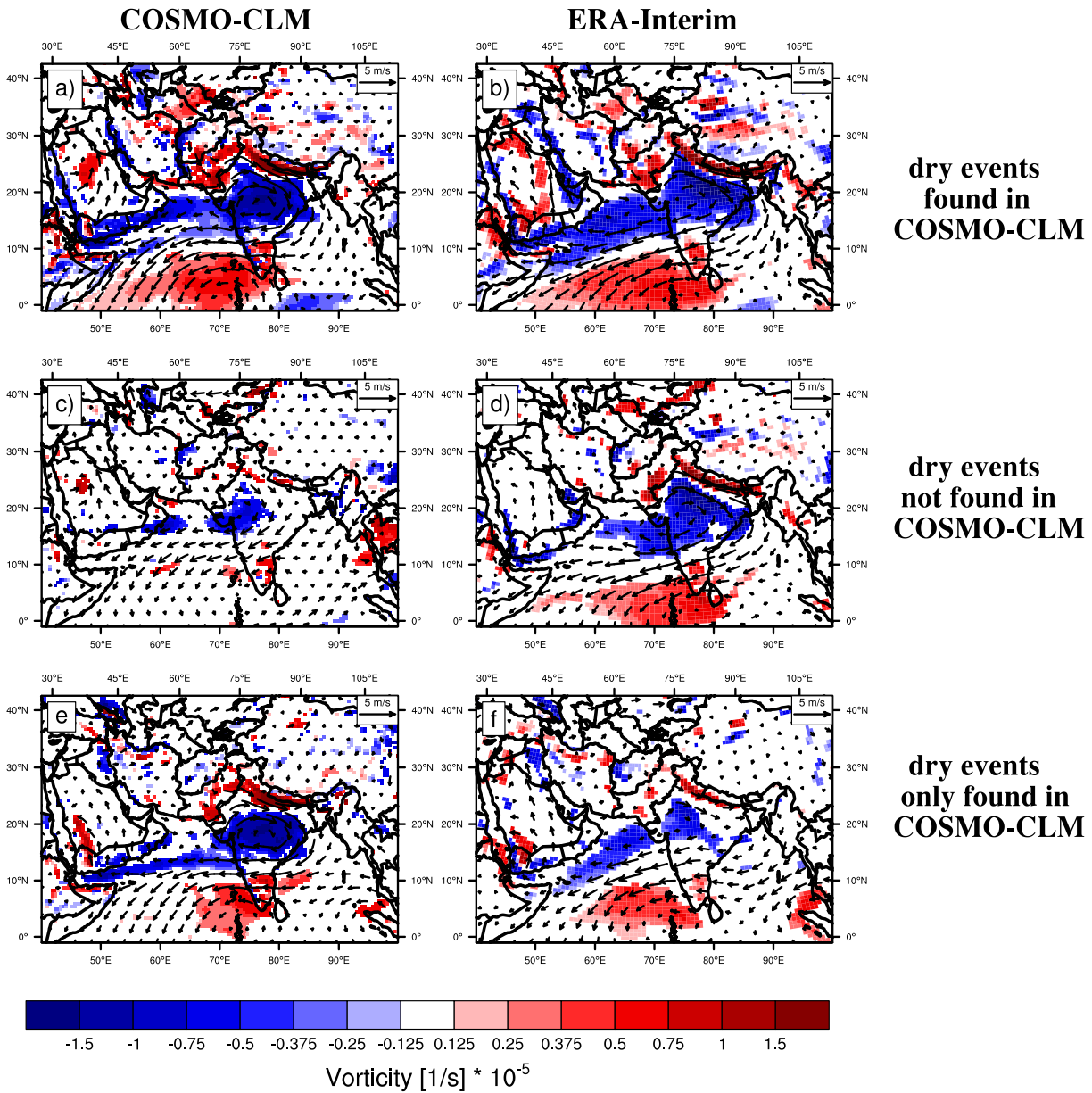


Figure 3.8: Anomaly composites of vorticity (shaded) + wind field (arrows) in 850 hPa for COSMO-CLM (a & c) and ERA-Interim data (b & d). a) & b): dry events simulated by COSMO-CLM; c) & d): dry event not simulated by COSMO-CLM; e) & f): dry events simulated by COSMO-CLM only. Shaded areas are significant with an p-value of 5% (t-test).

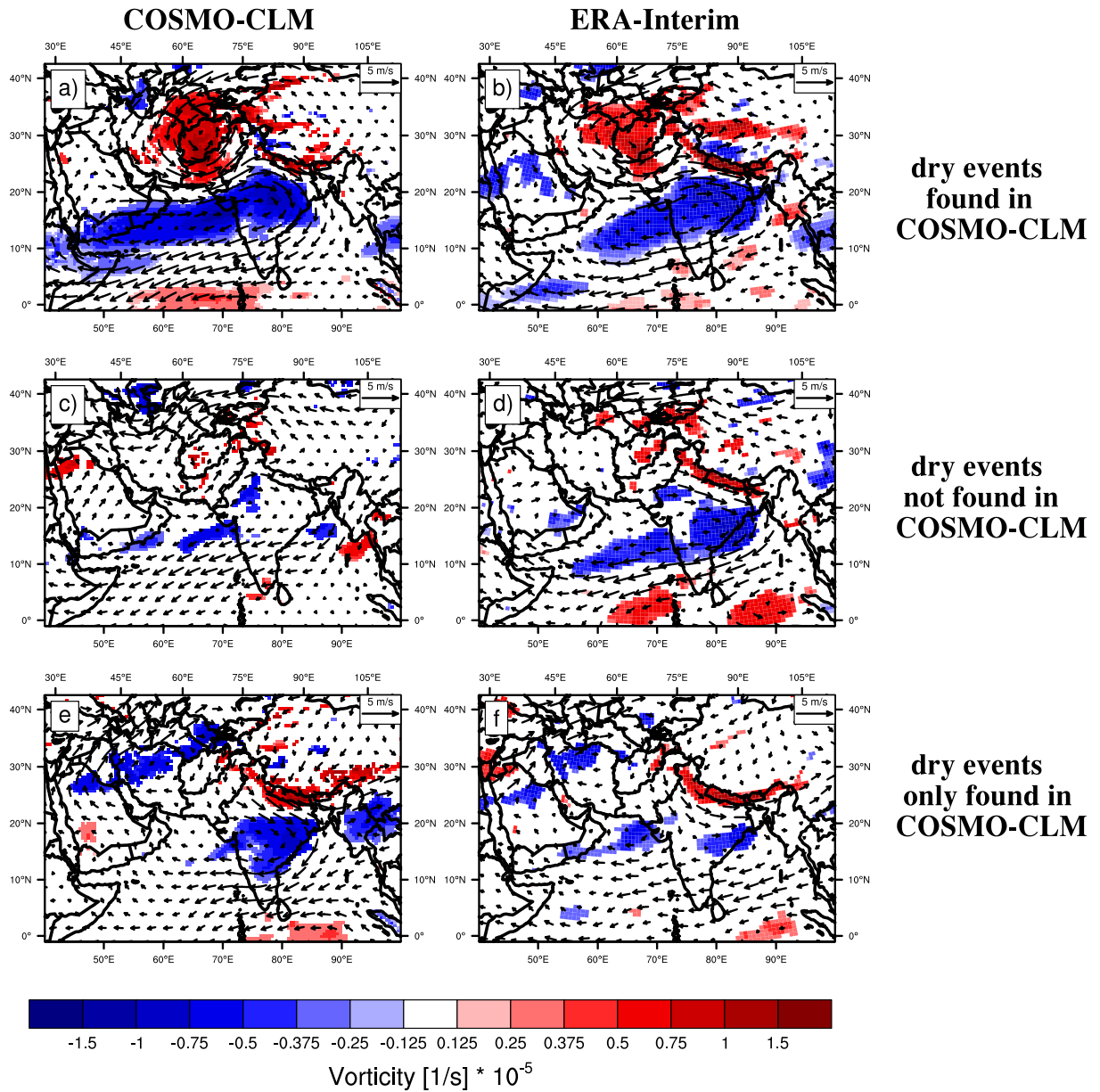


Figure 3.9: Anomaly composites of vorticity (shaded) + wind field (arrows) in 500 hPa for COSMO-CLM (a & c) and ERA-Interim data (b & d). a) & b): dry events simulated by COSMO-CLM; c) & d): dry event not simulated by COSMO-CLM; e) & f): dry events simulated by COSMO-CLM only. Shaded areas are significant with an p-value of 5% (t-test).

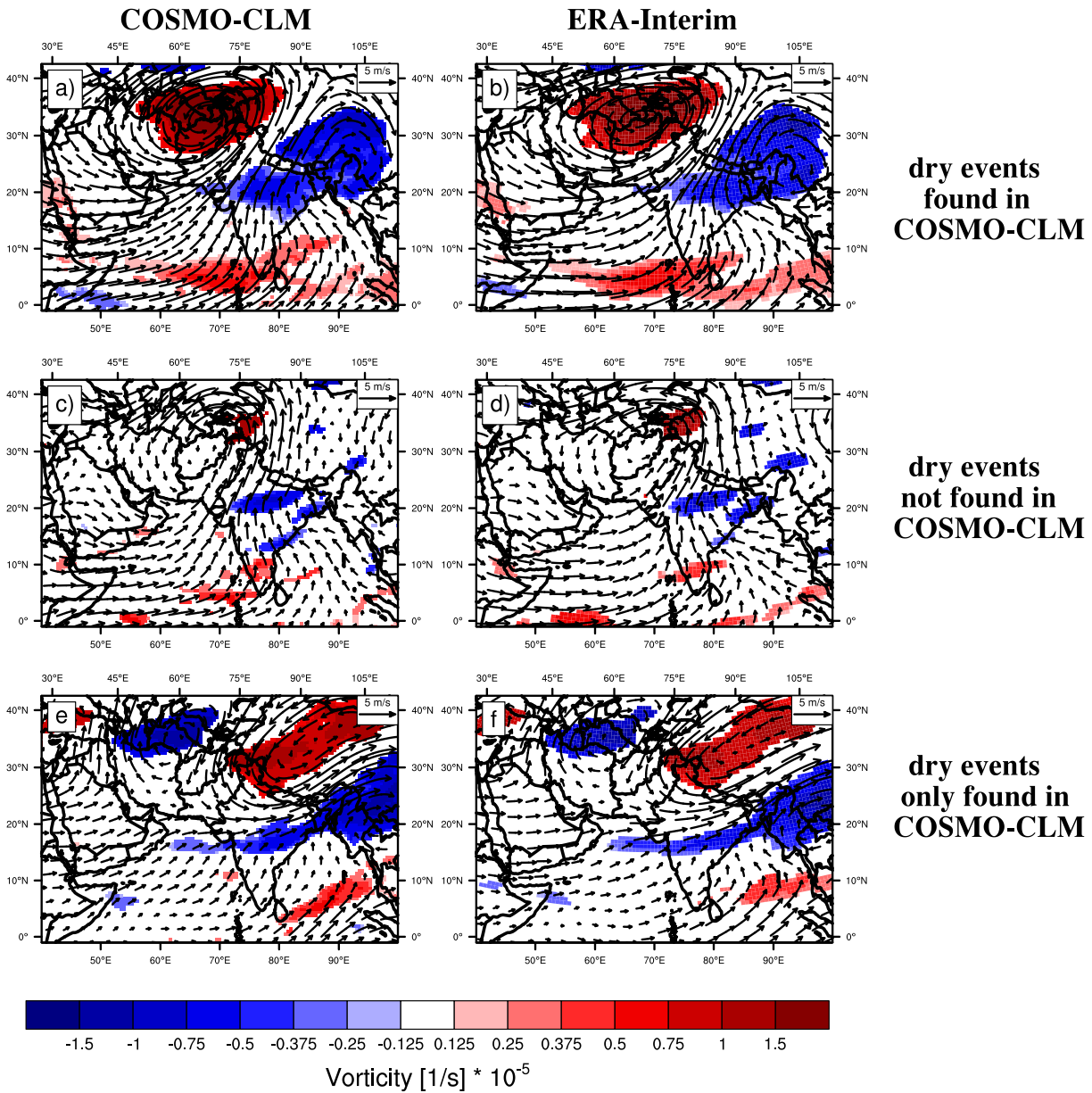


Figure 3.10: Anomaly composites of vorticity (shaded) + wind field (arrows) in 200 hPa for COSMO-CLM (a & c) and ERA-Interim data (b & d). a) & b): dry events simulated by COSMO-CLM; c) & d): dry event not simulated by COSMO-CLM; e) & f): dry events simulated by COSMO-CLM only. Shaded areas are significant with an p-value of 5% (t-test).

Wet Events

An analogue analysis for wet events affecting India is performed. Out of the total observed 81 wet events, 43 ($\approx 53\%$) observed wet events are also simulated by COSMO-CLM (category 1) and the main characteristic leading to these events is a strong cyclonic vorticity anomaly over India in 850 hPa (Figure 3.11b), which is well captured by the model (Figure 3.11a).

18 ($\approx 22\%$) observed observed wet events are not simulated by COSMO-CLM but found in ERA-Interim reanalysis (category 2). The vorticity anomaly composite for reanalysis data shows again a strong positive vorticity anomaly (Figure 3.11d), which is not captured by COSMO-CLM (Figure 3.11c).

30 wet events are simulated by COSMO-CLM but neither found in reanalysis nor in observation data (category 3). In these cases COSMO-CLM simulates a strong cyclonic vorticity anomaly over India (Figure 3.11e) which is stronger than in reanalysis data (Figure 3.11f). In the upper troposphere (200 hPa) a similar vorticity anomaly pattern with reversed sign is found for wet events compared to dry events (not shown). However, these upper-tropospheric features are not present in the mid-troposphere (500 hPa), which is characterised by a cyclonic vorticity anomaly over India only (not shown).

Our results suggest that dry events which are caused by both, changes in the lower tropospheric circulation over India as well as changes in the upper tropospheric circulation over Pakistan, are better captured by COSMO-CLM than dry events which are only caused by changes of the lower tropospheric circulation over the Indian subcontinent only. One explanation is that tropical-extratropical interactions are mainly induced by a strong upper level cyclonic anomaly over Pakistan (Krishnan et al., 2009), which is forced by lateral boundary conditions supplied by ERA-Interim reanalysis. In contrast to this, the lower level anticyclonic anomaly over India might be much more influenced by changes of the circulation over the tropical oceans. In our model setup COSMO-CLM is forced by observed sea surface temperatures but it is likely that model parameterizations might play an important role in configuring the local climate conditions over the tropical oceans, which in turn affects monsoon variability over India.

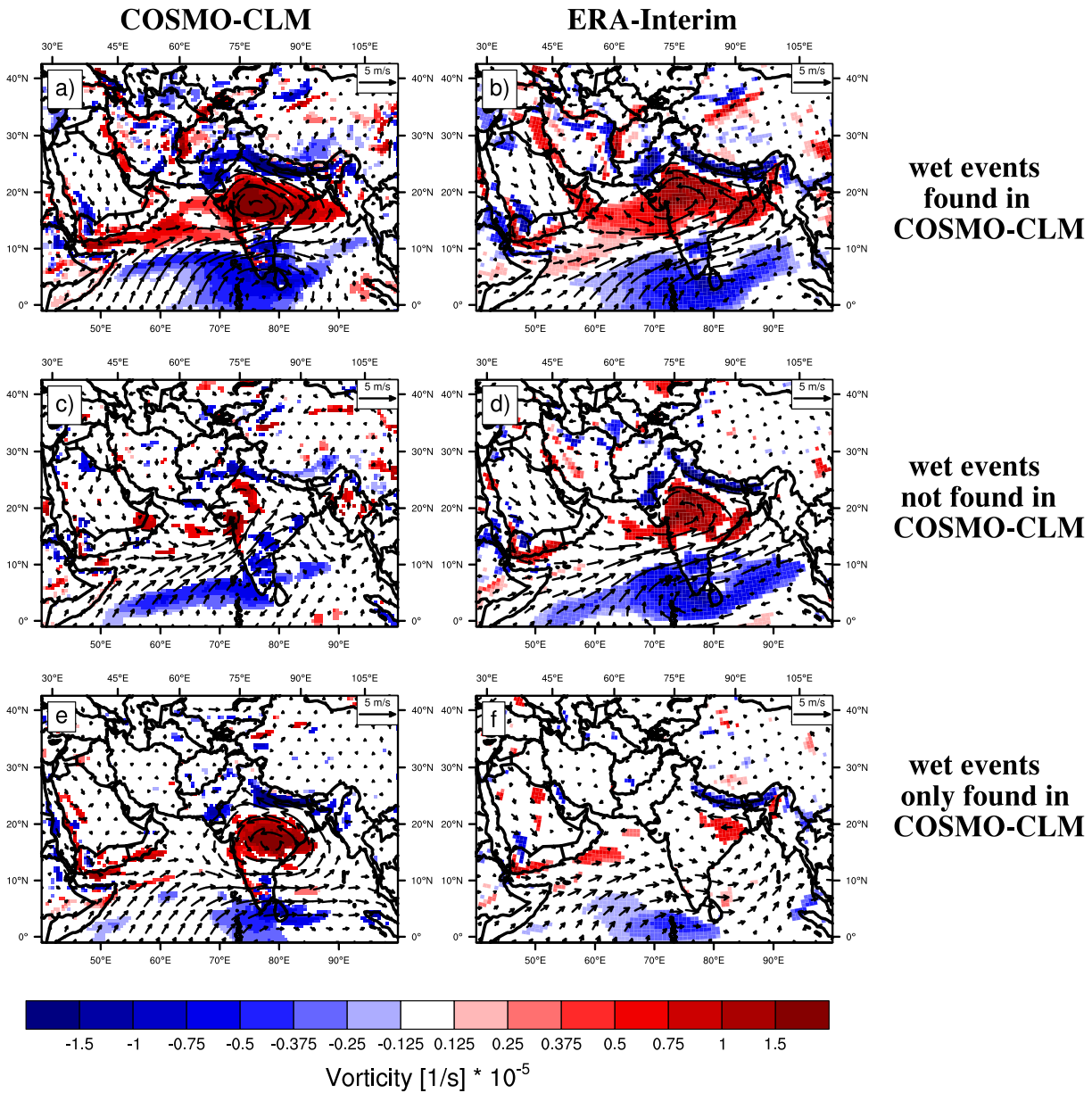


Figure 3.11: Anomaly composites of vorticity (shaded) + wind field (arrows) in 850 hPa for COSMO-CLM (a & c) and ERA-Interim data (b & d). a) & b): wet events simulated by COSMO-CLM; c) & d): wet event not simulated by COSMO-CLM; e) & f): wet events simulated by COSMO-CLM only. Shaded areas are significant with an p-value of 5% (t-test)

3.2 Conclusion

In this study we investigate the ability of the regional climate model, COSMO-CLM, driven by ERA-Interim reanalysis data at its lateral boundaries to represent the intraseasonal variability of the Indian summer monsoon. Furthermore, we focus on daily rainfall variability, northward propagation of monsoon intraseasonal oscillations and longer lasting extreme precipitation events.

We find that the general underestimation of rainfall in COSMO-CLM during the summer monsoon season (found by Dobler and Ahrens, 2010), is mainly due to too little rainfall amounts during the period from July to September. However, modelled daily rainfall anomalies over all India show a high correlation with observations.

We investigate the model's capability to simulate observed northward propagation of rainfall during the summer monsoon season (Turner and Slingo, 2009a; Suhas et al., 2013). It is found that COSMO-CLM simulates the observed northward propagation, however lag correlations between zonally averaged rainfall and rainfall at a reference point over India reveal smaller correlations for the model than for observations.

Northward propagation for specific years have been investigated using the method developed by Suhas et al. (2013). The originally proposed method to calculate MISO indices (Suhas et al., 2013) has been modified to suit the limited area of the RCM simulation. It is shown that these indices show similar results for the smaller domain compared to the original domain. The application of this approach on COSMO-CLM data shows that the model is able to simulate the temporal evolution of the LMISO1 and LMISO2 indices. However, the correlation of the intensity (LMISO-Int and LMISO-C-Int) between observed and simulated events is smaller compared to the individual correlation of both time series.

Further on, the models ability of simulating longer lasting extreme intraseasonal events have been investigated. To account for systematic model errors regarding absolute rainfall amounts, we use the standardised precipitation index (SPI) to detect extreme events on a weekly time scale. The spatial variability of COSMO-CLM regarding SPI timeseries is in good agreement with observational data. An analysis of the models ability to represent observed extreme dry and wet weeks at the same time with a similar magnitude, shows reasonable skill of the model. Even if ERA-Interim reanalysis data shows higher skill, COSMO-CLM is comparable to results deduced from satellite based rainfall estimates from TRMM and GPCP data. The latter has to be discussed carefully as only ten years of data are available for TRMM and GPCP data. Thus, the fit of the gamma distribution, which is needed to derive the SPI values, is likely to be not as robust as using a longer dataset.

To identify driving mechanisms leading to dry and wet events on a weekly time scale, we analyse atmospheric circulation in 200 hPa, 500 hPa and 850 hPa during dry and wet events over the Indian subcontinent excluding the northeastern part of the country. Three different

categories are defined: 1) found in Aphrodite and COSMO-CLM, 2) found in observations and ERA-Interim but not simulated by COSMO-CLM and 3) simulated by COSMO-CLM but neither observed in Aphrodite data nor simulated by ERA-Interim. It is found that COSMO-CLM performs better in simulating dry events associated with an anomalous upper tropospheric cyclonic vortex over Pakistan and an anomalous lower tropospheric anti-cyclonic vortex over India compared to dry events which are characterised by an anomalous lower tropospheric anticyclonic vortex over India only. We hypothesise that the upper level vortex over Pakistan is largely influenced by boundary conditions supplied by ERA-Interim but that the lower troposphere anticyclonic vortex over India is heavily influenced by the surrounding tropical oceans. Due to the high sensitivity of regional climate model results to physical parameterizations, e.g. convection (Srinivas et al., 2013), we assume that improvements of these parameterizations are necessary to enhance the skill of COSMO-CLM to capture events which are mainly forced by the anomalous anti-cyclonic vortex over India. A slightly better agreement between model and observations for dry events compared to wet events is found. This might be caused by the fact that the upper tropospheric circulation anomaly found for dry events is also present in the middle troposphere, which is not the case for wet events. Thus, the circulation during dry events might be more influenced by upper-tropospheric features, which are in turn in better agreement with observations compared to lower tropospheric circulation anomalies in COSMO-CLM. Even though not all observed dry/wet events could be identified in COSMO-CLM at the same time with a similar magnitude it is found that the mechanisms between lower level circulation anomalies and rainfall over India on the intraseasonal timescale are well represented in COSMO-CLM.

3.3 Intraseasonal Variability of the Indian Summer Monsoon under Recent Climate Conditions

As shown in Section 3.1, most of the observed features of the Indian Summer Monsoon on intraseasonal time scales are captured by COSMO-CLM if driven by ERA-Interim reanalysis data. However, as observations are assimilated within the ERA-Interim product, the general circulation is expected to be close to reality in this dataset. Thus, the results shown in Section 3.1 indicate that COSMO-CLM is able to represent intraseasonal features of the ISM if driven by a model capturing these features on its own. This must not necessarily mean that ECHAM5 driven CLM simulations are able to depict the northward propagation of rainfall. Thus, in this section the ability of CLM in representing these features if driven by ECHAM5 at its lateral boundaries is analyzed. This is done for the CLM simulation carried out in this study as well as those described in Dobler and Ahrens (2011) as they differ with respect to model version and setup (see Chapter 2). Furthermore, the performance of ECHAM5 itself is analyzed. Thus, to assess the ability of these models in capturing northwards propagation under recent climate conditions the following simulations are used: for ECHAM5 the simulation *EH5-REC* (1800-2000), for the first model setup of CLM the simulation *CCLM-REC-wet* (1943-1973) and for the second setup of CLM the simulation *CLM-COM* (1960-2000) (see Table 2.2). To calculate BSISO⁴ and MISO⁵, all datasets have been bilinear interpolated to a regular 1° x 1° grid. For consistency only the years 1943 to 1973 are used from *EH5-REC* to match those years from *CCLM-REC-wet*.

3.3.1 BSISO

The general pattern of the boreal summer monsoon oscillation (BSISO) of *EH5-REC* and *CCLM-REC-wet* (driven by *EH5-REC*) and *CLM-COM* compares well to observations (Figure 3.12). This can be assessed by calculating lagged correlations of band-pass filtered precipitation with respect to a certain reference point (Figure 3.12). The northward propagation is more pronounced in *EH5-REC* compared to both CLM simulations with correlations exceeding 0.7, whereas CLM reaches values between 0.5 and 0.6, only. However, in all models correlations are too small south of about 8° north. In observations there is a well defined corridor of correlations above 0.5 (between -10 and zero days). Here, *EH5-REC* shows only correlations above 0.3, which tend to be even smaller for both CLM simulations. This might be associated with the location of the southern boundary in both CLM simulations, which are around 5° south for *CCLM-REC-wet* and around the equator for *CLM-COM*.

⁴Boreal Summer Intraseasonal Oscillations

⁵Monsoon Intra-seasonal Oscillations

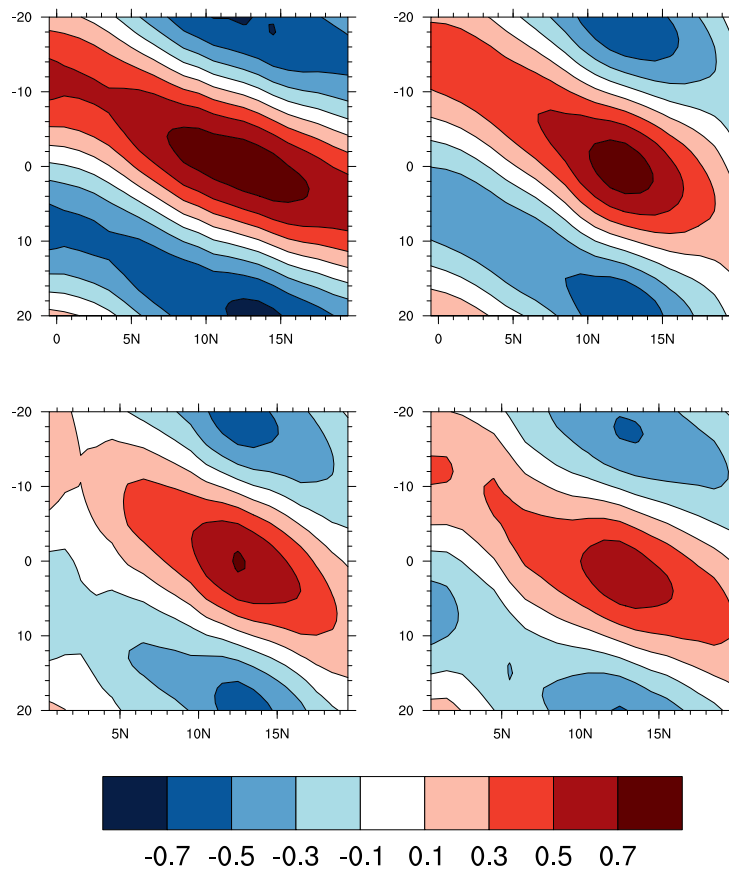


Figure 3.12: Cross-Correlation of zonally average precipitation (for longitudinal section between 70° - 100°) against a reference point near 85° east and 12.5° north for GPCP (topleft), *EH5-REC* (topright), *CCLM-REC-wet* (bottomleft) and *CLM-COM* (bottomright).

3.3.2 MISO

Monsoon intraseasonal Oscillations (MISO) are calculated according to Suhas et al. (2013), but using the smaller domain (see Section 3.1.4) due to the limited domain of the CLM simulations. The principal components of CLM and ECHAM5 are calculated by projecting the EEOF⁶ derived from GPCP data onto the GCM⁷/RCM⁸ precipitation fields.

Composites for all eight MISO phases show a distinct pattern of a northward moving rainbelt in observations (Figure 3.13). The first two phases are characterized by dry conditions over India and wetter conditions over the equatorial Indian Ocean. Phases 3 and 4 show wetter conditions over southern India, whereas phases 5 and 6 indicate wetter conditions over central India. The last two phases show wetter conditions over the Himalayan foothills and drier conditions over southern India and the tropical oceans. General patterns are similar

⁶Extended Empirical Orthogonal Function

⁷General Circulation Model

⁸Regional Climate Model

for *EH5-REC*, *CCLM-REC-wet* and *CLM-COM*. However, the northward propagating rainbelt occurs to be limited to 15° north in all simulations, which is in line with other studies (Abhik et al., 2014) showing a reduced northward propagation in ECHAM5. Spatial correlations reveal a good agreement between observations and *EH5-REC*, as well as observations and *CCLM-REC-wet* for most phases. Interestingly, correlations between *CCLM-REC-wet* and *EH5-REC* are above 0.7 for all phases except the first one (0.58). This suggests that the MISO in CLM is related to the representation of the MISO in the driving model. However, it should be noted that ECHAM5 data is interpolated to a 1° grid, due to the method applied. Thus, only the CLM experiments allows the interpretation of the smaller scale (spatial) precipitation, as the resolution is about 0.55°. A shortcoming of all simulation is the representation of the tilted rainband in phases 5-6, which is clearly found in observations but only to a minor extend in the models (Figure 3.13).

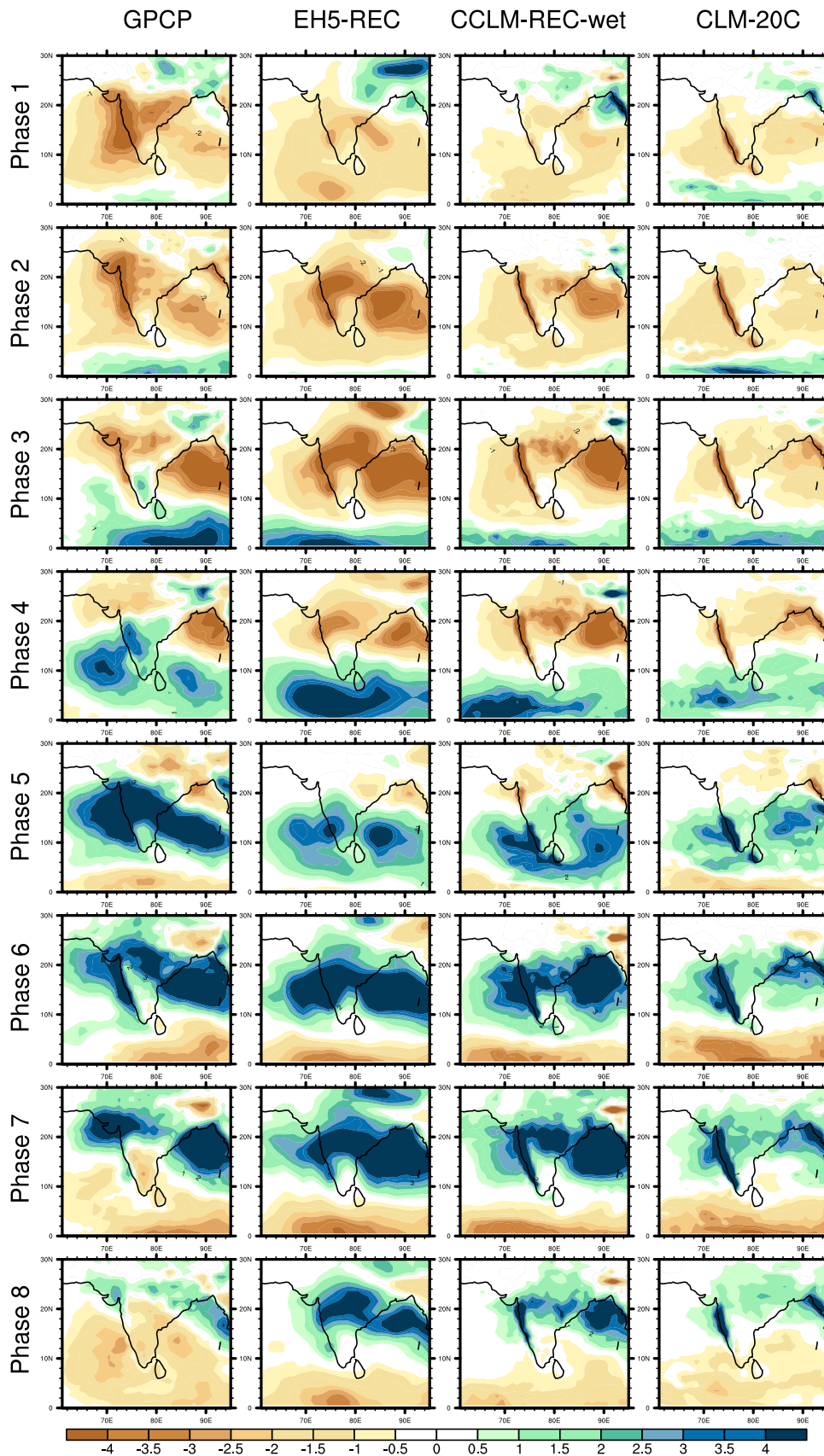


Figure 3.13: Composites anomalies [mm/d] for the eight MISO phases for left column: GPCP, 2nd left column: ECHAM5 REC, 3rd left column: CCLM-REC-wet and right: CLM-20C.

3.4 Conclusion

In this Chapter the ability of CLM and ECHAM5 simulations to reproduce observed ISV⁹ features of the ISM have been validated. It has been shown that, CLM driven by ERA-Interim at its lateral boundaries is able to simulate the mean spatial structure of rainfall over India during the summer season, as well as the boreal summer monsoon intraseasonal oscillations (BSISO) and northward propagation of rainfall (MISO). CLM has positive skill in simulating observed dry and wet events if driven by ERA-Interim and these extreme events are associated with similar atmospheric circulation patterns compared to ERA-Interim reanalysis data. Additionally, ECHAM5 and CLM simulations driven by ECHAM5 have been validated. As the setup for future climate simulations with CLM differ from those used for paleo-climate, two CLM simulations under recent climate conditions have been analyzed. Results indicate that all models (ECHAM5 and both CLM setups) are able to reproduce the northward propagation to some extent. Composite of the eight different MISO phases reveal similar pattern as found in observations. However, composite anomalies are mostly smaller compared to GPCP. It is found that composite anomaly patterns between the driving host (ECHAM5) and the RCM (CLM) are in better agreement than CLM and observations revealing the dependency of CLM results on the forcing model. The results for the representation of MISOs in ECHAM5 compares well to those from other studies (Sperber and Annamalai, 2008; Abhik et al., 2014). Sperber and Annamalai (2008) investigated the BSISO in several CMIP3 models. Their findings suggest that ECHAM5 has difficulties in simulating some aspects of the BSISO, e.g. the northwest mode over the Western Pacific, however it is able to simulate the northwards propagation of rainfall over India.

Based on the results described in this chapter as well as those derived in other studies (Sperber and Annamalai, 2008; Abhik et al., 2014) it can be concluded that the model chain used in this study is suitable to investigate changes of the ISV of the ISM under paleo and future climate conditions. This statement is mostly based on the ability of the models to capture the northward propagation over India, however, it should be kept in mind that other components of the BSISO, which are not well represented in the model, e.g. westward propagating mode may also affect limitations in northward propagation in ECHAM5 (Abhik et al., 2014).

⁹intraseasonal variability

Variability of the Indian Summer Monsoon during the Holocene

4

In this chapter, the tempo-spatial variability of the ISM¹ during the past 6000 years is investigated. Using coarse resolved AOGCM², AGCM³ and high resolved RCM⁴ datasets it focuses on the influence of changes in active and break phases on intraseasonal time scales onto multi-decadal to centennial scale variability of the ISM. The chapter is divided into three sections, firstly giving an introduction into the current state of research to long-term ISM variability (Section 4.1). The remaining two sections focus on the last Millennium using the full model chain (Section 4.2) as well as analysing the past 6000 years using AOGCM and AGCM experiments (Section 4.3). Thus, after successfully validating the models used in this study (Chapter 3), this chapter is dedicated to answer Task 2:

IN HOW FAR ARE EXTREME PHASES OF THE ISM RELATED TO A DOMINANT RAINFALL ANOMALY PATTERN DURING THE HOLOCENE? IS THIS ASSOCIATED WITH MORE ACTIVE/BREAK SPELLS ON THE INTRASEASONAL TIME SCALE?

¹Indian Summer Monsoon

²Atmosphere-Ocean General Circulation Model

³Atmosphere-only General Circulation Model

⁴Regional Climate Model

4.1 Introduction

Several proxy and model based studies address the variability of the ISM during the past. In general, the Indian Summer Monsoon is related to changes in orbital parameters as well as glacial boundary conditions. From the model perspective, the effect of changed orbital parameters and glacial conditions onto the global climate is investigated within PMIP⁵. Within this project climate model simulations under conditions during the LGM⁶ (21ka BP), the mid-Holocene (6.000 years BP) and during the past Millennium are carried out (see <https://pmip3.lscce.ipsl.fr/>, <https://pmip2.lscce.ipsl.fr/>, Joussaume and Taylor 2000; Braconnot et al. 2007; Haywood et al. 2011).

During the LGM glaciers covered most of northern America and also parts of northern Europe, which makes these simulations suitable to investigate the impact of increased global land-ice onto the earth's climate. A model-proxy intercomparison for the LGM over the Asian monsoon regions has been undertaken by Chabangborn et al. (2014). From 21ka BP onwards, the global ice volume decreased, leading to the formation of the Lake Agassiz in northern America. The drainage of Lake Agassiz happened around 8.2ka BP, associated with a huge amount of freshwater entering the North Atlantic. This event appears prominent in several proxy records (Gupta et al., 2003; Dixit et al., 2014b, Prasad and Enzel, 2006 and references therein). It is thought that the freshwater release into the North Atlantic Ocean caused a weakening of the AMOC⁷ leading to a cooling over the northern Atlantic due to decreased northward heat transport, which in turn caused a southward shift of the ITCZ⁸ (Cheng et al., 2009). These findings based on proxies have been generally confirmed by model-based studies (Kageyama et al., 2013; Marzin et al., 2013). Kageyama et al. (2013) show that a freshwater flux into the North Atlantic has a weakening effect on the Indian monsoon system in most climate model simulations. Furthermore, the influence of North Atlantic SST⁹s onto Indian monsoon rainfall has also been analysed by Goswami et al. (2006a), who showed a link via the AMO¹⁰. The impact of the freshwater influx into the North Atlantic is not limited to the Indian monsoon but also found in proxies over Eastern Asia (Liu et al., 2013).

The time period around 6ka BP (mid-Holocene) was characterised by increased summer solar insolation at the northern latitudes. This also affected the Indian monsoon, which was generally strengthened during this period (Overpeck et al., 1996; Joussaume et al., 1999;

⁵Paleoclimate Modelling Intercomparison Project

⁶Last Glacial Maximum

⁷Atlantic Meridional Overturning Circulation

⁸inter-tropical convergence zone

⁹Sea Surface Temperatures

¹⁰Atlantic Multi-decadal Oscillation

Braconnot et al., 2002; Fleitmann et al., 2003, 2007). Overall, global and regional climate models are able to capture increased rainfall over northern India during the mid-Holocene (Joussaume et al., 1999; Braconnot et al., 2002; Polanski et al., 2012), but there is some model spread concerning the magnitude of changes (Braconnot et al., 2002).

Information about climate variability derived from proxy data is thought to be more reliable for the past 1000 years. During this period, two major climate epochs can be distinguished: the Medieval Climate Anomaly (MCA) and the Little Ice Age (LIA). Proxy records reveal changes during the Little Ice Age, which are again thought to be linked to the North Atlantic Climate (Gupta et al., 2003). Proxies reveal stronger monsoonal winds during MCA¹¹ compared to LIA¹² (Gupta et al., 2005). This is in line with results obtained by Sinha et al. (2011b) who found more drought conditions during the 14th to 15th century in a proxy from central India. The strength of the ISM during the MCA and LIA has been further discussed by Rehfeld et al. (2013) based on results obtained from a paleoclimatic proxy network. They show that the linkage between India and China is stronger during MCA compared to LIA, which they relate to a stronger ISM season during MCA.

Findings about long-term variability of the Indian monsoon throughout the Holocene reveal, that changes in solar insolation play an important role due to their associated changes in the land-sea contrast. Thus, the decreasing trend in summer insolation over the northern latitudes within the past 11,000 years is associated with a decreasing strength of the Indian monsoon (see Gupta et al., 2003 - their Figure 2b; Zheng et al., 2014 - their Figure 3c). However, studies suggest that monsoon intensity lagged maximum solar insolation during the early Holocene, which might be associated to glacial boundary conditions (Overpeck et al., 1996; Fleitmann et al., 2007) suggesting the importance of remaining ice sheets onto the Indian summer monsoon. The relationship between solar insolation and monsoon strength is recorded to be more robust after 6000 years BP (Overpeck et al., 1996). The decreasing trend in monsoonal rainfall over India has been also shown by Dallmeyer et al. (2015) for four different climate models (see their Figure 7) confirming results from several model-based studies (Kutzbach and Otto-Bliesner, 1982; Braconnot et al., 2002).

Despite the long-term trend, results from proxy-based studies suggest short-term fluctuations (Gupta et al., 2003; Fleitmann et al., 2003; Cai et al., 2012; Prasad et al., 2014), which are most likely not to be explained by changes of orbital parameters. Here, small changes in solar activity are thought to have also influenced ISM variability throughout the Holocene (Thamban et al., 2007; Cai et al., 2012). A study from Gupta et al. (2005) reveals a link between sunspot numbers and the Indian summer monsoon variability.

¹¹Medieval Climate Anomaly

¹²Little Ice Age

Despite changes in solar insolation, anomalous surface conditions over the oceans influence ISM variability. The impact of the North Atlantic is well known from the 8.2ka BP event, which could be supported by several model studies as already discussed.

However, also the tropical ocean basins have vast impact on the ISM. This has been recently supported by Prasad et al. (2014), who show that drought conditions over India are linked to anomalously warm conditions over the IPWP¹³ region. The influence of the surface conditions over the Indo-Pacific onto Indian monsoon have been further analysed by several studies (Gopinathan and Sastry, 1990; Graham et al., 2011; Kim et al., 2012). Results obtained by Graham et al. (2011) reveal that climatic changes during the MCA are heavily influenced by changes in the Indo-Pacific SST gradient. Using observational datasets Gopinathan and Sastry (1990) reveal the relationship between the position of the Pacific Warm Pool Position (POWP) and Indian monsoon rainfall on monthly time-scales. Their results suggest that an easterly shift is associated with deficient rainfall over India and vice versa. Furthermore, the sensitivity of the Indian monsoon to changed SSTs over the Indian and Pacific ocean basins has been studied by Meehl and Arblaster (2002). They show that anomalously cold conditions over the eastern Pacific enhance precipitation over India by modulating the large-scale east-west circulation. For the Indian Ocean they find that rainfall anomalies are sensitive to the location of increased SSTs. Homogeneous anomalies north of 10° south tend to increase rainfall over southern Asia, whereas if SST anomalies are restricted to the equatorial Indian Ocean it causes decreased rainfall rates over India.

A difficulty of using proxies to assess climate variability over India exists due to the low number of proxy datasets available as well as due to the high spatial variability of rainfall over the Indian subcontinent. Ramesh (2001) compared existing proxy records for India and concluded that the integration of different proxy results into a single timeseries (comparable to the All-Indian rainfall timeseries) needs further knowledge about the temporal variability of rainfall over different regions of India during the past. Here, global climate model simulations are helpful to explain associated circulation changes between e.g. warmer and colder climates. Furthermore, due to the fact that climate models provide physically consistent fields, temporal and spatial variability of e.g. rainfall can be analysed to a higher degree compared to results obtained from proxies, as these include dating uncertainties as well as only giving point information.

Thus, in this chapter global climate model as well as regional climate model simulations are used to assess the spatio-temporal variability of the ISM. Focus is put on decadal to centennial-scale variability and their potential drivers. This includes the quantification in how far changes on the intraseasonal time-scale play a role in influencing longer-term variability as hypothesised by Sinha et al. (2011a,b). Besides, other factors, e.g. anomalous conditions over the Indo-Pacific Warm Pool region are analysed.

¹³Indo-Pacific Warm Pool

4.2 The Last Millennium

4.2.1 Data & Methods

GCM and RCM times-periods

As part of the HIMPAC project and this study, a five member COSMOS AOGCM ensemble for the past 1200 years in a resolution of T31L19 (Jungclaus et al., 2010) is analyzed regarding ISM variability. According to Section 1.2, these investigations are needed to select time periods with a length of 200 years, which are further simulated using ECHAM5 in a higher resolution of T63L31 to provide the boundary conditions for the COSMO-CLM simulations. In this project three AGCM simulations: Medieval Climate Anomaly (800 AD - 1000 AD; *EH5-MCA*), Little Ice Age (1515 AD - 1715 AD; *EH5-LIA*) and the last 200 years of the 20th century (1800 AD - 2000 AD; *EH5-REC*) in a resolution of T63L31 are carried out and analyzed regarding changes of the ISM in these different climate epochs (Polanski et al., 2014). Extensive work has been undertaken to carry out focusing on the best interpolation method of sea ice cover and sea surface temperature fields from the AOGCM simulations to obtain physically consistent AGCM simulations presented in Polanski et al. (2014). This includes the application of a specific software tool to ensure that monthly characteristics of SST and SIC¹⁴ fields are obtained in the T63L31 atmosphere-only ECHAM5 simulations. Finally, output from these ECHAM5 simulations is used to drive the regional climate model CLM¹⁵ at its lateral boundaries.

Here, for each GCM timeslice experiment (*EH5-MCA*, *EH5-LIA* and *EH5-REC*) two 30 year periods are chosen to be downscaled in a resolution of approx. 55 km. As this thesis aims to quantify the intraseasonal contribution to ISM variability on longer time-scales, the AIMR¹⁶ from the GCM simulations smoothed by a 31 year running mean is used to identify dry and wet periods. In general, for each GCM time-slice the driest and wettest 31 year period is chosen to be downscaled, however, for the recent climate GCM simulation (*EH5-REC*) the secondary minimum around 1910 is used instead of the global minimum around 1820. This is motivated to cover the abrupt change in monsoonal rainfall between 1900 and 1960 seen in the GCM simulation (Figure 4.1).

All model simulations used in this chapter as well as their identifiers are listed in Table 4.1.

¹⁴Sea Ice Concentrations

¹⁵COSMO-CLM

¹⁶All-Indian Monsoon Rainfall

Identifier	Modeltype	Time-period	Forcing Model
<i>EH5-MCA</i>	AGCM	900 - 1100 AD	<i>COSMOS-mil0014</i> (Jungclaus et al., 2010)
<i>EH5-LIA</i>	AGCM	1515 - 1715 AD	<i>COSMOS-mil0014</i> (Jungclaus et al., 2010)
<i>EH5-REC</i>	AGCM	1800 - 2000 AD	<i>COSMOS-mil0014</i> (Jungclaus et al., 2010)
<i>CCLM-MCA-wet</i>	RCM	956 - 987 AD	<i>EH5-MCA</i> (Polanski et al., 2014)
<i>CCLM-MCA-dry</i>	RCM	1041 - 1071 AD	<i>EH5-MCA</i> (Polanski et al., 2014)
<i>CCLM-LIA-wet</i>	RCM	1562 - 1592 AD	<i>EH5-LIA</i> (Polanski et al., 2014)
<i>CCLM-LIA-dry</i>	RCM	1597 - 1627 AD	<i>EH5-LIA</i> (Polanski et al., 2014)
<i>CCLM-REC-wet</i>	RCM	1943 - 1973 AD	<i>EH5-REC</i>
<i>CCLM-REC-dry</i>	RCM	1895 - 1925 AD	<i>EH5-REC</i>

Table 4.1: Overview to model simulations used in Chapter 4

Overview to Diagnostics

In this part of the study daily and seasonal rainfall amounts over the Indian subcontinent are used to investigate how active and break phases on intraseasonal time scales influence extreme phases of the ISM on longer time scales. As hypothesised by Sinha et al. (2011a) abrupt changes are associated with changes in active and break phases, which demands a methodology to detect those breakpoints in timeseries. Here, the method developed by Bai and Perron (2003) is used, which allows for the detection of multiple breakpoints in a specific timeseries. Furthermore, active and break spells are identified using a method similar to the one developed by Rajeevan et al. (2010), based on daily rainfall amounts. Rajeevan et al. (2010) use normalised precipitation over the CMZ¹⁷ (65°- 88°east; 18°- 28°north) for the months of July and August to identify active and break spells, which are characterised by at least 3 consecutive days below -1.0 or above +1.0, respectively. In this study, SPI¹⁸ values rather than normalised rainfall rates are used, which is motivated by results obtained in Chapter 3 showing a good agreement of spatio-temporal characteristics of observed and CLM SPI values if driven by ERA-Interim at its lateral boundaries. SPI values are calculated for each day in July and August and in accordance to Rajeevan et al. (2010) an active or break spell is characterised by three consecutive days with an SPI above +1.0 or below -1.0, respectively. For ECHAM5 simulations SPI values are derived for each time-period (200 years) by fitting a Gamma distribution to the rainfall data of each GCM simulation respectively. Due to the fact that the time-periods covered by the CLM simulations are disjoint, a reference period (*CCLM-REC-wet*) is chosen. Thus the parameters for the Gamma distribution are derived from *CCLM-REC-wet* only and the parameters are further used to derive SPI values for all CLM simulations.

¹⁷Core Monsoon Region

¹⁸Standardized Precipitation Index

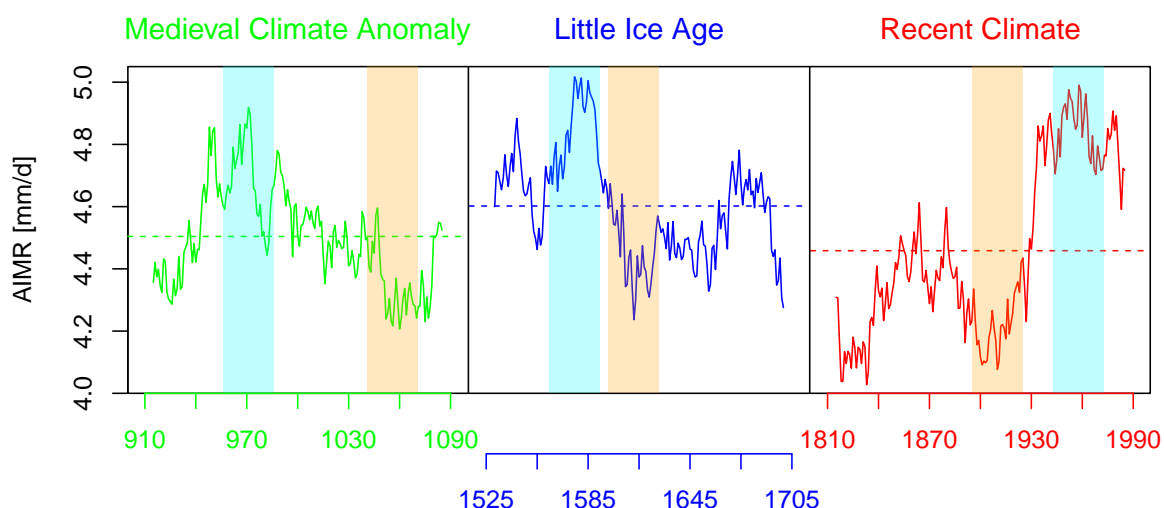


Figure 4.1: All Indian Monsoon Rainfall (AIMR) for all three ECHAM5 simulations during the last Millennium: MCA (900-1100, green), LIA (1515-1715, blue) and REC¹⁹ (1800-2000, red). Indicated in cyan and orange are the selected wet & dry time periods, respectively (each 31 years), which are downscaled using CLM.

4.2.2 Relationship between AIMR and Active/Break spells in COSMO-CLM

As shown in Chapter 3, COSMO-CLM is able to simulate observed dry and wet events on the intraseasonal time scale for the right reasons. Thus, it can be used to analyse changes of the ISM under different climate conditions, as here during the Millennium. First, climatological rainfall distributions and their differences between the CLM simulations are investigated. An anomalous rainfall dipole pattern with one centre over central India and a secondary one over northeastern India between two simulations is expected if changes on the intraseasonal time scale dominate general ISM changes. Next, active and break spells are assessed in the RCM data for each time period, which is performed similar to the method developed by Rajeevan et al. (2010). However, as the method by Rajeevan et al. (2010) has never been applied to rainfall timeseries for different climate periods, it is tested in how far this method is applicable for the datasets used in this study. Eventually, a new index based on seasonal rainfall rates is developed and it is tested in how far it is suitable to detect periods with an increased number of active (break) spells and decreased number in break (active) spells on intraseasonal timescales.

Climatological Rainfall

CLM experiments are used to analyse in how far wet and dry periods within MCA, LIA and REC differ significantly and in how far a prominent rainfall dipole pattern is present. In general, it is found that CLM simulations are in agreement with the selected GCM timeslices, meaning that a wet/dry period in ECHAM5 is also a wet/dry period in CLM.

Significant differences of mean summer (JJAS) rainfall are found for most CLM experiments at least over specific regions of India (Figure 4.2). However, regarding area-averaged rainfall means over India significant differences (using a Kolmorow-Smirnow test) are only found for four simulation pairs (Table 4.2.2): *CCLM-MCA-dry* and *CCLM-MCA-wet* (Figure 4.2a), *CCLM-MCA-dry* and *CCLM-LIA-wet* (Figure 4.2f), *CCLM-LIA-wet* and *CCLM-LIA-dry* (Figure 4.2j) and *CCLM-LIA-dry* and *CCLM-REC-wet* (Figure 4.2m).

simulation pair	AIMR diff. [mm/d]	Dipole Pattern	Active	Breaks
<i>CCLM-MCA-wet</i> vs. <i>CCLM-MCA-dry</i>	0.60	no	2.9	-0.19
<i>CCLM-MCA-wet</i> vs. <i>CCLM-LIA-wet</i>	-0.06	no	1.52	0.26
<i>CCLM-MCA-wet</i> vs. <i>CCLM-LIA-dry</i>	0.59	no	1.84	2.39
<i>CCLM-MCA-wet</i> vs. <i>CCLM-REC-wet</i>	0.07	no	2.03	0.32
<i>CCLM-MCA-wet</i> vs. <i>CCLM-REC-dry</i>	0.77	no	3.94	-6.55
<i>CCLM-MCA-dry</i> vs. <i>CCLM-LIA-wet</i>	-0.66	no	-1.39	0.45
<i>CCLM-MCA-dry</i> vs. <i>CCLM-LIA-dry</i>	-0.01	no	-1.06	2.58
<i>CCLM-MCA-dry</i> vs. <i>CCLM-REC-wet</i>	-0.53	no	-0.87	0.52
<i>CCLM-MCA-dry</i> vs. <i>CCLM-REC-dry</i>	0.17	yes	1.03	-6.35
<i>CCLM-LIA-wet</i> vs. <i>CCLM-LIA-dry</i>	0.65	no	0.32	2.13
<i>CCLM-LIA-wet</i> vs. <i>CCLM-REC-wet</i>	0.13	no	0.52	0.06
<i>CCLM-LIA-wet</i> vs. <i>CCLM-REC-dry</i>	0.83	yes	2.42	-6.81
<i>CCLM-LIA-dry</i> vs. <i>CCLM-REC-wet</i>	-0.52	no	0.19	-2.06
<i>CCLM-LIA-dry</i> vs. <i>CCLM-REC-dry</i>	0.18	yes	2.10	-8.94
<i>CCLM-REC-wet</i> vs. <i>CCLM-REC-dry</i>	0.70	yes	1.90	-6.87

Table 4.2: Differences in mean rainfall over India (AIMR), the presence of a rainfall anomaly dipole pattern, differences in active as well as break spells for all 15 possible simulation pairs from CLM simulations for MCA, LIA and REC. Significant differences using a Kolmorow-Smirnow test with an error probability of 0.1 are marked in bold.

For the first simulation pair (*CCLM-MCA-dry* and *CCLM-MCA-wet*, Figure 4.2a) differences are found mostly over the northern and partly western parts of India.

For the second simulation pair (*CCLM-MCA-dry* vs. *CCLM-LIA-wet*, Figure 4.2f) a generally homogeneous pattern is found, with lower rainfall rates in *CCLM-MCA-dry* compared to *CCLM-LIA-wet*. Significant differences are found over the Western Ghats and over north-western India (see Figure 4.2f).

The third simulation pair (*CCLM-LIA-wet* and *CCLM-LIA-dry*, Figure 4.2j) shows significant differences over the Western Ghats and northwestern India, similar to the differences found between *CCLM-MCA-dry* vs. *CCLM-LIA-wet* (Figure 4.2f) but with opposite sign.

Rainfall differences between *CCLM-LIA-dry* and *CCLM-REC-wet* (Figure 4.2m) reveal drier conditions over most of the country in *CCLM-LIA-dry*, however, these are only significant over parts of southern and northwestern India.

A prominent rainfall dipole pattern is found in none of the simulations with significant differences in AIMR. Regarding all simulation pairs, a dipole rainfall pattern is found for 27% (4 out of 15), namely *CCLM-MCA-dry* vs. *CCLM-REC-dry*, *CCLM-LIA-wet* vs. *CCLM-REC-dry*, *CCLM-LIA-dry* vs. *CCLM-REC-dry*, *CCLM-REC-dry* vs. *CCLM-REC-wet* (see Figures 4.2i,l,n,o). This indicates that changes on the intraseasonal timescale might play a role in determining ISM changes.

Despite using all possible combinations of simulations it is further analysed in how far mean wet and dry periods during the last Millennium differ. Therefore, the rainfall difference between the averages for all dry and all wet periods is calculated (Figure 4.2p). The difference pattern reveals a strong signal over the western core monsoon region and at the Western Ghats, but it is also positive over northeastern India. Thus, no rainfall dipole pattern is present. Based on the CLM simulations it can be concluded that rainfall differences between two time-periods are not structured into a clear pattern and most of the simulation pairs do not reveal a dipole rainfall anomaly pattern, contradicting the hypothesis from Sinha et al. (2011a). However, it must be noted that rainfall differences within the three time periods are comparably small. Furthermore, the hypothesis from Sinha et al. (2011a) is based on an abrupt change in rainfall, rather than differences between two disjunct time periods. Significant differences in AIMR between the wet and dry CLM simulation within one GCM²⁰ timeslice are found for *CCLM-MCA-dry* and *CCLM-MCA-wet* as well as for *CCLM-LIA-dry* and *CCLM-LIA-wet*, but the patterns do not reveal a prominent dipole rainfall pattern. Even though not significant rainfall anomalies between *CCLM-REC-dry* and *CCLM-REC-wet* within *EH5-REC* reveal a strong dipole pattern, which is in line with the hypothesis from Sinha et al. (2011a).

²⁰General Circulation Model

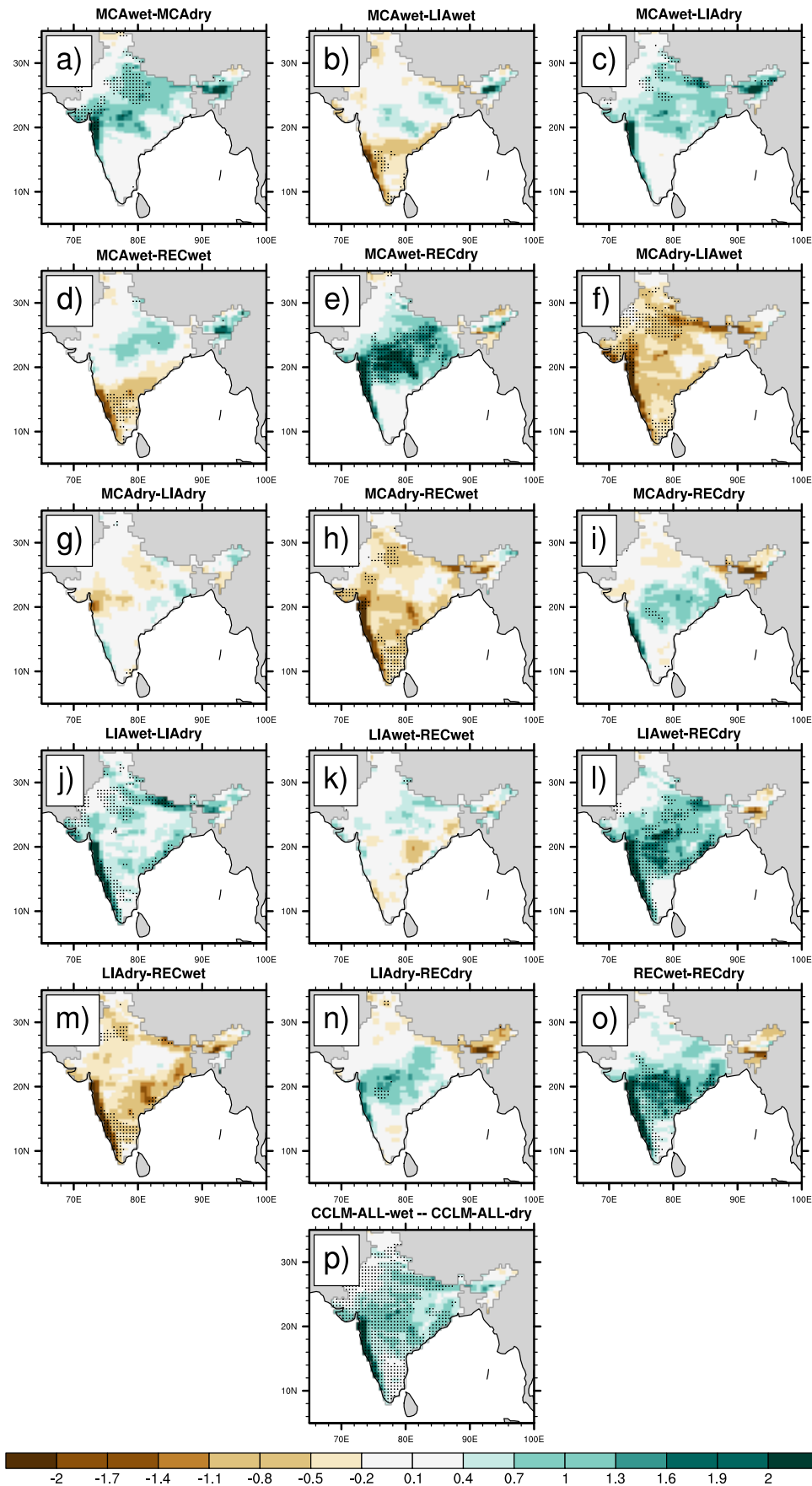


Figure 4.2: Mean rainfall difference [mm/d] between COSMO-CLM simulations for wet and dry periods selected from ECHAM5. Significant (p -value <0.05) rainfall anomalies are dotted.

Active and Break spells further to Rajeevan et al. (2010)

Next, it is analysed in how far active and break spells differ in all possible simulation pairs. Special focus is put on changes of active and break spells if significant changes in area-averaged AIMR are found and if a prominent rainfall dipole pattern between simulations is present. Active and break spells are identified similar to Rajeevan et al. (2010) but using SPI values instead of normalised rainfall rates (see Section 4.2.1). Significance of changes in active and break spells is tested using a one-sided Kolmogorov-Smirnov test. The decision whether to test if the number of active spells is greater or smaller in one experiment compared to another is based on the mean rainfall amount during the 31 year time period in CLM. Thus, if experiment "A" simulates higher rainfall rates compared to experiment "B" it is tested if breaks are more common as well as if active spells are less common in experiment "A" compared to experiment "B". Vice versa applies for an experiment with lower rainfall rates.

For breaks, significant differences (p-level: 10%) are found for three pairs, namely between *CCLM-REC-wet* vs. *CCLM-REC-dry*, *CCLM-REC-dry* vs. *CCLM-MCA-wet* and *CCLM-LIA-dry* vs. *CCLM-REC-dry* (Table 4.2.2). For all other simulation pair the distribution of breaks cannot be distinguished between each other. For active phases more significant differences are found: between *CCLM-MCA-wet* vs. *CCLM-MCA-dry*, *CCLM-MCA-wet* vs. *CCLM-REC-dry*, *CCLM-LIA-dry* vs. *CCLM-REC-dry* as well as between *CCLM-LIA-wet* and *CCLM-REC-dry* (Table 4.2.2). Thus, for three out of four simulation pairs showing a dipole rainfall anomaly pattern, significant differences in the occurrence of active and/or break spells are found. It should be noted that even though not significant differences are large between *CCLM-MCA-dry* and *CCLM-REC-dry*, especially for active spells.

The former analyses show that neither all simulation pairs with significant AIMR differences nor all simulation pairs showing a prominent dipole pattern are related to changes in active and break spells, with especially the latter contradicting the hypothesis by Sinha et al. (2011a). The reason for this behaviour could be two-sided: either seasonal rainfall anomalies are dominated by seasonal persistent patterns, which are not related to active and break spells or it is linked to the fact that different climate states (MCA, LIA and REC) are compared with each other.

The former explanation means that even a large number of break/active spells, which are associated with a dipole between northeastern and central India is not linked to the same rainfall anomaly pattern on seasonal timescales as its contribution is too small. This would be in line with earlier studies, e.g. Krishnamurthy and Shukla (2007).

The latter would mean that a general drier climate would lead to an increased/decreased number of break/active spells compared to a wetter climate. This would mean that not all of these identified active and break spells are associated with the characteristic circulation anomalies (as shown in Chapter 3) and thus not with a dipole rainfall pattern even on daily time scales.

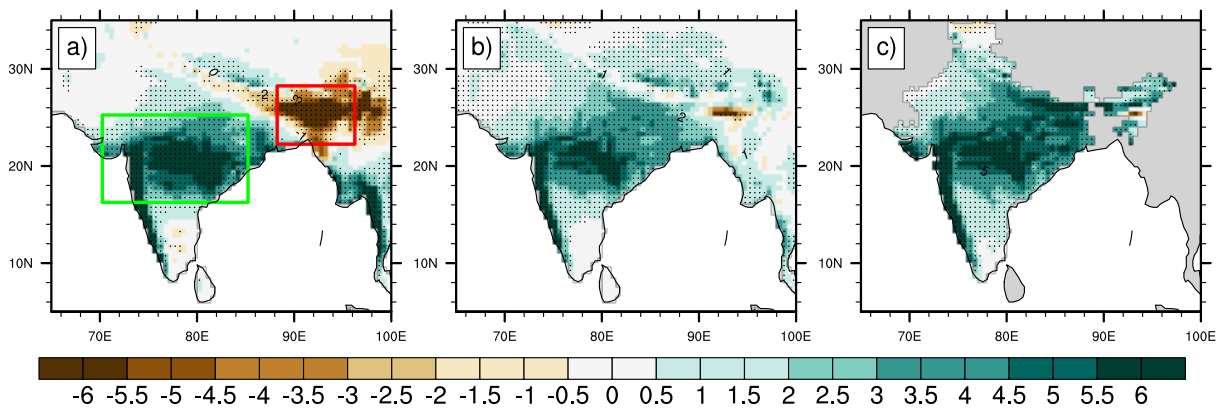


Figure 4.3: Composite anomaly for years with
 (a) high/low rainfall anomalies over central India and northeastern India. The green box indicates the region used as central India, and the red box the region used as northeastern India.
 (b) increased number of active/ decreased number of break days and vice versa.
 (c) high and low rainfall anomalies over the AIMR region, including all India.
 Areas for which rainfall between both composites differs significantly using a t-test with an error probability of 1% are dotted.

The impact of changes in active and break spells onto the seasonal average precipitation is tested by calculating the composite anomaly between all years with an increased/reduced number of break/active days and an increased/reduced number of active/break days. Here, all years above half a standard deviation are considered to obtain a larger sample size. It is found that years with an increased number of active days and decreased number of breaks are associated with higher rainfall amounts over central India compared to years with a decreased number of active days and increased number of breaks (Figure 4.3b). This is expected as active and break spells are identified using SPI values over the Core Monsoon Region (CMZ). There is no sign of a rainfall dipole pattern as the negative anomaly over northeastern India is rather small in its extent.

As explained it might also be the case that the method to identify active and break spells is not suited for this dataset, as different climate states are compared to each other. This is partly supported as more than 30% of all years with a large number of break days and decreased number of active days are from one CLM simulation (*CCLM-REC-dry*). It is worth mentioning that the active/break spell composite is similar to the composite between years (JJAS²¹ mean) with increased/decreased rainfall over all-India (Figure 4.3c).

²¹June-September

Active and Break spells related to Dipole-Pattern

Overall, the results suggest that the method applied is not suitable to detect break-active spell dipole rainfall pattern in these datasets. However, the existence of a rainfall dipole pattern is the backbone of the hypothesis from Sinha et al. (2011a), who found indications for this pattern in proxy data. A method is needed to identify this dipole pattern in seasonal mean rainfall. Therefore, for each simulation mean summer rainfall amounts over central India (70°-85° east; 19°-25° north) and north-east India (88°-96° east; 22°-28° north) are calculated and years with anomalous wet conditions over central India and dry conditions over northeastern India and vice versa are selected. To obtain a larger sample size years with above/below half a standard deviation are selected. In accordance to the calculation of active and break spells a common reference period for the calculation of mean and standard deviation is used (*CCLM-REC-wet*).

The composite difference of the respective years in each sample reveals the expected dipole rainfall pattern on seasonal time-scale (Figure 4.3a), which resembles closely the pattern related to active and break spells on intraseasonal time-scales (Figure 1.3). Additionally rainfall anomalies along the Himalayan foothills tend to share the same sign as northeastern India, similar to the pattern related to active and break spells on intraseasonal time-scales. Next, it needs to be verified in how far these selected years (associated with a rainfall dipole pattern) are characterised by changes in the occurrence of active and break spells. Density distributions between the number of active and break days i) in all 180 years, ii) years with wet conditions over central India (CI) and dry conditions over north-east India (NEI) and iii) years with dry conditions over central India and wet conditions over north-east India reveal remarkable differences (Figure 4.4).

The number of active days is significantly increased during years with anomalous wet conditions over central India and dry conditions over NEI²², whereas the number of break days is significantly decreased (using a bootstrap two-sided Kolmorow-Smirnow test with an error probability of 5%). In contrast, active spell days are significantly decreased whilst break days are increased during years with dry conditions over CI²³ and wetter conditions over NEI. This confirms that the anomalous rainfall dipole pattern in seasonal mean rainfall is associated with an increased/decreased number of active/break spells on the intraseasonal timescale in CLM. Thus, the representation of the pattern in seasonal mean rainfall can be used as a proxy for changes in active and break days on the intraseasonal time-scale. As 40% of all simulation pairs show a dipole pattern in rainfall over CI and NEI it might be concluded that changes on the intraseasonal time-scale steer ISM variability on longer time-scales to some extent. However, it is difficult to obtain a robust result using these CLM simulations only as differences between the simulations regarding rainfall are rather small and mostly not significant.

²²North-eastern India

²³Central India

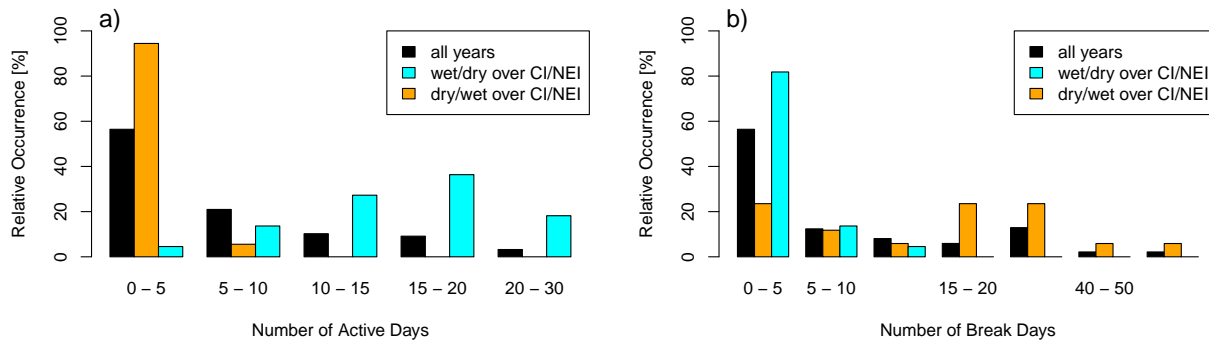


Figure 4.4: Relative occurrence of active days (a) and break days (b) for all years, years with anomalous wet conditions over CI and dry conditions over NEI as well as years with anomalous dry conditions over CI and wet conditions over NEI in COSMO-CLM.

4.2.3 Relationship between AIMR and Active/Break spells in ECHAM5

As discussed in the previous section some rainfall difference patterns (derived from CLM simulations) between dry and wet periods show a dipole rainfall anomaly pattern, which has in turn showed to be related to a higher occurrence of breaks or active days (depending on the sign of the pattern itself). To quantify in how far multi-decadal to centennial scale variability during the last Millennium is influenced by changes on the intraseasonal timescale all three GCM timeslice experiments are used (*EH5-MCA*, *EH5-LIA*, *EH5-REC*). In accordance to the analyses carried out for the CLM simulations, active and break spells are identified using the method based on daily rainfall over the CMZ (see Section 4.2.1) to test in how far changes in AIMR are related to changes in the intraseasonal variability. Next, seasonal rainfall rates over CI and NEI are analysed together with total rainfall over India (AIMR). Eventually, it is tested in how far the hypothesis by Sinha et al. (2011a) can be verified by analysing if breakpoints in rainfall over all-India identified using the method developed by Bai and Perron (2003) (see Section 4.2.1) are associated with rainfall changes over northeastern and central India.

Active and Break Spells further to Rajeevan et al. (2010)

Firstly, active and break spells are identified in all GCM simulations using daily SPI values over the CMZ during July and August (Figure 4.5). High correlations between the number of active spell days and AIMR is found for the *EH5-MCA* and *EH5-REC* period (correlation coefficients above 0.7). For these two experiments breaks are also negatively correlated with AIMR with correlation coefficient values of -0.3 for *EH5-MCA* and -0.75 for *EH5-REC*. Smaller correlations are found for the *EH5-LIA* experiment, for which active days correlate with only 0.14 and breaks with 0.11. Looking at the timeseries of AIMR and the number

of active spell days and break days (Figure 4.5), similarities for *EH5-MCA* and *EH5-REC* are clearly seen due to the relationship between breaks, active days and all-Indian monsoon rainfall. This is not the case for LIA. Especially the maximum in AIMR around 1570 is not associated with an increased number of active or a decreased number of break spell days. Analyses show that this can be explained as most of the change between maximum AIMR (around 1580 AD) and the following minimum AIMR (around 1610 AD) is associated with differences in rainfall in June and September. As the method to identify active and break spells is only based on July and August rainfall it does not capture the transition between maximum and minimum AIMR. It might be argued that the maximum of AIMR in *EH5-LIA* is mainly due to a prolonged monsoon season or mostly due to changes in active and break spells rather than during peak monsoon season (July & August). However, analysis of changes in the onset and offset of the monsoon is beyond the scope of this study, which focuses on the contribution of active and break spells. As active and break spells show high correlations for *EH5-MCA*, *EH5-REC* and the second half of *EH5-LIA* (excluding the maximum in AIMR) it is further argued that changes during the peak monsoon season are likely to be the main reason for rainfall variability over India in these AGCM simulations.

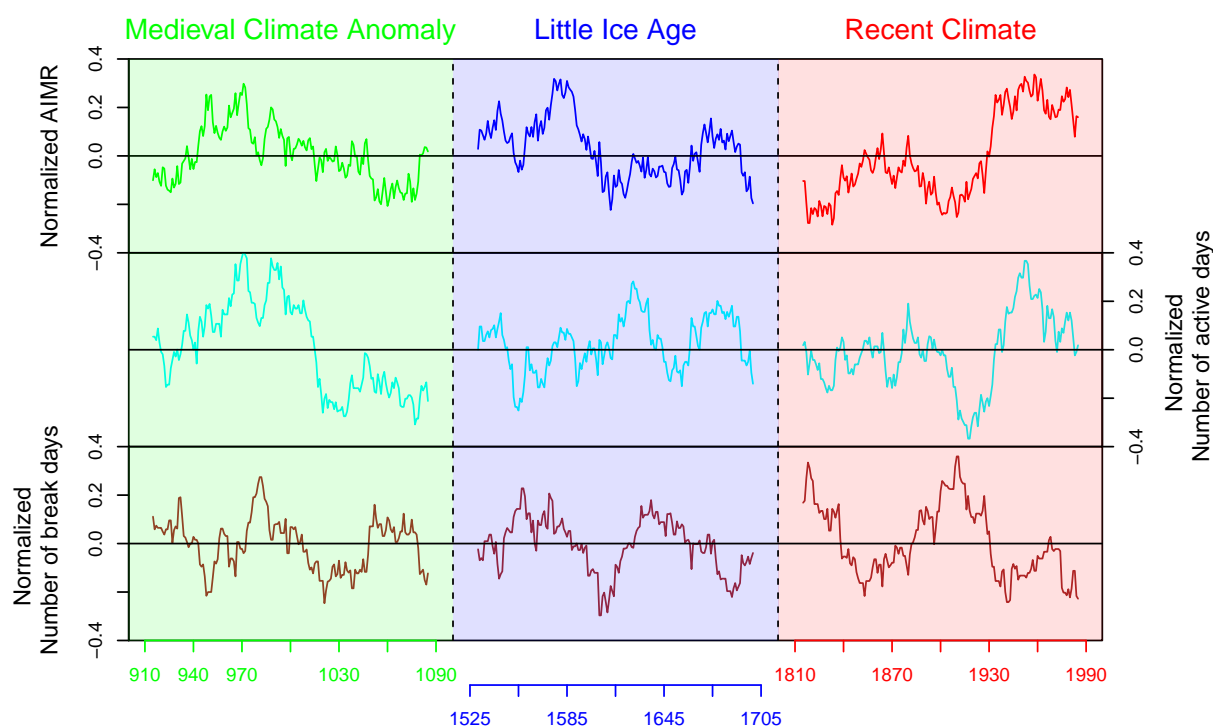


Figure 4.5: (top) 31 year running mean of normalised AIMR time series for MCA, LIA and REC.
 (middle) 31 year running mean of normalised number of active spell days
 (bottom) 31 year running mean of normalised number of break spell days

In general, these results support the hypothesis from Sinha et al. (2011a) that rainfall anomalies during the last Millennium are associated with more active or break spells on the intraseasonal time scale. However, it has been found that the definition of active and break spells according to Rajeevan et al. (2010) (but based on SPI values) does not lead to a well marked dipole rainfall pattern in seasonal mean rainfall in CLM simulations (Section 4.2.2). Similar results are obtained for the GCM simulations as rainfall composite anomalies of years, which are characterised by an increased number of breaks and decreased number of active days and vice versa do not show a prominent dipole rainfall pattern (Figure 4.6b). Thus, it is concluded that this method is not suitable to detect the rainfall anomaly dipole pattern on seasonal time-scales. The reasons for this are discussed in the former Section 4.2.2 and are thought to be the same for the ECHAM5 simulations: either seasonal persistent rainfall patterns are dominant compared to the occurrence of active and break spells or the application to rainfall data including different climate states is not suitable.

Active and Breaks Spells related to Dipole-Pattern

Motivated by the study of Sinha et al. (2011a) the dependency between all Indian monsoon rainfall and rainfall over central (CI) and northeastern India (NEI) is analysed for all three time periods. For CLM simulations it could already be verified that years with opposite rainfall rates over these two regions are associated with a dipole rainfall pattern on seasonal time-scales as well as with changes in the occurrence of active and break days. This might not be the case for ECHAM5 simulations. Thus, two questions have to be answered: 1) Are years with high rainfall anomalies but different signs over CI and NEI associated with a dipole like pattern restricted to the core monsoon region? and 2) Are these years marked by a high occurrence of active and break spells?

Anomalies in rainfall during years with high precipitation over CI and low rainfall over NEI and vice versa are shown in Figure 4.6a. Analogue to the analysis carried out for CLM, selected years are characterised by rainfall anomalies over both regions above half a standard deviation to obtain a larger sample size. The dipole structure is clearly found in the anomaly composite, with large rainfall deviations over the CI and NEI regions and little changes over southern India. The pattern is very similar to the one obtained from CLM simulations (Figure 4.3a) as well as the pattern related to active and break spells (Figure 1.3). However, in CLM the region over NEI and along the Himalayan foothills share the same sign, which is not found in ECHAM5. This might be related to the coarse resolution and the representation of orography in the GCM.

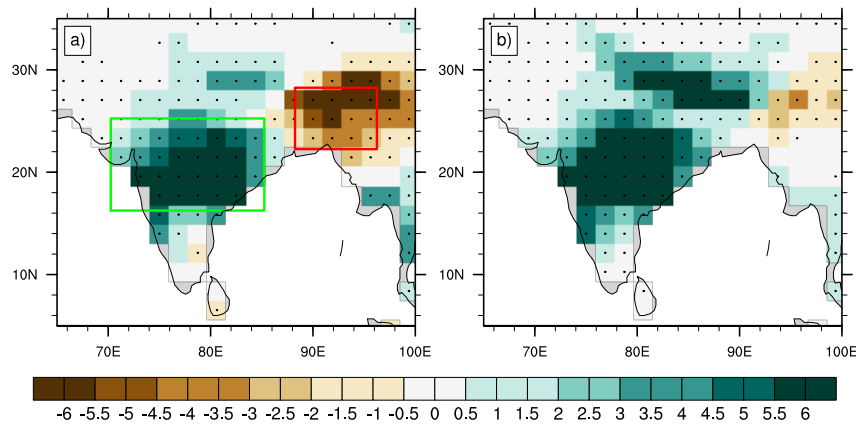


Figure 4.6: (a) Rainfall composite anomaly [mm/d] for years with high/low rainfall anomalies over central India and northeastern India. The green box indicates the region used as central India, and the red box the region used as northeastern India. (b) Rainfall composite anomaly [mm/d] for years with high/low number of active spell days and low/high number of break spell days. Areas for which rainfall between both composites differs significantly using a t-test with an error probability of 1% are dotted.

Next, active and break spell days are identified in all years included in the composite. It is found that active/break days are significantly ($p.\text{level} < 0.01$) increased/decreased during years with positive anomalies over CMZ and negative anomalies over NEI region, and vice versa (Figure 4.7). The results of these analyses indicate that the combination of both time-series can be used as a proxy for changes of active and break spells in GCM data, similar to the results obtained for CLM (Section 4.2.2).

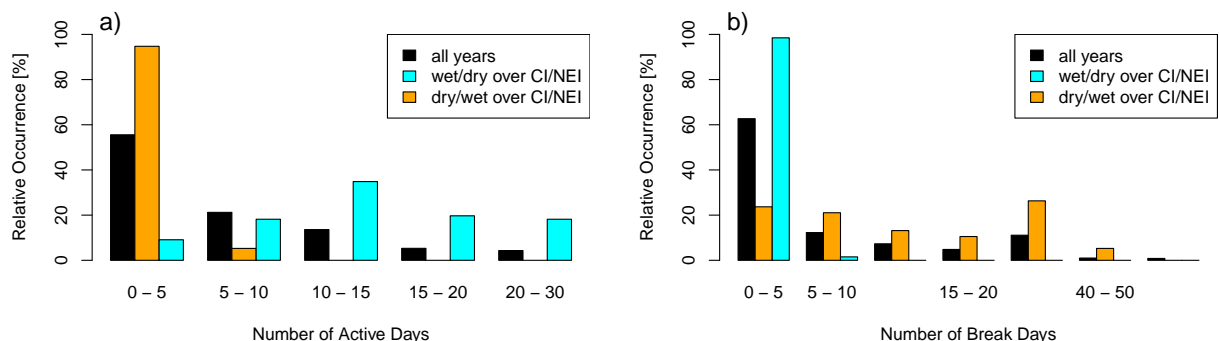


Figure 4.7: Relative occurrence of active days (a) and break days (b) for all years, years with anomalous wet conditions over CI and dry conditions over NEI as well as years with anomalous dry conditions over CI and wet conditions over NEI in ECHAM5.

After successfully testing in how far a dipole pattern is associated with changes in active and break spells over India, it is analysed in how far the hypothesis developed by Sinha et al. (2011a) can be supported using the AGCM simulations. This hypothesis claims that abrupt changes in ISM precipitation during the last Millennium are associated with changes in active and break spells. Therefore, rainfall over the AIMR as well as over the CI region and NEI region are smoothed using a 31 year running mean. Breakpoints are identified in the AIMR time series based on the method developed by Bai and Perron (2003). Figure 4.8 shows AIMR, CI and NEI timeseries for all three GCM timeslices.

For *EH5-MCA*, AIMR increases until around 950 followed by a decreasing trend until 1050. Obviously, rainfall variability over CI explains most of the total rainfall variability (correlation above 0.9) due to the fact that India receives most rainfall during JJAS over this region. AIMR is only poorly correlated with rainfall over NEI (correlation of -0.06 and rainfall over CI and NEI is moderately correlated with -0.32. Four breakpoints at the years 945 AD, 976 AD, 1014 AD and 1048 AD are identified using the method following Bai and Perron (2003). If the hypothesis by Sinha et al. (2011a) holds true one would expect changes in both: CI and NEI rainfall with opposite signs at the identified breakpoints. To test this, linear regression models are fitted to the AIMR, CI and NEI timeseries for each breakpoint. The first breakpoint (945 AD) is associated with an increase in AIMR and CMZ rainfall, which are both significant with an error probability of 5%. Additionally, rainfall over NEI decreases significantly, which supports the hypothesis. The second breakpoint is associated with a significant decrease in AIMR and CI rainfall. However, in this case, NEI rainfall shows a significant decreasing trend, which is not in line with hypothesis. For the third breakpoint, CI and NEI rainfall reveal opposite signs with only the slope for rainfall over the CMZ being significant. However, as can be seen in Figure 4.8 the whole time period from around 1000 AD until 1030 AD is marked by opposite trends in NEI and CMZ rainfall, which is line with the overall decreasing trend for this time period in All-Indian monsoon rainfall. The fourth breakpoint (1048 AD), reveals no relation to active and break spells as NEI and CMZ rainfall share the same sign.

For *EH5-LIA*, three breakpoints at 1571 AD, 1596 AD and 1661 AD are identified. AIMR rainfall at the first breakpoint is marked by a sharp significant increase. As hypothesised NEI and CI rainfall reveal different signs in trends, which are both significant (p -level=0.05). Additionally, the significant decrease in AIMR rainfall during the second breakpoint is marked by a decrease in CI and an increase in NEI rainfall, which are again both significant. Only the third breakpoint does not support the hypothesis, as AIMR, CI and NEI rainfall trends share the same sign. The second breakpoint marks the transition between *CCLM-LIA-wet* and *CCLM-LIA-dry*, for which no dipole rainfall pattern is found. Furthermore, changes in active and break spells (further to Rajeevan et al. 2010) do not reveal any significant

changes, which somehow contradicts different trends over central and northeastern India. However, a strong rainfall dipole pattern is found in June and September. As the method according to Rajeevan et al. (2010) only takes into account July and August rainfall rates over the core monsoon region, these anomalies are not captured by this method. If rainfall trends over NEI and CI are calculated using seasonal means derived from July and August rainfall rates only, changes in AIMR can not be related to a dipole-like rainfall structure. As discussed above, this is due to the fact that most of the overall rainfall anomaly (JJAS) origins from changes during September and June.

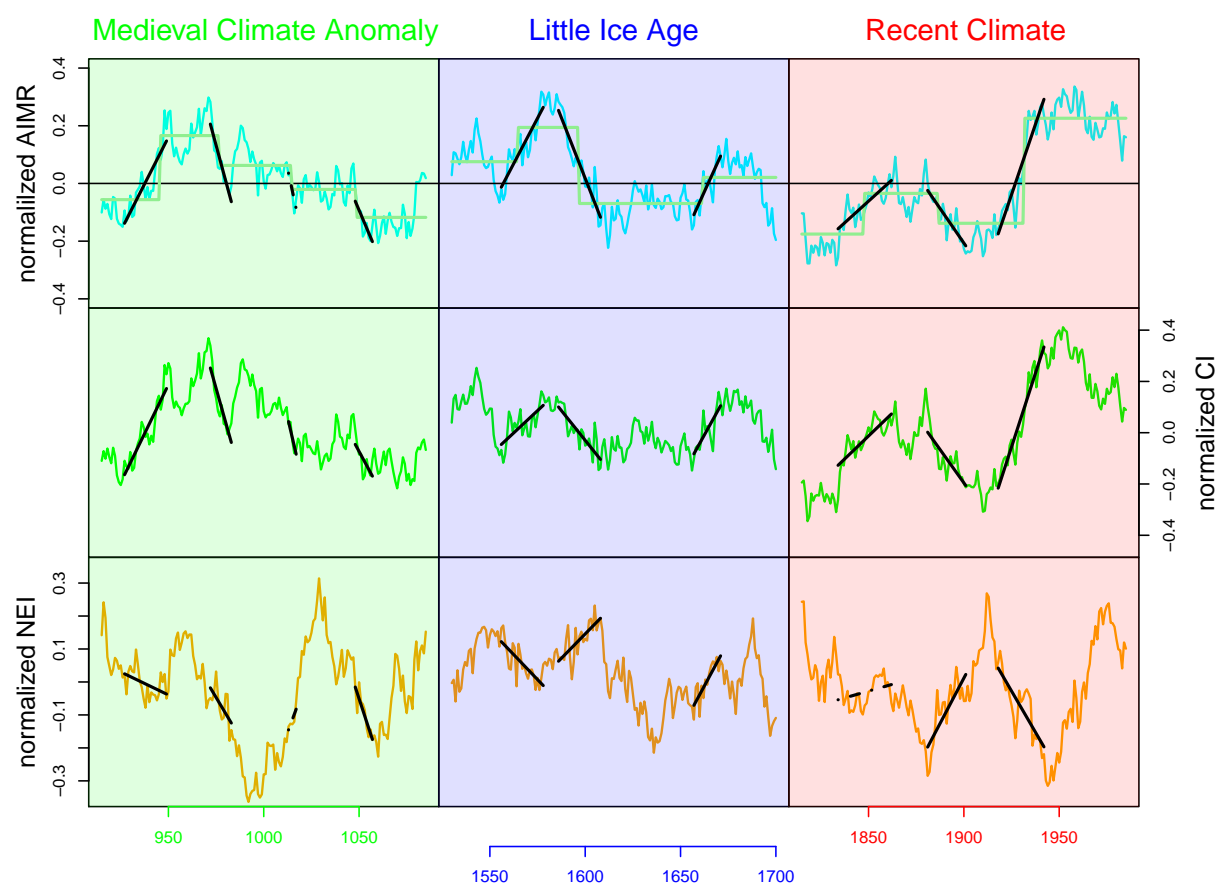


Figure 4.8: Standardised rainfall timeseries, smoothed by a 31 year running mean, for precipitation over all India (AIMR; top panel), over the core monsoon region (CI; middle panel) and over northeastern India (NEI; lower panel). Breakpoints (green lines in upper panel) are calculated following Bai and Perron (2003). A linear regression model is fitted to each breakpoint (black lines) for all rainfall time series. Significant slopes different to zero are marked as solid, not significant ($p.\text{level} > 0.01$) are marked as dashed-dotted lines. All timeseries are firstly normalised and then smoothed by a 31 year running mean.

For *EH5-REC*, three breakpoints in AIMR rainfall are found at 1847 AD, 1886 AD and 1931 AD. The first breakpoint is associated with increased rainfall over AIMR, CI and NEI region, indicating that the occurrence of active and break days is not responsible for the shift in overall precipitation. The decreasing trend in AIMR rainfall during the second breakpoint (1886 AD) is accompanied by opposite signs in trends of NEI and CI rainfall, supporting the hypothesis. This is also true for the third breakpoint, which is marked by a large increase in AIMR rainfall. Here CI and NEI rainfall reveal opposite signs and both linear regression models show slopes significantly different to zero. This is in line with the results obtained from RCM simulations, which show a strong dipole rainfall pattern between *CCLM-REC-dry* and *CCLM-REC-wet*. However, the two CLM simulations (*CCLM-REC-dry* and *CCLM-REC-wet*) alone do not allow to analyse the transition between these phases as the periods covered by each simulation are disjunct. Here, the transient GCM simulation have an additional value as results for *EH5-REC* reveal the overall transition to be marked by changes in the occurrence of active and break spells.

It has been shown that not all breakpoints in AIMR rainfall are associated with changes in active and break spells. To analyse in how far changes in the occurrence of active and break phases are related to the magnitude of the AIMR change itself, the difference in rainfall before and after each breakpoint for all 10 identified breakpoints is calculated. It is found that 50% of all breakpoints can be associated to changes in rainfall over CI and NEI region with opposite signs (Figure 4.9, filled points). Furthermore, the two breakpoints with the largest decrease in AIMR and three out of four breakpoints with the largest increase in AIMR are related to changes in active and break spells. These results strongly support the hypothesis from Sinha et al. (2011a) as especially large and abrupt changes in AIMR are related to a dipole rainfall pattern.

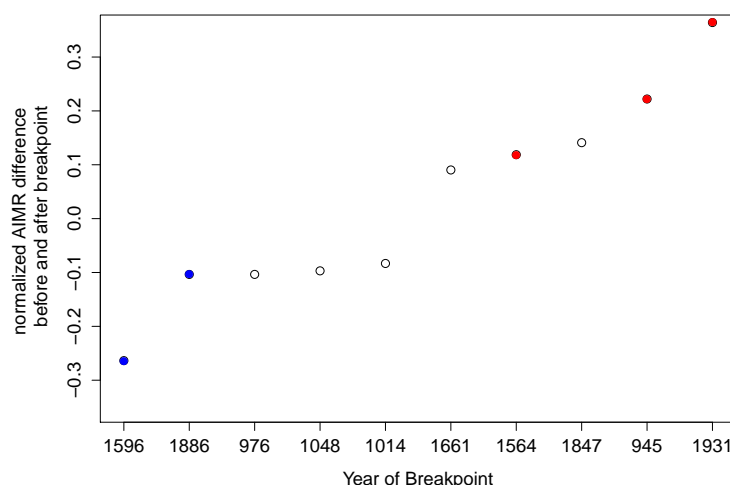


Figure 4.9: Difference in smoothed & standardised AIMR rainfall before and after each respective breakpoint for all 10 breakpoints found in ECHAM5 simulations for MCA, LIA and REC. Breakpoints, which could be linked to changes in active and break spells as hypothesised by Sinha et al. (2011a) are indicated as filled points.

Synthesis By analysing CLM simulations during the last Millennium for dry and wet epochs (each 31 years) it is found that not all selected wet and dry time periods reveal significant changes in active and/or break days or a prominent dipole rainfall anomaly pattern. However, if the dipole rainfall anomaly pattern over central and northeastern India is present on seasonal time-scales it is associated with a higher occurrence of active and break days on the intraseasonal time-scale, respectively.

Using rainfall data from the three 200 year timeslice experiments for MCA, LIA and REC (*EH5-MCA*, *EH5-LIA*, *EH5-REC*) it is shown that the number of active and break days shows significant correlation with all-Indian monsoon rainfall. However, composite analysis of years with increased active and decreased break days (and vice versa) show that rainfall anomalies are spread over most of India and (similar to results carried out for CLM) a prominent dipole pattern could not be found using this method as rainfall anomalies over northeastern India tend to be small. Rainfall timeseries over northeastern and central India have been used to select years with anomalous wet/dry conditions over CI/NEI and vice versa. In accordance to results for CLM simulations, it is shown that this pattern on seasonal time-scales is associated with changes in the occurrence of active and break spells and can be thus used as a proxy for intraseasonal variability. The analysis of the respective three rainfall timeseries over central and northeastern India reveal that some variability of rainfall over India is associated with changes of active and break spells. Especially, large abrupt changes in AIMR associated with a dipole rainfall pattern could be associated to changes in rainfall over northeastern and central India with different signs.

4.3 The Past 6000 years

It has been shown in Section 4.2 that the rainfall variability over Indian during the last Millennium in ECHAM5 global climate model simulations is partly related to the occurrence of active and break phases. Especially the breakpoints with the largest changes in rainfall are associated with different trends in precipitation over central India and northeastern India. In how far the hypothesis that abrupt changes of the ISM are caused by changes on the intraseasonal time scale also applies for the time period from 6000 years BP until present is focus of this section.

This part of the study is structured as following: first rainfall over India from the COSMOS (AOGCM) simulation over the past 6000 years together with those time series over central India and northeastern India are discussed. This analysis answers the question in how far changes in active and break spells dominant changes in rainfall variability over India during the Holocene. Next, a dry and wet epoch identified by using rainfall over the all Indian region is selected and simulated in a higher resolution of T63L31 using ECHAM5. This is primarily done to analyze possible driving mechanisms leading to drier and wetter conditions over India despite changes on the intraseasonal time scale. Furthermore, possible mechanisms steering ISM variability are analyzed using atmosphere-only sensitivity experiments. Eventually, a synthesis of the results obtained in this section is given.

4.3.1 Data & Methodology

Here, a transient fully-coupled COSMOS simulation covering the past 6000 years in a resolution of T31L19 is used (Fischer and Jungclaus, 2011). Precipitation data is available on a monthly basis for this dataset and is further aggregated to seasonal rainfall means for the summer monsoon period (June to September). It cannot be validated in how far years with increased rainfall over CI and decreased rainfall over NEI are associated with a higher occurrence of active spells and lower occurrence of breaks (and vice versa) in this model simulation, as daily rainfall data would be necessary for this analysis. It is assumed that the relationship found for higher resolved ECHAM5 simulations remains true also for coarse resolved (T31L19) simulations. Rainfall time series are calculated for CI and NEI, which are the same regions as used for the analysis carried out in Section 4.2 (CI: 70°- 85°east; 19°- 25°north and NEI: 88°- 96°east; 22°- 28°north).

ECHAM5 AGCM model simulations in T63L31 are carried out for a dry and wet period (each 50 years) identified in the coupled global model simulations. The atmosphere-only simulations in T63L31 are driven by SST and SIC conditions taken from the 6000 year model simulation. CO_2 , CH_4 and N_2O concentrations are set to constant pre-industrial values according to Fischer and Jungclaus (2011).

Additionally, GCM sensitivity simulations using different sea-surface temperatures from different ocean basins are carried out to separate effects of North Atlantic, Pacific and Indian Ocean SST's onto the Indian summer monsoon rainfall. Each of these sensitivity experiments span 30 years. All model simulations used in this section are listed in Table 4.3.

As discussed, the long-term variability of the ISM is related to changes in insolation due to varying orbital parameters. Here, orbital parameters are calculated according to Berger (1978); Berger and Loutre (1991). Based on the values for eccentricity, obliquity and longitude of perihelion solar insolation can be calculated for each day of a specific year and each latitude. There are two different possibilities to compute daily insolation. The first approach is called equinoctial type and the second the calendar day insolation (Berger, 1978). The first calculates daily insolation for fixed positions relatively to the vernal equinox, whereas the second approach calculates the insolation for a specific date of the year. In this study daily insolation for calendar dates are calculated. The differences between both techniques can be quite large in terms of absolute insolation values (see Section 3 in Berger 1978). However, a high linear relationship between the daily insolation timeseries of both approaches with a correlation coefficient of above 0.999 is found for the past 6000 years at 25° north. Thus, both approaches can be used to relate rainfall over India to changes in solar insolation.

Identifier	Model-type	Time-period	Forcing Model
<i>COSMOS-Holocene</i>	AOGCM	6000 BP - 0 BP	Fischer and Jungclaus (2011)
<i>EH5-2ka</i>	AGCM	2008 BP - 1958 BP	<i>COSMOS-Holocene</i>
<i>EH5-1.7ka</i>	AGCM	1662 BP - 1612 BP	<i>COSMOS-Holocene</i>
<i>EH5-1.7ka-NA</i>	AGCM	sensitivity exp. (30 years)	<i>COSMOS-Holocene</i>
<i>EH5-1.7ka-PO</i>	AGCM	sensitivity exp. (30 years)	<i>COSMOS-Holocene</i>
<i>EH5-1.7ka-IO</i>	AGCM	sensitivity exp. (30 years)	<i>COSMOS-Holocene</i>

Table 4.3: Overview to model simulations used in Chapter 4, Section 4.3

4.3.2 Rainfall over AIMR during the past 6000 years in COSMOS

As this section focuses on centennial scale variability, area-averaged seasonal mean rainfall over India (JJAS) is smoothed using a 201 year running mean (Figure 4.10, upper plot). The rainfall in *COSMOS-Holocene* is marked by a general decreasing trend from 6000 years BP until present, however, with some remarkable extremes on shorter (multi-decadal to centennial) time-scales. The general decreasing trend in rainfall can be explained by reduced solar irradiance (shown as blue line in Figure 4.10), which is calculated according to Berger and Loutre (1991). Increased solar irradiance at northern latitudes during summer increases the thermal heat contrast between the Asian landmasses and the Indian Ocean, which in turn leads to a strengthening of the monsoonal southerlies and hence an inten-

sification of the monsoon. By regressing the solar irradiance on the seasonal rainfall over India, the residuals are calculated, which are shown in Figure 4.10 (lower plot). Three wet phases and three dry phases are detected, for which a value above or below 2 standard deviations is found. The wet phases are identified around 4.7ka BP, 3.9ka BP and 1.7ka BP and the dry phases around 3.7ka BP, 2ka BP and 900 BP. Interestingly, a shift from one state to the other within a short period of time is found twice: 1) between 3.9ka BP and 3.7ka BP and 2) between 2ka BP and 1.7ka BP, whereas the latter is more pronounced.

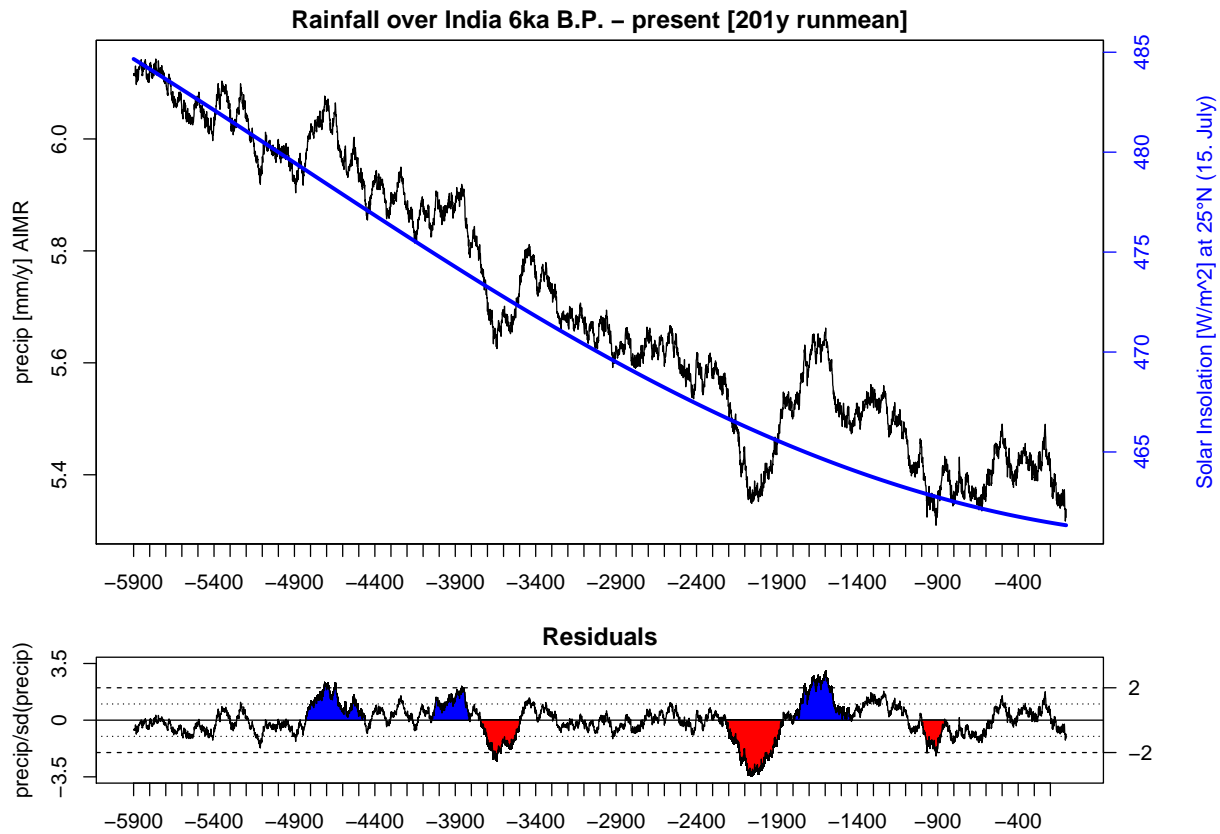


Figure 4.10: top: Precipitation over the All-Indian subcontinent (AIMR) smoothed by a 201 year running mean (black line) and solar insolation at 25°North during 15th of July calculated following Berger and Loutre (1991) (blue line). bottom: Normalised residuals of standardised precipitation minus regressed solar insolation onto precipitation over AIMR region. Phases, for which standardised precipitation exceeds $+2/-2$ are indicated in blue/red.

To investigate in how far these anomalous phases of the ISM (with respect to area-averaged AIMR) in *COSMOS-Holocene* are present over all of India or only parts of it, a linear regression based on solar irradiance and precipitation at each grid point over India is carried out (Figure 4.11). For most of the grid points the linear relationship is positive, meaning that decreased solar irradiance is associated with decreasing rainfall over these regions. However, four grid boxes show a negative relationship, meaning that rainfall increases with decreasing solar irradiance.

From Figure 4.11 it can be concluded that an abrupt change between 2ka BP and 1.7 ka BP is found for southern India, as well as northwestern India and parts of Central India. The dry phase around 2ka BP affects most of the grid points, except the two grid points over central India. In contrast the dry event around 3.7ka BP affects the core monsoon region to a higher extent and is not associated with extreme dry conditions over southern India. Generally, dry and wet events over northeastern India are not in phase with those found for all India. Overall, this result indicates that dry and wet phases of the ISM on centennial time-scales in COSMOS show different spatial distribution and might thus also be caused by different mechanisms.

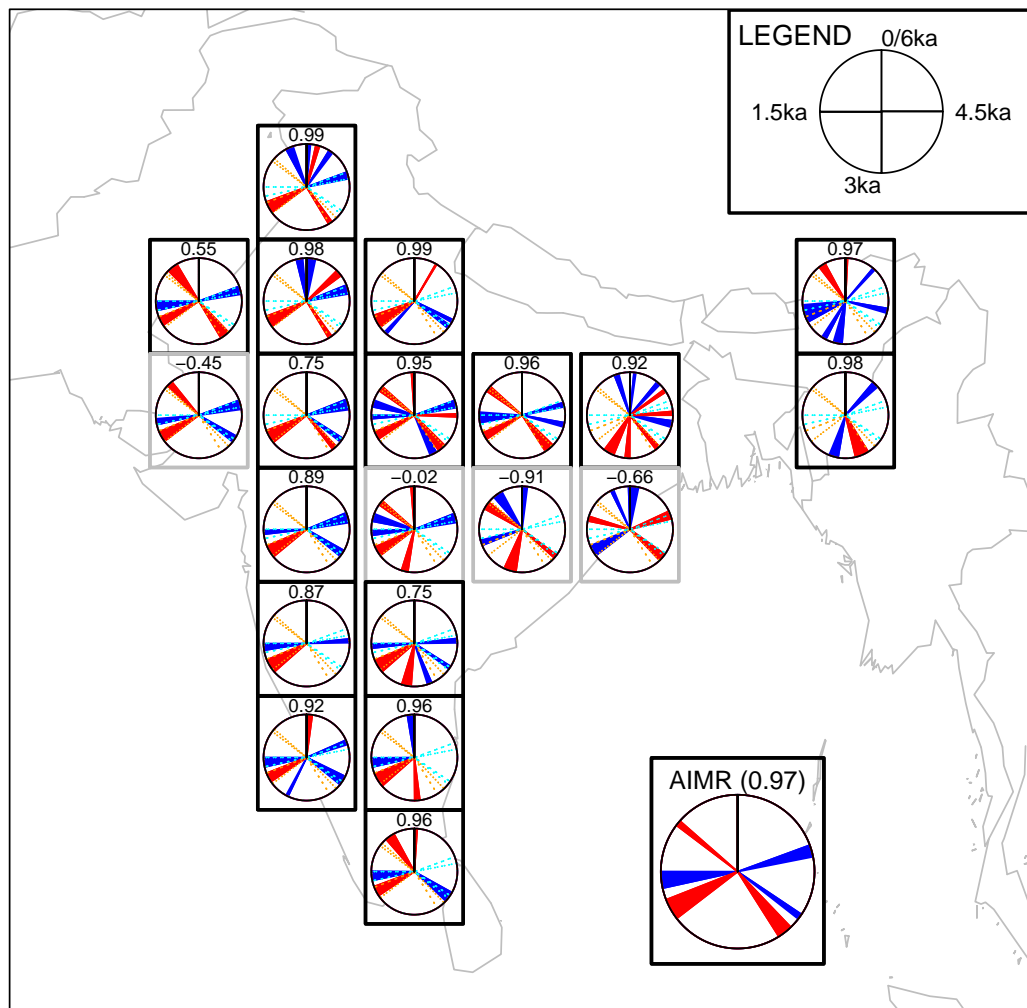


Figure 4.11: Pie diagrams indicating phases for which standardised rainfall exceeds +2 (indicated in blue) or -2 (indicated in red). Precipitation at each grid point has been detrended by regressing the insolation at 25° North calculated according to Berger and Loutre (1991). Black rectangles indicate grid points with positive correlations between original precipitation time series and insolation at 25° North, whereas grey rectangles indicate negative correlations between both time series. Numbers within the rectangles give the correlation coefficient. Dashed pie-segments in the pie-diagrams of each grid points indicate wet and dry phases calculated using All-Indian monsoon rainfall (left-bottom pie-diagram).

4.3.3 Variability of Active and Break spells

To answer the main hypothesis of this work, seasonal rainfall amounts during summer monsoon season are calculated over NEI, CI as well as over the whole country (Figure 4.12). As it is not expected that the long-term (decreasing) rainfall trend is caused by changes on the intraseasonal time scale, all smoothed timeseries are linearly detrended and standardised. A linear detrending method is used instead of using insolation (as done in the previous section) as to use the same method for all three time series to make the results better comparable. From the AIMR timeseries (Figure 4.12; top) it can be concluded that most of the extremes found by detrending the time series using the linear regression between AIMR and insolation (see Section 4.3.2) are also present by simple linear detrending. However, the wet phase around 3.9ka BP²⁴ is not exceptional dry using the latter method. Additionally, the last centuries are in general wetter using a linear detrending method. Still, the main extremes, especially the one around 2ka BP is very pronounced using the linear detrending method. Thus, using a linear detrending method does not influence the results obtained in this section.

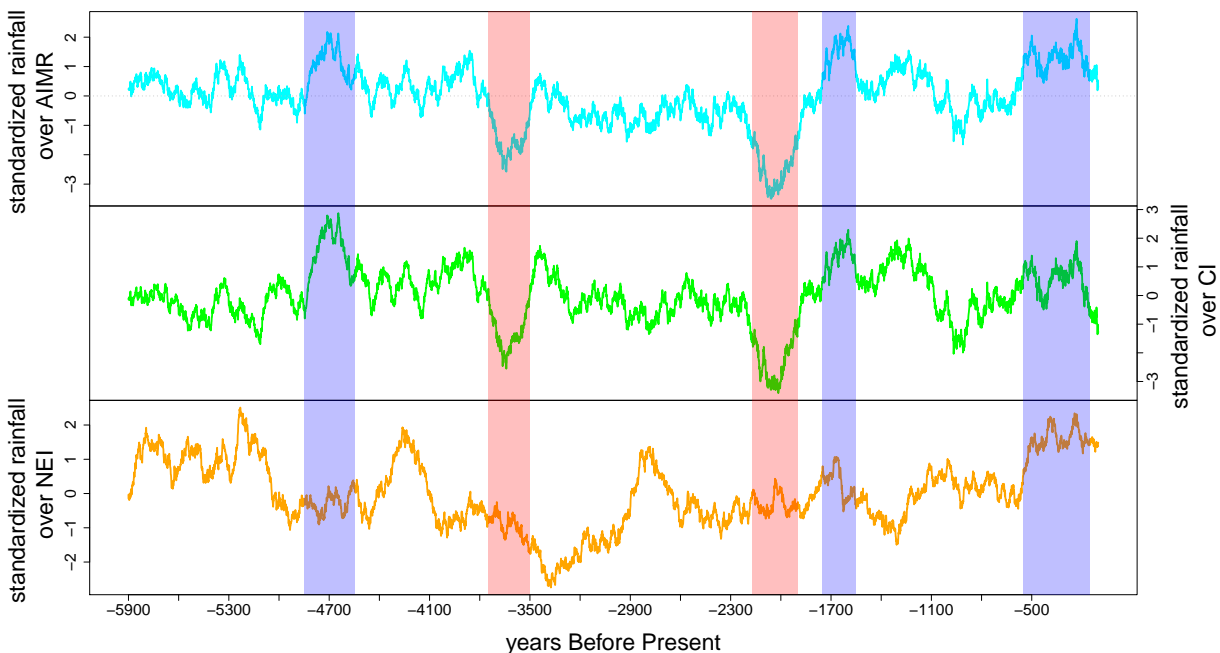


Figure 4.12: Standardised, linearly detrended rainfall time series over AIMR (top), CI (middle) and NEI (bottom). All time series are firstly smoothed by a 201 year running mean, detrended and eventually normalized by its own standard deviation. Extreme dry and wet periods are indicated by red and blue bars.

²⁴Before Present

Similar to the results obtained for the last Millennium, a high correlation between rainfall over all-India and central India is found ($r = 0.88$), whereas correlations between AIMR and NEI is much smaller ($r = 0.35$) (Figure 4.12). By analysing the time series around abrupt changes of the ISM it is found that there is no marked increase in rainfall over NEI when AIMR decreases (see dry AIMR events around 3.7ka BP and 2ka BP). Also increases in AIMR are not marked by decreasing trends in rainfall over NEI (see wet AIMR events around 4.7ka BP, 1.7ka BP and after 500 years BP). Thus from these analysis it can be concluded that abrupt changes of rainfall over all-India are not associated with changes in rainfall over NEI and CI with opposite signs in the coarse resolved AOGCM COSMOS²⁵ simulations, which contradicts the hypothesis from Sinha et al. (2011a).

4.3.4 Changes of dry and wet events on the intraseasonal time-scale between 2ka BP and 1.7 ka BP

It has been shown that trends in rainfall over the AIMR region are not related to opposite trend in rainfall over CI and NEI regions, which contradicts with main hypothesis that abrupt changes are related to the occurrence of dry and wet events as hypothesised by Sinha et al. (2011a). Due to the availability of data it could not be proven that a rainfall dipole-pattern is related to active and dry events in the coarse resolved AOGCM. It might be well argued that this resolution is not sufficient to simulate intraseasonal features of the ISM in general. This is supported by results from Abhik et al. (2014) showing that northward propagation in ECHAM5 is less well represented using 19 vertical levels compared to using 31 vertical levels.

To test in how far the results might be affected by the coarse resolution of the AOGCM, two ECHAM5 simulations in a resolution of T63L31 for the abrupt change in ISM precipitation between 2ka BP and 1.7 BP are carried out (*EH5-2ka* & *EH5-1.7ka*). Due to limited computational resources only two transient 50 year simulations during the peak of the dry and wet period have been carried out, which are subsequently called *EH5-2ka* (dry period) and *EH5-1.7ka* (wet period) (see Table 2.2). If the occurrence of active and break spells would be the dominating factor in steering both the dry and wet period, one would expect a dipole pattern to occur in seasonally averaged rainfall differences between both periods. Figure 4.13 shows differences in seasonally averaged rainfall amounts between *EH5-2ka* and *EH5-1.7ka* from T63L31 AGCM simulation (Figure 4.13b) as well as for both periods derived from the coarse resolved AOGCM simulation (Figure 4.13a). As expected, wetter conditions during 1.7ka BP compared to 2ka BP are found and the pattern in T63L31 AGCM simulations is similar to the one from the T31L19 AOGCM simulation. This shows that general rainfall characteristics from the coarse resolved COSMOS simulation, used to drive the higher resolved AGCM simulations are reproduced. In general, largest differences in rainfall

²⁵Community Earth System Models

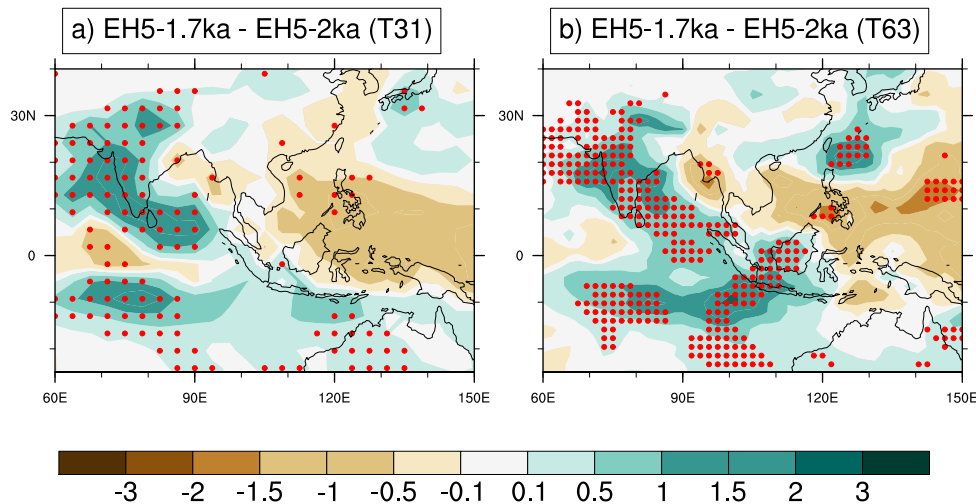


Figure 4.13: Rainfall difference [mm/d] between a) *EH5-1.7ka* and *EH5-2ka* event derived from T31 AOGCM simulation (*COSMOS-Holocene*) and b) difference between *EH5-1.7ka* and *EH5-2ka* derived from T63L31 AGCM simulations (*EH5-2ka* & *EH5-1.7ka*). Regions with significant differences (plevel=0.1) are dotted in red (using a two-tailed t-test).

between *EH5-2ka* and *EH5-1.7ka* are found over northwestern, western, southern India and along the Himalayan foothills. This is in line with rainfall patterns in the coarse resolved model simulation and the results shown previously (see Figure 4.11). However, a prominent dipole rainfall structure is neither found in the coarse resolved simulation nor in the higher resolved AGCM simulations. This suggests that changes in the occurrence of wet and dry events on the intraseasonal time-scale do not cause the increase in AIMR between 2ka BP and 1.7ka BP independent of the resolution of the climate model simulation. These results raise two new research questions:

I. WHAT IS THE MECHANISM STEERING THE ABRUPT CHANGE IN AIMR RAINFALL AROUND 2KA BP?

II. CAN SUCH A MECHANISM ALSO EXPLAIN OTHER DRY AND WET PHASES FOUND IN THE AOGCM SIMULATION COVERING THE PAST 6000 YEARS?

, which are addressed in the remaining part of the section. To answer the first research question ECHAM5 simulations with a horizontal resolution of T63L31 are analysed with respect to changes in local and large-scale circulation features. In addition to the two simulations already discussed (*EH5-2ka* & *EH5-1.7ka*), several sensitivity experiments are carried out to reveal potential drivers of ISM variability. Next, it is tested in how far the mechanism derived from the former analyses are generally driving ISM variability on centennial time-scales. This is done using the coarse resolved AOGCM simulation (*COSMOS-Holocene*).

4.3.5 Mechanisms steering ISM rainfall variability between 2ka BP and 1.7ka BP

Only orbital parameters are changed during integration time of the AOGCM simulation while other factors, e.g., greenhouse gas concentrations are kept constant (see Fischer and Jungclaus 2011). Due to varying orbital parameters, solar insolation during boreal summer decreases between 2ka BP and 1.7ka BP, which is expected to lead to a decreased monsoon intensity. This contradicts to what is found in AIMR rainfall, which increases during that time period (Figure 4.12). Additionally, changes in insolation between 2ka BP and 1.7ka BP are comparably small, leading to the conclusion that varying orbital parameters are not the dominant factor steering ISM variability during both extreme phases.

Changes in sea surface temperature conditions are more likely to cause the abrupt change in rainfall over India around 2ka BP. Differences in SSTs between 1.7ka BP and 2ka BP are found over most ocean basins (Figure 4.14 left). The most striking features are: 1) a tripole-like SST pattern in the North Atlantic, 2) cold central Pacific Ocean and eastern part of Indo-Pacific Warm Pool (IPWP) and 3) warm northern Arabian Sea as well as eastern Indian Ocean.

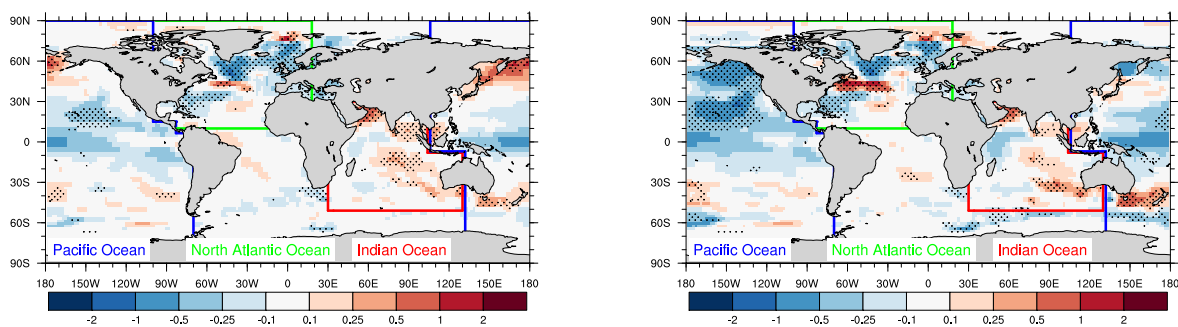


Figure 4.14: Sea surface temperature difference (June to September) between
left: $EH5-1.7ka$ (50 years) and $EH5-2ka$ (50 years) [K].
right: $EH5-1.7ka$ (30 years) and $EH5-2ka$ (30 years) [K]
Regions with significant changes ($p_{level}=0.05$) are dotted. Coloured lines display the boundaries of the regions used for sensitivity studies.

Known SST patterns over the NA²⁶ steering the ISM are e.g., the AMO, but also tripole-like SST patterns are found to be related to monsoonal rainfall (Goswami et al., 2006a; Feng and Hu, 2008; Krishnamurthy and Krishnamurthy, 2016). Over the Indian Ocean, the IOD²⁷ is known to be a factor influencing ISM variability (Ashok et al., 2001) and over the

²⁶North Atlantic

²⁷Indian Ocean Dipole

Pacific Ocean ENSO²⁸ is the dominant mechanism steering monsoon rainfall (Webster et al., 1998 and references therein). Besides, ENSO the PDO²⁹ as well as the IPWP are known to influence ISM variability (Gopinathan and Sastry, 1990; Krishnan and Sugi, 2003; Krishnamurthy and Krishnamurthy, 2014). However, it is impossible to disentangle the effects from the different ocean basins by solely using the two AGCM simulations during 1.7ka BP and 2ka BP (*EH5-2ka* & *EH5-1.7ka*). Thus, to determine the drivers of ISM variability in these AOGCM and AGCM simulations, further sensitivity experiments are necessary.

Setup of Sensitivity Experiments

To separate the effects from the North Atlantic (NA), Pacific Ocean (PO³⁰) and Indian Ocean (IO³¹) three sensitivity studies are carried out. Due to computational resources each simulation spans only 30 years. However, mean SST differences during the first 30 years in *EH5-2ka* and *EH5-1.7ka* are very similar to those for all 50 years (compare Figure 4.14 left and right).

To disentangle the effect of SSTs over the NA during 1.7ka BP (wet phase) on the ISM, SSTs over all ocean grid points are set to values corresponding to *EH5-2ka* (dry phase), except those over the North Atlantic Ocean (see green box in Figure 4.14) which are set to values corresponding to *EH5-1.7ka* (wet phase). Similarly, to extract the effect of the PO, SST's are set to values from *EH5-2ka* (dry phase) for all ocean grid points except those over the Pacific Ocean (see blue box in Figure 4.14), which are set to values of *EH5-1.7ka* (wet phase). Likewise, the effect of the IO is disentangled by setting SST values over all ocean basins to *EH5-2ka* (dry phase) values except over the Indian Ocean (see red box in Figure 4.14), where SSTs correspond to *EH5-1.7ka* (wet phase) values. These sensitivity experiments will subsequently be called *EH5-1.7ka-NA* (for changed North Atlantic), *EH5-1.7ka-IO* (for changed Indian Ocean) and *EH5-1.7ka-PO* (for changes Pacific Ocean) (see Table 4.3).

It should be noted that all experiments carried out are transient with varying lower boundary conditions instead of timeslice experiments with no interannual variability in SST and SIC conditions. This is motivated by the fact that the intention for the first two AGCM simulations for 1.7ka BP and 2ka BP (*EH5-1.7ka* and *EH5-2ka*, see Table 4.3) has been to use the same boundary conditions as for the coarse resolved AOGCM simulation to make the comparable to each other. Furthermore, the setup is chosen to fit the general approach undertaken within HIMPAC (see Section 1.2), which has also been used for AGCM simulations for the last Millennium (see Section 4.2). However, due to the interannual variability of SSTs large horizontal gradients might be partly imposed at the boundaries of the chosen regions (see Figure 4.14) in the sensitivity experiments. Possible effects are discussed at the end of the section.

²⁸El Niño Southern Oscillation

²⁹Pacific Decadal Oscillation

³⁰Pacific Ocean

³¹Indian Ocean

Results from Sensitivity Experiments

As *EH5-1.7ka* and *EH5-2ka* span 50 simulation-years each, but each sensitivity experiment does only cover the first 30 years of *EH5-1.7ka* or *EH5-2ka* (depending on the ocean basin), only the first 30 years from *EH5-1.7ka* and *EH5-2ka* are used for the comparison with the sensitivity experiments. However, rainfall differences are similar for the first 30 years and the complete 50 year period (Figure 4.15). This is somehow expected as the main SST difference characteristics between *EH5-2ka* and *EH5-1.7ka* found in the 50 year average are also present in the 30 year average (see Figure 4.14).

The aim of the sensitivity experiments is to unravel the influence of changed SSTs over all three ocean basins on the ISM. This is done by analysing changes in seasonal rainfall amounts, moisture fluxes and upper and lower tropospheric velocity potential.

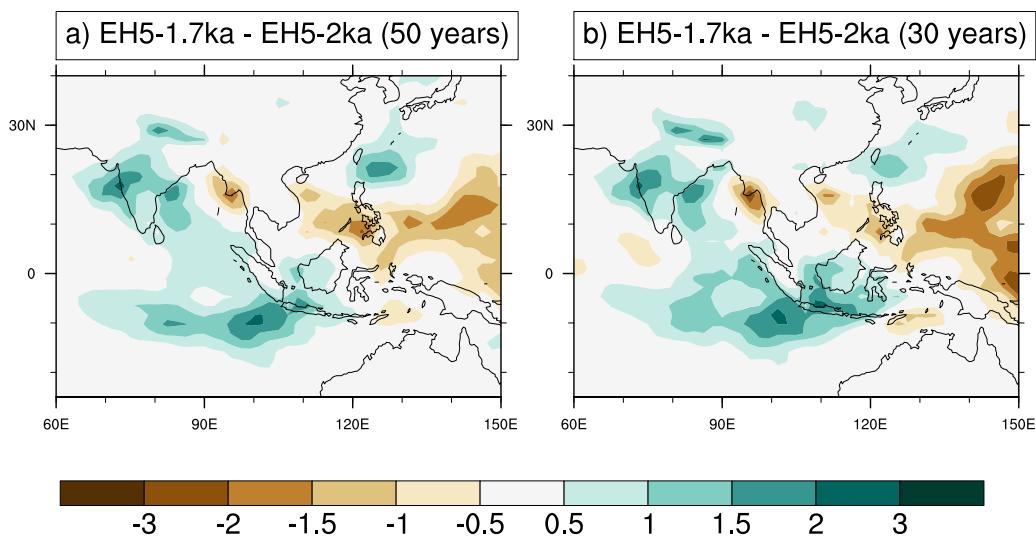


Figure 4.15: Rainfall difference [mm/d] between a) *EH5-1.7ka* and *EH5-2ka* (50 years), b) *EH5-1.7ka* and *EH5-2ka* (30 years)

Rainfall

As discussed, the rainfall difference between *EH5-1.7ka* and *EH5-2ka* reveals wetter conditions over most of India, along the Himalayan foothills and over the east-equatorial Indian Ocean, whereas drier conditions are found over the western Pacific (Figure 4.16a). The sensitivity experiments test to what extent these differences are caused by SST conditions over a specific ocean basin. This is illustrated by calculating the differences between each sensitivity experiment and *EH5-2ka*. If large differences are present it can be concluded that these differences are caused by the specific ocean basin for which SSTs are set to *EH5-1.7ka* values (wet phase) for the respective sensitivity experiment.

EH5-1.7ka-IO reveals higher precipitation amounts compared to *EH5-2ka* along the Himalayan foothills and over southern India, however, rainfall rates are similar over central India (Figure 4.16b). This is different for *EH5-1.7ka-PO*, which shows wetter conditions over central India and along the coast of the Bay of Bengal compared to *EH5-2ka* (Figure 4.16c). Interestingly, the wetter conditions between *EH5-1.7ka* and *EH5-2ka* over the equatorial eastern Indian Ocean, are not found in *EH5-1.7ka-IO* but in *EH5-1.7ka-PO*, which indicates that local SST's over the equatorial eastern Indian Ocean are not the dominant factor for steering rainfall changes over this region. *EH5-1.7ka-NA* reveals slightly drier conditions over India, especially over central India and along the eastern Himalayan foothills (Figure 4.16d). These results indicate that both the Pacific Ocean and Indian Ocean most likely steer the abrupt change in ISM rainfall between 2ka BP and 1.7ka BP.

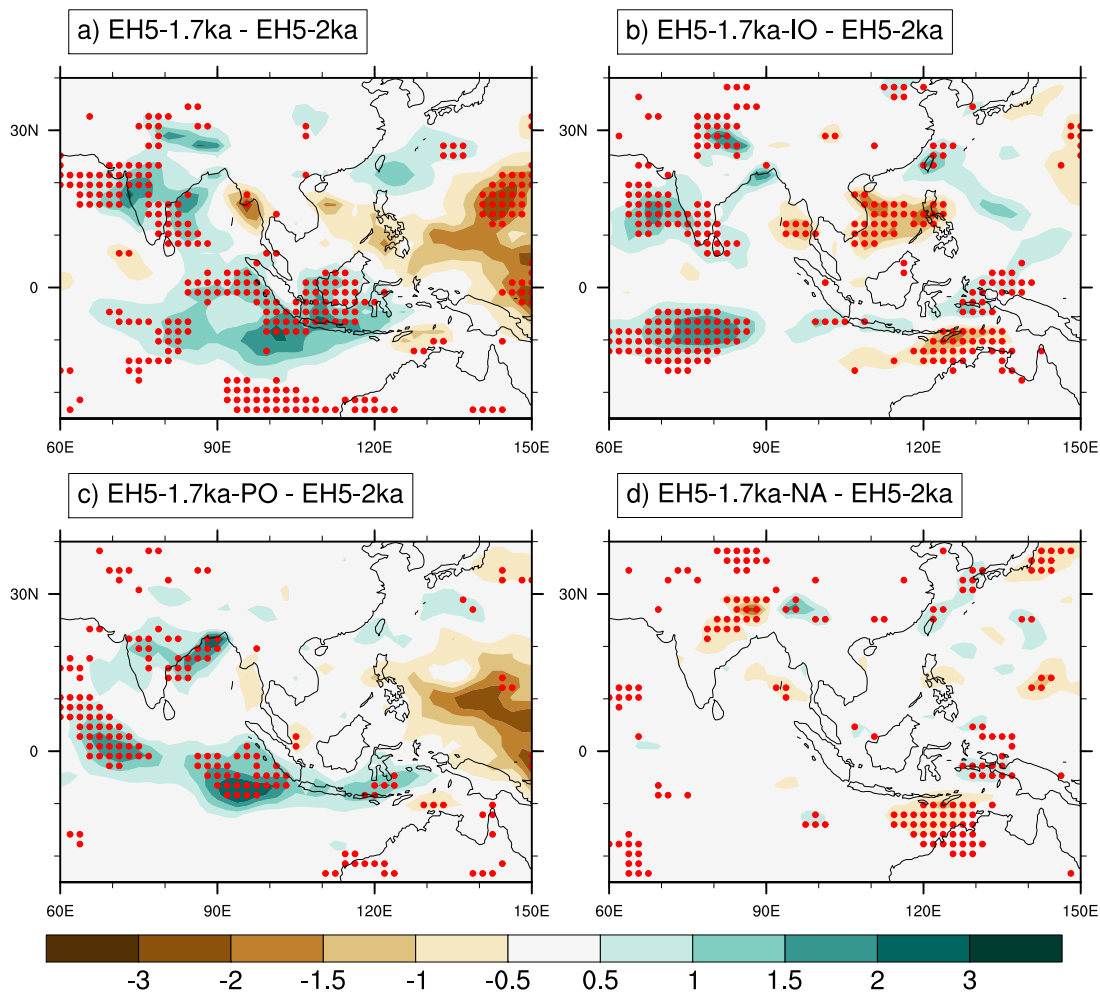


Figure 4.16: Rainfall difference [mm/d] between a) *EH5-1.7ka* and *EH5-2ka* event (30 years), b) *EH5-1.7ka-IO* and *EH5-2ka*, c) *EH5-1.7ka-PO* and *EH5-2ka* and d) *EH5-1.7ka-NA* and *EH5-2ka*. Regions with significant differences (plevel=0.1) are dotted in red (using a two-tailed t-test for a) and a paired t-test for b),c),d)).

Moisture Flux

As the formation of precipitation is linked to the availability of sufficient moisture in the lower atmosphere, moisture fluxes in 850 hPa are analysed for all available model simulations (Figure 4.17). On average, the typical monsoon moisture flux pattern is found in 850 hPa for *EH5-1.7ka* during the summer monsoon season (Figure 4.17a), where moisture is transported into northern India during summer from the Arabian Sea as well as from the northern part of the Bay of Bengal.

For *EH5-1.7ka* an anomalous easterly moisture flux is found stretching from the western Pacific into India compared to *EH5-2ka*. The additional moisture advected from the Bay of Bengal into central and northern India is likely to enhance precipitation over these regions, which is in line with overall precipitation changes (see Figure 4.16a). Additionally, an anomalous moisture flux from the northern Arabian Sea into northwestern India is found in *EH5-1.7ka* compared to *EH5-2ka* (Figure 4.17b).

The moisture flux difference pattern for *EH5-1.7ka-IO* shows a easterly moisture flux over the Bay of Bengal, which is not as large as found between *EH5-1.7ka* and *EH5-2ka* (compare Figure 4.17b and Figure 4.17c). However, *EH5-1.7ka-IO* reveals an anomalous moisture flux from the northern Arabian Sea into northwestern India (Figure 4.17c), similar to the one found between *EH5-1.7ka* and *EH5-2ka* (Figure 4.17b). This suggests that these circulation changes are driven by SST changes over the IO. Similarities are also found for moisture transport over the Bay of Bengal, however the circulation anomaly between *EH5-1.7ka-IO* and *EH5-2ka* differs to the one from *EH5-1.7ka* and *EH5-2ka* (Figure 4.17b) over central India.

EH5-1.7ka-PO simulates a larger anomalous moisture transport from the western Pacific into the Bay of Bengal (Figure 4.17d), which shares high similarities to the overall difference between *EH5-1.7ka* and *EH5-2ka* (Figure 4.17b). However, the anomalous moisture transport is located further to the south and the additional moisture transport into central and northern India is smaller in *EH5-1.7ka-PO* compared to *EH5-1.7ka*, which is in line with the smaller precipitation change in *EH5-1.7ka-PO* compared to *EH5-1.7ka* over these regions (Figure 4.16b & d). These results suggest that a substantial part of the anomalous easterly moisture transport from the western Pacific is driven by Pacific SSTs rather than Indian Ocean SSTs. Nevertheless, the anomalous moisture transport from the Bay of Bengal is likely to be driven by Pacific and Indian Ocean SST's, as it can neither be completely reproduced by *EH5-1.7ka-IO* nor *EH5-1.7ka-PO*. Here, the choice of the ocean boundary for Indian and Pacific Ocean and their associated imposed SST gradients in the sensitivity experiments might be one explanation for the mismatch.

Differences in moisture transport between *EH5-1.7ka-NA* and *EH5-2ka* are comparably small (Figure 4.17 e), which is again in line with little precipitation changes in *EH5-1.7ka-NA* (Figure 4.16e). Overall, it can be concluded that the large-scale circulation changes in moisture transport between *EH5-1.7ka* and *EH5-2ka* are dominated by changes in Pacific SSTs. However, on a local scale SSTs over the Indian Ocean seem to play also an important role, as it determines the moisture transport from the Arabian Sea.

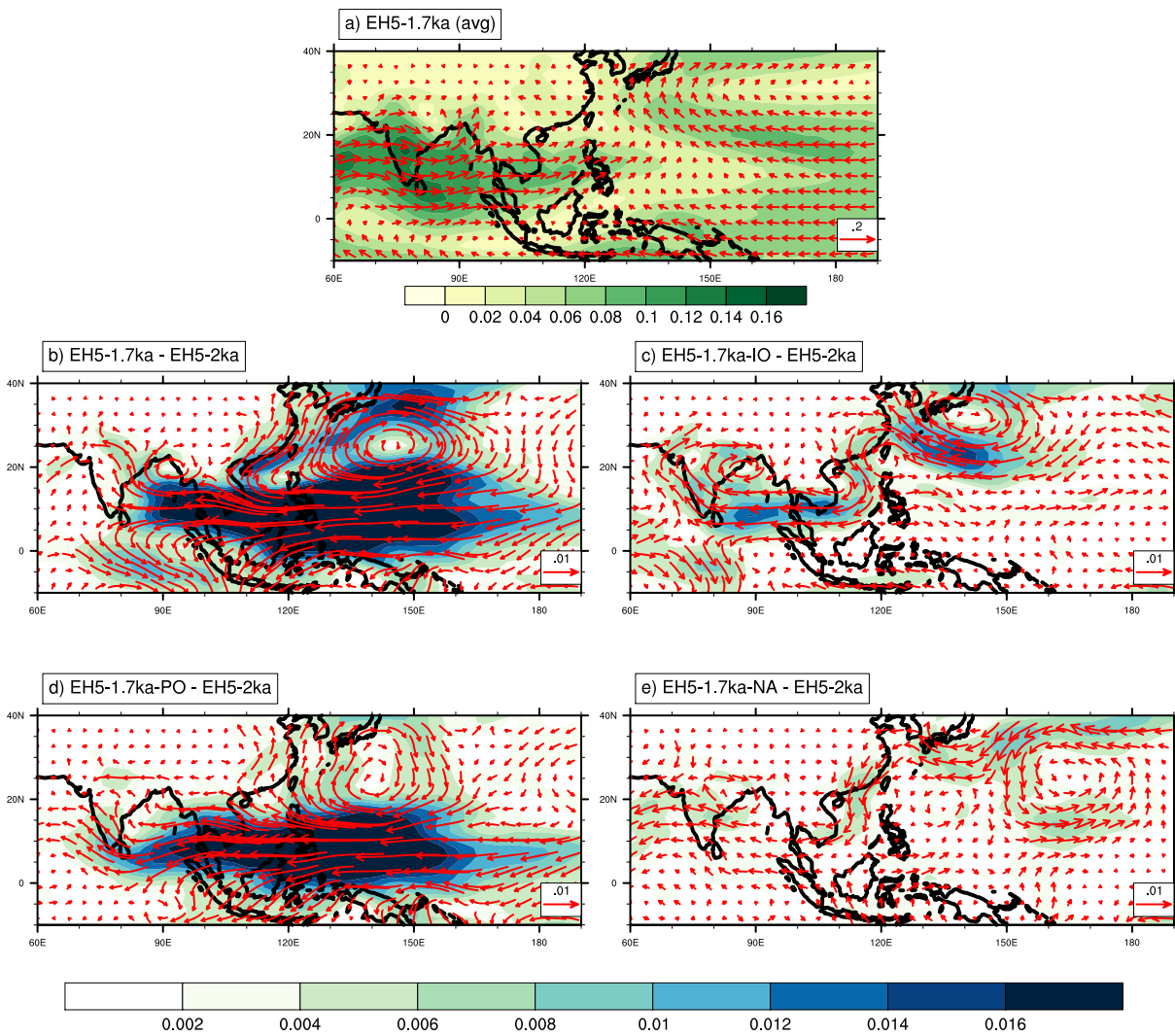


Figure 4.17: Anomalous moisture transport in 850 hPa (contour & vector).

a) Averaged moisture transport derived from *EH5-1.7ka*; b) Difference between *EH5-1.7ka* and *EH5-2ka*, c) Difference between *EH5-1.7ka-IO* and *EH5-2ka*, d) Difference between *EH5-1.7ka-PO* and *EH5-2ka* and e) Difference between *EH5-1.7ka-NA* and *EH5-2ka*. Velocity potential is given in $m/s \cdot kg/kg$

Upper and lower tropospheric Velocity Potential

To analyse changes in the large-scale monsoonal circulation, velocity potential fields in 200 hPa and 850 hPa are investigated (Figures 4.18 and 4.19). Averaged over 30 years two divergent centres over the western and eastern Pacific are found in 200 hPa (Figures 4.18a). The convergent counterparts are found over the southern tropical Atlantic and western Indian Ocean as well as over the eastern tropical Pacific. In the lower troposphere (850 hPa), centres of activity are found in a similar location as in 200 hPa but with opposite signs, however the divergent centre over the eastern Pacific being less pronounced in the lower troposphere (Figures 4.19a).

Upper Troposphere In 200 hPa velocity potential differences between *EH5-1.7ka* and *EH5-2ka* reveal positive anomalies over the entire Pacific Ocean and negative anomalies over the Indian Ocean and at the western coast of Africa (Figure 4.18b). This suggests a westward shift of the divergent centre over East Asia towards India in 200 hPa in *EH5-1.7ka* compared to *EH5-2ka*, which is consistent with an increase in the upper-tropospheric divergent flow over the Indian subcontinent. Thus, rainfall anomalies over India are in line with potential velocity anomalies between *EH5-1.7ka* and *EH5-2ka*. This easterly shift of the Walker circulation is also associated with ENSO (Thomas et al., 2000, Laing and Evans, 2011 and references therein).

Results obtained from *EH5-1.7ka-IO* show negative anomalies in 200 hPa over the western Indian Ocean, however, changes over the Pacific Ocean are much smaller compared to differences between *EH5-1.7ka* and *EH5-2ka* (Figure 4.18c). In contrast, differences between *EH5-1.7ka-PO* and *EH5-2ka* reveal large negative anomalies in 200 hPa over the entire Indian Ocean and large positive anomalies over the tropical Pacific Ocean (Figure 4.18d). This indicates that most of the westerly shift of the divergent centre towards the Indian Ocean is induced by changes in Pacific Ocean SSTs.

Changes in upper-tropospheric velocity potential between *EH5-1.7ka-NA* and *EH5-2ka* are small, which is consistent with only minor changes in surface moisture transport and precipitation changes over India.

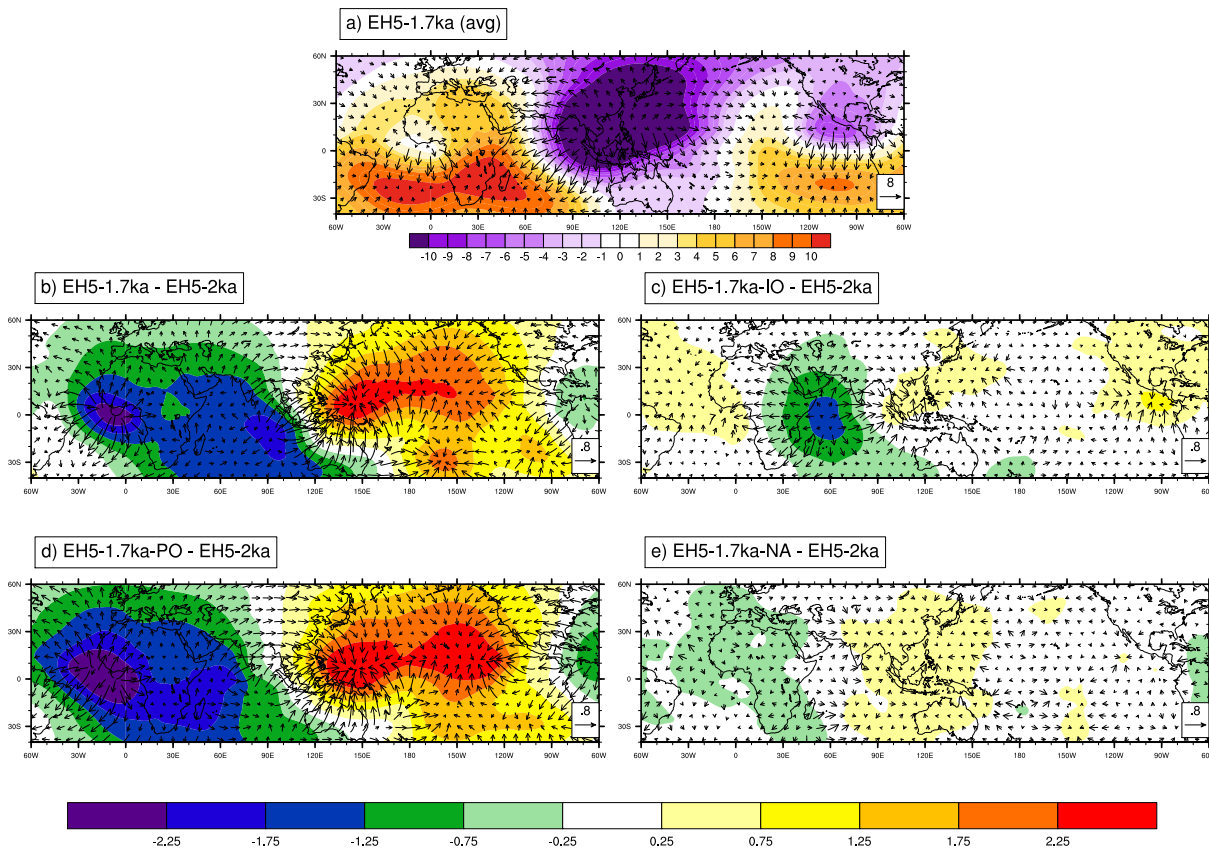


Figure 4.18: Velocity potential in 200 hPa (contour) and divergent winds (vector).

a) Averaged velocity potential derived from *EH5-1.7ka*; b) Difference between *EH5-1.7ka* and *EH5-2ka*, c) Difference between *EH5-1.7ka-IO* and *EH5-2ka*, d) Difference between *EH5-1.7ka-PO* and *EH5-2ka* and e) Difference between *EH5-1.7ka-NA* and *EH5-2ka*. Velocity potential is given in $10^6 m^2/s$

Lower Troposphere The velocity potential difference pattern between *EH5-1.7ka* and *EH5-2ka* in the lower troposphere is similar to its counterpart in the upper troposphere, but with reversed sign (compare Figure 4.19b to Figure 4.18b). Higher velocity potential values connected with a convergent flow over India are found in 850 hPa during *EH5-1.7ka* compared to *EH5-2ka* (Figure 4.19b), which is in line with higher precipitation rates over this region. Differences between *EH5-1.7ka-IO* and *EH5-2ka* are comparably small and less pronounced than in 200 hPa, however, a small increase in velocity potential values is found over western Indian Ocean.

Differences in lower tropospheric velocity potentials between *EH5-1.7ka-PO* and *EH5-2ka* resemble largely the difference pattern found between *EH5-1.7ka* and *EH5-2ka* (compare Figure 4.19b to Figure 4.19d). These results suggest that changes in the large-scale circulation via an anomalous Indo-Pacific Walker circulation found between *EH5-1.7ka* and *EH5-2ka* are steered by ocean temperatures over the Pacific and only to a lesser extent due to SSTs over the Indian Ocean, which is similar to results found for 200 hPa.

Velocity potential anomalies between *EH5-1.7ka-NA* and *EH5-2ka* are comparably small, which is in line with the little precipitation change observed for *EH5-1.7ka-NA*.

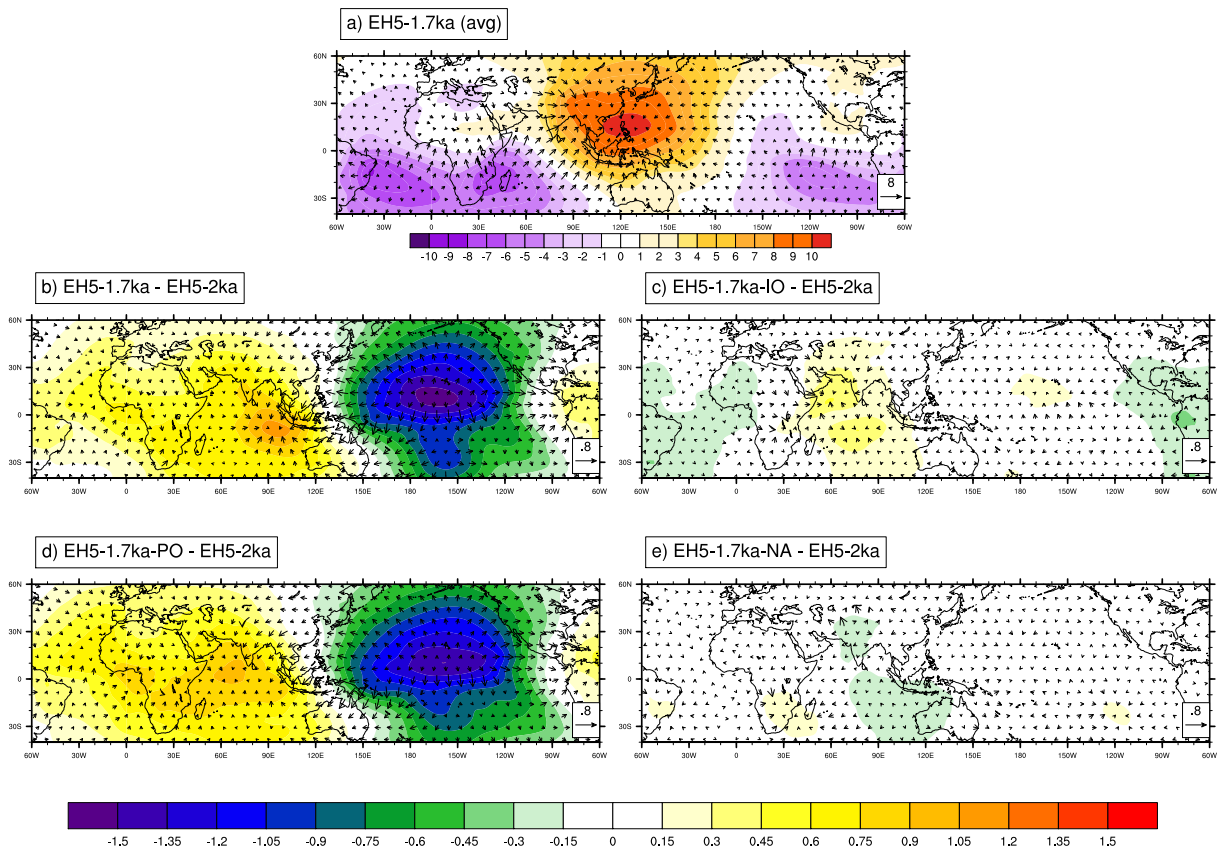


Figure 4.19: Velocity potential in 850 hPa (contour) and divergent winds (vector).

a) Averaged velocity potential derived from *EH5-1.7ka*; b) Difference between *EH5-1.7ka* and *EH5-2ka*, c) Difference between *EH5-1.7ka-IO* and *EH5-2ka*, d) Difference between *EH5-1.7ka-PO* and *EH5-2ka* and e) Difference between *EH5-1.7ka-NA* and *EH5-2ka*. Velocity potential is given in $10^6 m^2/s$

Evaporation and Moisture Advection The most prominent pattern found for evaporation differences between *EH5-1.7ka* and *EH5-2ka* is enhanced evaporation over the northern Arabian Sea (Figure 4.20) (positive values mean condensation due to the convention for vertical fluxes that downwards is positive). Thus, this region describes an anomalous moisture source during *EH5-1.7ka* compared to *EH5-2ka*.

The only sensitivity experiment showing this anomaly is *EH5-1.7ka-IO*. As expected neither *EH5-1.7ka-PO* nor *EH5-1.7ka-NA* show any evaporation anomaly here, as this source of moisture is triggered by higher SSTs over the northern Arabian Sea during *EH5-1.7ka* compared to *EH5-2ka* (see Figure 4.14).

This additional moisture source leads to enhanced moisture advection from the northern Arabian Sea into northwestern India in *EH5-1.7ka* compared to *EH5-2ka* (Figure 4.21a). This enhanced moisture advection with a similar magnitude is not found for *EH5-1.7ka-PO* or *EH5-1.7ka-NA* because of the missing SST anomaly over this region. In contrast, the anomalous moisture advection is found in *EH5-1.7ka-IO* compared to *EH5-2ka*. The results indicate that the enhanced moisture supply over this region due to warmer SSTs outweigh

the effect of a decreased land-sea contrast between northwestern India and the surrounding ocean. This is in line with comparable AGCM model studies (Levine and Turner, 2012). These results also reveal how local SST anomalies might affect longer-term ISM variability.

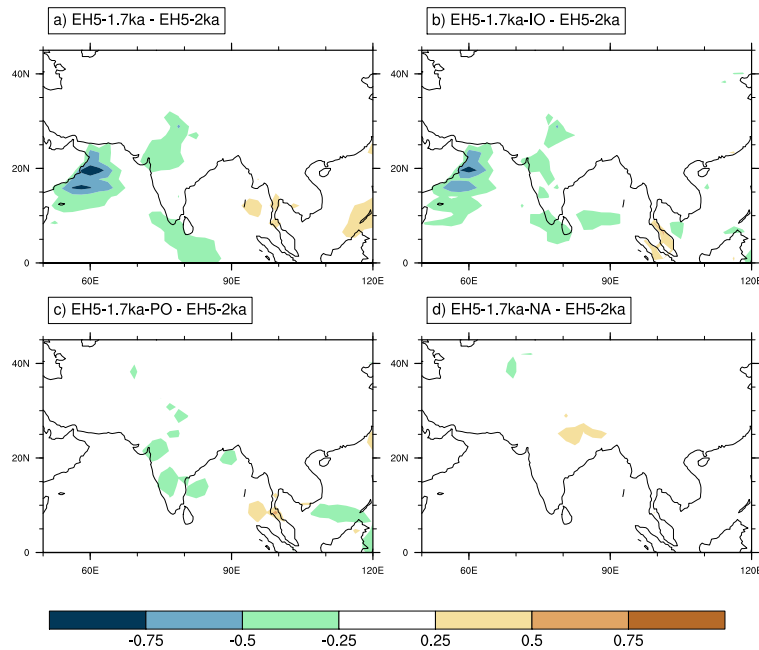


Figure 4.20: Difference in evaporation in mm/d between a) *EH5-1.7ka* and *EH5-2ka*, b) *EH5-1.7ka-IO* and *EH5-2ka*, c) *EH5-1.7ka-PO* and *EH5-2ka* and e) *EH5-1.7ka-NA* and *EH5-2ka*. Note that a downward evaporation flux is defined positively, thus condensation is defined positive and evaporation linked to negative values.

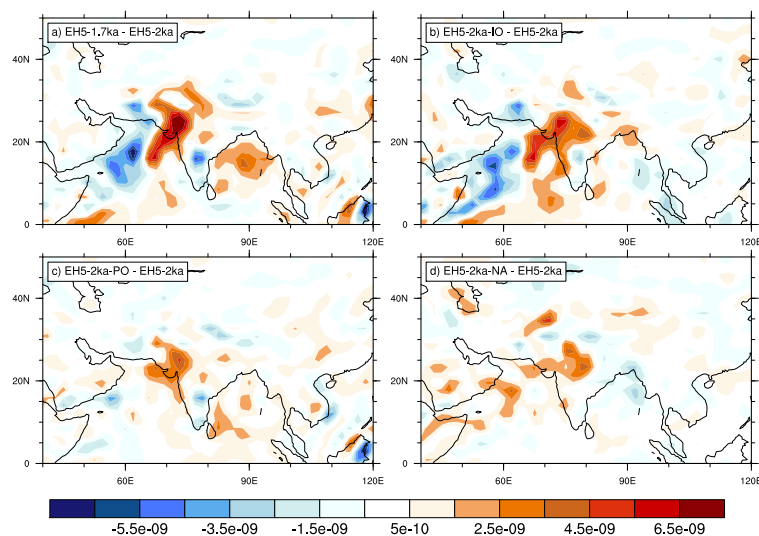


Figure 4.21: Difference in moisture advection [$m/s \cdot kg/kg$] between a) *EH5-1.7ka* and *EH5-2ka*, b) *EH5-1.7ka-IO* and *EH5-2ka*, c) *EH5-1.7ka-PO* and *EH5-2ka* and e) *EH5-1.7ka-NA* and *EH5-2ka*. Daily mean wind speeds and specific humidity values are used to derive moisture advection.

4.3.6 Mechanisms influencing the ISM on inter-annual to centennial time scales

Results obtained from the sensitivity studies suggest that changes of the SST's over the Pacific and Indian Ocean are responsible for the wetter conditions during 1.7ka BP and drier conditions around 2ka BP. However, results might be heavily affected by the short time period each simulation covers, e.g. only 50 years for *EH5-1.7ka* and *EH5-2ka*. To analyse, in how far changes in sea surface temperature conditions over particular areas in the Pacific and Indian Ocean are in phase with changes found in Indian monsoon rainfall, several SST based oceanic indices are calculated, which have been found to be related to the intensity of the ISM in earlier studies. Here sea surface temperatures are calculated over the following regions: NINO1+2, NINO3, NINO4, NINO3+4, NARAB³² and NEIO³³. NARAB and NEIO are chosen because significant changes between 1.7ka BP and 2ka BP are found over these regions (see Figure 4.14). Additionally, the position of the Indo-Pacific Warm Pool is calculated by the mean longitudinal position of all ocean grid cells exceeding 29° C in the area from 30° - 230° east and 40° south to 40° north similar to Kim et al. (2012) (c.f. Table 4.4). All oceanic indices are based on yearly means, except the IPWP which is based on JJAS SSTs. These indices are calculated from the original coarse AOGCM model simulation data in a resolution of T31L19.

NINO1+2	NINO3	NINO3+4	NINO4	NARAB	NEIO	IPWP
90°W-80°W, 10°S-0°	150°W-90°W, 5°S-5°N	170°W-120°W, 5°S-5°N	160°E-150°W, 5°S-5°N	50°E-70°E, 15°N-30°N	80°E-100°E, 5°N-15°N	mean position of SST>29°C

Table 4.4: Regions used for the calculation of sea surface temperature based oceanic indices.

SSTs in all NINO regions show high anti-correlations with rainfall over India, especially NINO4 region (0.80, see Table 4.5). Annual time series between NARAB and AIMR are only weakly correlated, and SST's over NEIO region show a moderate anti-correlation. A high temporal correlation is found between the AIMR and the position of the IPWP (-0.82), which indicates that a westward shift of the warm pool region leads to increased rainfall over India (Table 4.5). It is worth mentioning that SST over the NINO4 region and the position of the IPWP are highly correlated (0.86), as parts of the NINO4 region are also included in the IPWP region.

To investigate mechanisms controlling ISM strength on multi-decadal to centennial time scales all time series are smoothed using a 51-year running mean (Figure 4.22). The dry event around 2ka BP coincides with an anomalous eastward shift of the IPWP, cold SST's over NARAB and NEIO, as well as warmer ocean temperatures over all NINO regions. The

³²Northern Arabian Sea

³³North Eastern Indian Ocean

	NINO1+2	NINO3	NINO4	NINO3+4	NARAB	NEIO	IPWP
Correlation	-0.69	-0.68	-0.80	-0.74	0.22	-0.57	-0.82
Correlation (51 year)	-0.53	-0.62	-0.72	-0.75	0.62	-0.08	-0.75

Table 4.5: Correlation coefficients between oceanic index and rainfall over India (AIMR), based on yearly values (upper row) and after smoothing each time-series with a 51 year moving average (lower row).

period with the highest AIMR amount does coincide with the most westerly position of the IPWP. Interestingly, AIMR rainfall rates show similar increased rainfall amounts for the 40 years preceding the absolute rainfall maximum. This plateau is well represented in the position of the IPWP. Correlations between smoothed time series between AIMR and NINO regions are similar to yearly values, which also applies for the position of the IPWP (Table 4.5). This indicates that the Indo-Pacific Warm Pool plays an important role in influencing the ISM on these time scales. Largest differences are seen for NARAB region, where correlations increased from 0.22 to 0.62 for the smoothed timeseries compared to the NEIO region, for which the correlation coefficient drops to around zero for the smoothed time-series (Table 4.5). The correlation coefficient found between smoothed AIMR and SST's over the NARAB region of 0.62 is statistically significant on the 99% level, which is tested by calculating correlation coefficients of 1000 random time-series, smoothed by a 51 year running mean. This indicates, that enhanced moisture availability over the north Arabian Sea plays an important role in determining temporal characteristics of the Indian monsoon on these time scales. Even though correlation coefficients between SST's over the NINO regions and AIMR are high for the smoothed time series, the position of the IPWP and the SST over NARAB region are the only two indices showing robust minima and maxima during the weak and strong monsoon period (Figure 4.22). Thus, it can be concluded that changes of the position of the Indo-Pacific Warm Pool and temperatures over the Northern Arabian Sea play the most important role in influencing the long-term ISM strength between 2 ka and 1.7 ka BP in this respective model simulation.

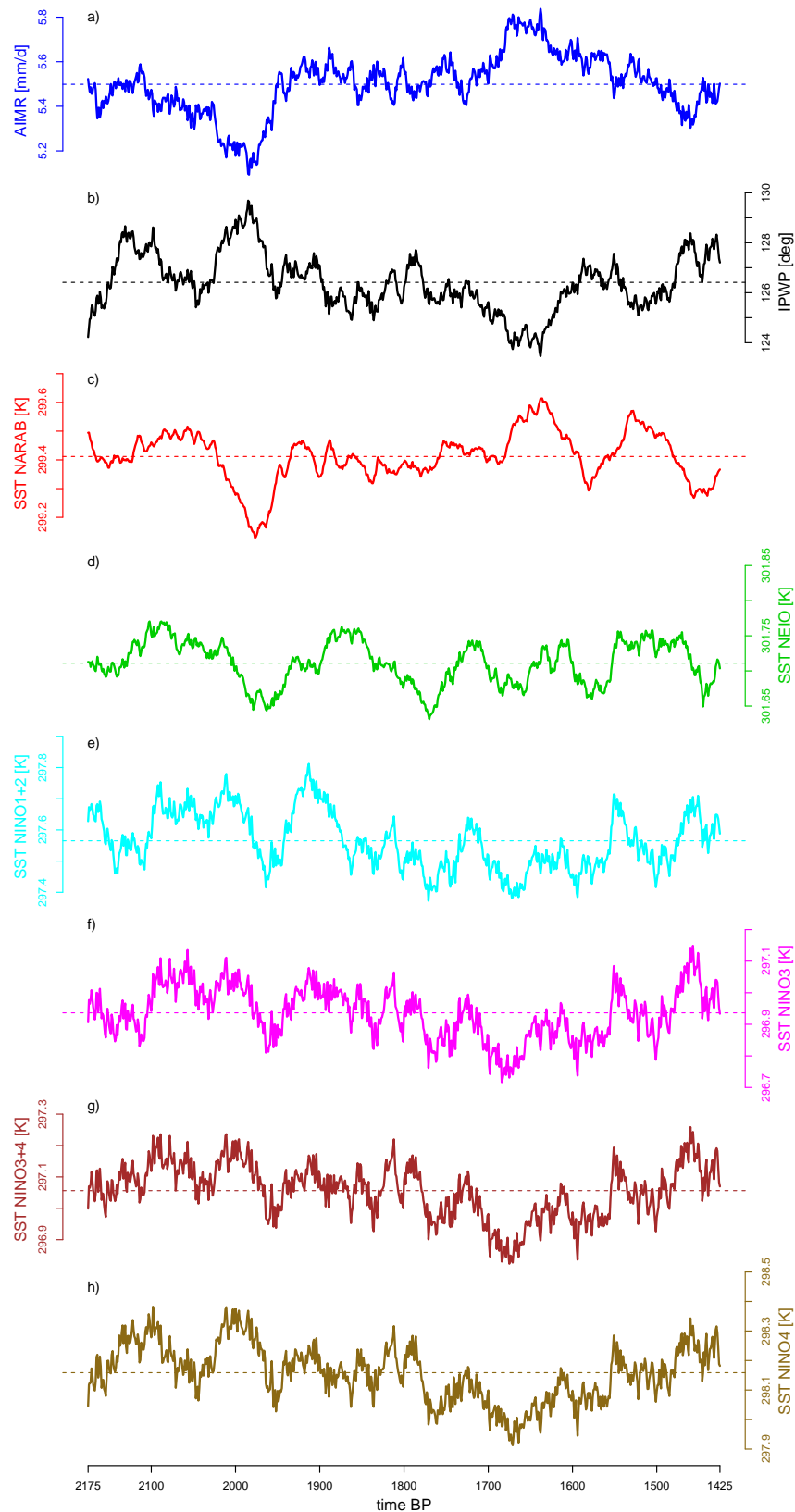


Figure 4.22: a) AIMR b) Position of IPWP c) SST over NARAB d) SST over NEIO e) SST over NINO1+2 region f) SST over NINO3 region g) SST over NINO3+4 region h) SST over NINO4 region. All time series are derived from T31L19 COSMOS AOGCM simulation (Fischer and Junglaus, 2011) and smoothed using a 51 year running mean.

Influence of the position of the IPWP and the SST over the northern Arabian Sea during the last 6000 years

The former analysis focused on the mechanisms steering the abrupt change in ISM intensity between 1.7ka BP and 2ka BP, which is found to be related to the position of the IPWP and the SST's over the NARAB region. To analyse in how far these two factors are also important for the other extreme events found in the 6000 year AOGCM simulation, both indices are calculated using the complete dataset. The respective time series are linear detrended and smoothed using a 201 year running mean to focus on centennial scale ISM variability (Figure 4.23).

The AOGCM simulations suggests two major droughts during the past 6000 years (one at around 3.6ka BP and another around 2ka BP), and three wet periods: one around 4.7ka BP, 1.7ka BP and another one around 700 years BP (Figure 4.23). However, the latter is thought to be due to the simple linear detrending method applied as solar insolation did not vary linearly during the past 6000 years (see Figure 4.10). The position of the IPWP is anomalously westerly shifted around 5.2ka BP, 1.7ka BP and 500 years BP, as well as anomalously easterly shifted around 3.7ka BP, 3.1ka BP and 2ka BP. The SST over the NARAB region is found to be anomalously warm around 4.7ka BP, 4ka BP, 3.3ka BP, 2.7ka BP and 1.7ka BP, whereas it is anomalously cold around 3.7ka BP, 2.9ka BP and 2ka BP.

Comparing the two major dry conditions over India with the SST over the NARAB region and the position of the IPWP it is found that for both time periods (3.7ka BP and 2ka BP) the IPWP is anomalously shifted to the east and the SST over the NARAB region is comparably cold. Similarly, for the wet epoch over India around 1.7ka BP the IPWP is shifted to the west and the SST over the northern Arabian sea is comparably warm. However, the second wet epoch around 4.7ka BP is linked to an anomalous warm SST over the NARAB region only but not to a shift of the IPWP. All other epochs with anomalous positions of the IPWP or anomalous SST's over the NARAB region do not have a huge influence on the ISM. As it can be inferred from Figure 4.23, none of these epochs is found to happen simultaneously. Thus, the combination of both: an anomalous shift of the position of the IPWP and changes of the SST over the NARAB region have the potential to influence the ISM on centennial time scales. This relationship is especially pronounced for extreme dry epoch, which are always associated with changes in the position of the IPWP and changes in SSTs over the NARAB region.

It is important to note that changes of the SST over the NARAB regions are comparably small, which is due to the 201-year filter, the coarse spatial resolution of the AOGCM simulation and the small size of the NARAB region. In fact, the NARAB region consists only of a few grid points. Higher resolved AOGCM simulations are necessary to analyse the influence of the NARAB in more detail.

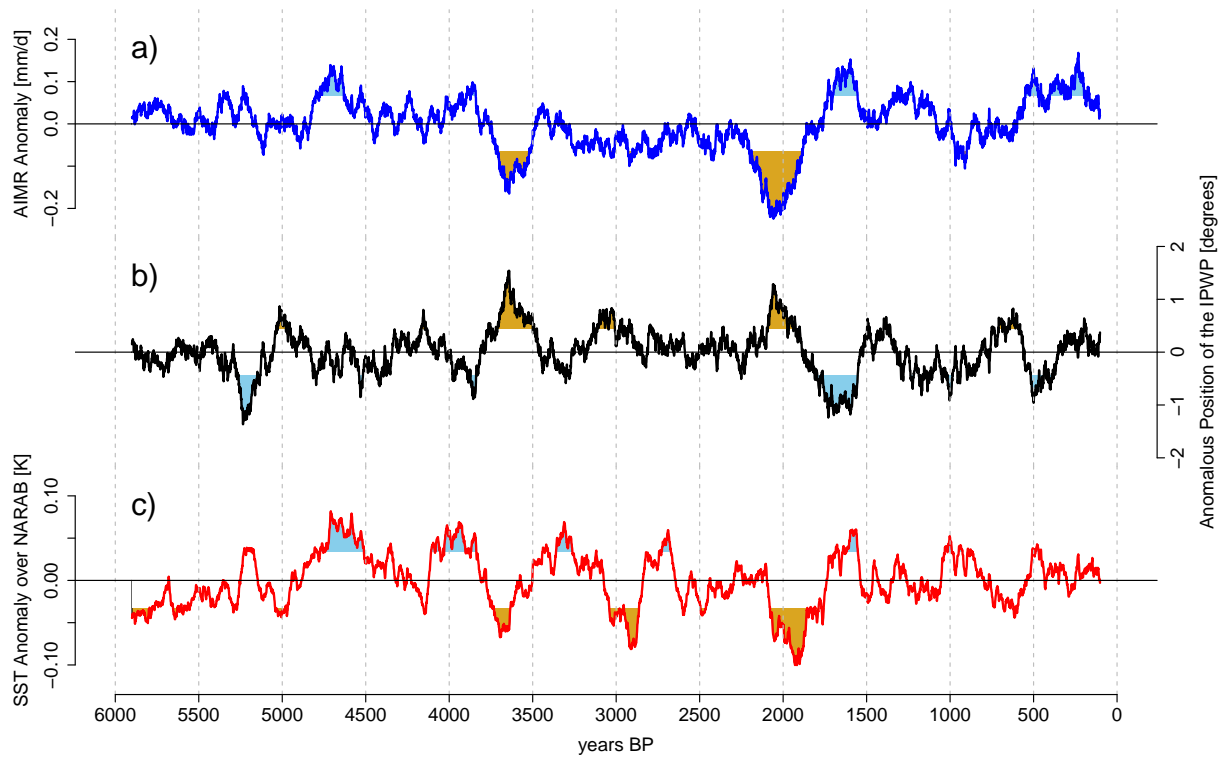


Figure 4.23: AOGCM time series for a) AIMR anomaly, b) anomalous position of IPWP and c) SST anomaly over NARAB region. Time-series are linearly detrended and smoothed using a 201-year running mean. Time periods for which the respective value exceeds the standard deviation are marked in blue if wetter conditions over India would be expected and brown if drier conditions over India would be expected.

Synthesis

The analysis of a transient AOGCM simulation covering the past 6000 years driven by constant GHG³⁴ concentrations but varying orbital parameters shows that extreme phases of the ISM on centennial time-scales could not be attributed to changes in the occurrence of active and break spells on the intraseasonal time-scale. Based on these results, the focus has been to answer two research questions: I) What is the mechanism steering the abrupt change in AIMR rainfall around 2ka BP? and II) Can such a derived mechanism also explain other dry and wet phases found in the AOGCM simulation covering the past 6000 years?.

For the strongest abrupt change in ISM precipitation between 1.7ka BP and 2ka BP (in the model data) sensitivity experiments with different sea surface temperatures using an AGCM in a resolution of T63L31 are carried out. These simulations indicate that the position of the IPWP and local surface temperatures over the Northern Arabian Sea are important in influencing the ISM during the transition between wet and dry periods.

The second research question is answered by testing in how far other extreme phases of the ISM in the whole 6000 model years can be attributed to changes in the position of the IPWP and SST's over the NARAB region. These results suggest that extreme phases of the ISM are in most cases associated with simultaneous changes of the position of the IPWP and SSTs over the NARAB. Extremes of only one of the mentioned factors (IPWP or SST over NARAB) are in general not sufficient to trigger an extreme phase of the All-Indian Monsoon Rainfall on centennial time-scales in this model simulation.

³⁴Greenhouse Gas Concentrations

4.4 Conclusion & Discussion

Last Millennium

In this chapter the hypothesis from Sinha et al. (2011a) has been tested using global and regional climate model data from atmosphere-only model simulations as well as coupled model simulations. First, transient 200 year AGCM simulations with a resolution of T63L31 for three time periods during the past 1000 years: Medieval Climate Anomaly, Little Ice Age and Recent Climate are carried out (Polanski et al., 2014). Lower boundary conditions as SST and SIC are taken from a coarse resolved (T31L19) fully-coupled AOGCM COSMOS simulation covering the last Millennium (Jungclaus et al., 2010). These simulations are further analysed regarding ISM variability on decadal to multi-decadal time scales using summer monsoon rainfall over the Indian subcontinent. For each AGCM time slice one dry and one wet phase (each 30 years) are dynamically downscaled using the RCM CLM with a horizontal resolution of approximately 55 km.

Sinha et al. (2011a) hypothesised that abrupt changes of the ISM are related to changes in the occurrence of active and break spells on the intraseasonal time scale. First, the high-resolved CLM simulations are used to verify this hypothesis, by identifying active and break spells using daily rainfall amounts. Rajeevan et al. (2010) identified active and break spells for the months July and August based on normalised precipitation over the Core Monsoon Region, defining an active (break) spell as an event with rainfall above (below) one standard deviation for at least 3 consecutive days. In this study, daily SPI values are used instead of normalised rainfall, motivated by the fact that spatial variability and dry and wet events on weekly time scale have been shown to be in good agreement with observations (see Chapter 3). However, it is shown that the identification of active and break phases using this method is not suitable as anomaly composites of years with an anomalous high number of active (break) phases do not show a specific dipole-like rainfall anomaly pattern, but rather a uniform rainfall anomaly pattern over India. This confirms the results from other studies indicating that most of the seasonal anomalous rainfall over India stems from seasonal persisting rather than intraseasonal variability patterns (Krishnamurthy and Shukla, 2000, 2007).

However, Sinha et al. (2011a) based their assumption on different trends in rainfall over CI and NEI in proxy data during the abrupt change in monsoon intensity and thus a dipole-like rainfall anomaly pattern. A new method has been developed based on rainfall time series over CI and NEI. Composite anomalies for rainfall for years with anomalous high rainfall rates over CI and low rainfall rates over NEI, and vice versa, show the expected dipole precipitation pattern. Additionally, it is shown that this seasonal dipole rainfall pattern is in

turn associated with a shift of the probability of occurrence of active and break days. Thus, it could be shown that rainfall time series of both regions can be used as a proxy for active and break days on the intraseasonal time scale. Furthermore, it is shown that the same method can be applied to both CLM and ECHAM5 data.

Comparing the different CLM simulations to each other shows that not all of the differences reveal a dipole-like rainfall pattern over CI and NEI. However, for 4 out of 15 differences a dipole pattern is present especially between CCLM-REG-wet and CCLM-REG-dry. As most of the simulations do not reveal significant changes of active and break phases the hypothesis by Sinha et al. (2011a) could not be entirely confirmed. However, it should be noted that most of the differences in rainfall over India are comparably small. Thus, it might not be expected that all these differences are caused by changes on the intraseasonal time scale. Additionally, the time difference between most of the time periods exceeds hundreds of years, whereas Sinha et al. (2011a) thesis is based on abrupt shifts in ISM precipitation.

Using the AGCM simulations, abrupt changes in rainfall over all-India, CI and NEI are detected using an objective algorithm identifying breakpoints in time series (Bai and Perron, 2003). It is shown that 50% of all identified breakpoints in All-Indian monsoon rainfall, especially the breakpoints associated with largest differences, are associated with changes of active and break phases on the intraseasonal time-scale. This partly confirms the hypothesis from Sinha et al. (2011a) but there are further mechanisms driving monsoon variability during the last Millennium in ECHAM5.

Changes in all-Indian monsoon rainfall might also be related to changes in monsoon onset and retreat and thus duration. However, the analysis suggest that most of the dry and wet events in ECHAM5 are associated with changes during the core monsoon months (July & August) and only the wet event during LIA is strongly associated with large rainfall changes during June and September. Thus, changes in the duration of the monsoon season do not drive the decadal to multi-decadal variability in AIMR in these ECHAM5 simulations.

It should be noted that the study presented here analyses only one AGCM-RCM combination, which limits the interpretation of the obtained results. However, RCM and AGCM reveal consistent results, e.g. rainfall dipole patterns found in CLM time slices are also indicated in rainfall timeseries calculated from ECHAM5. Furthermore, the simulations carried out within HIMPAC and partly within this thesis are shown to be in good agreement with multi-proxy archives (Polanski et al., 2014). However, RCM simulations couldn't be compared to proxies over the Indian subcontinent as no such datasets representing rainfall on intraseasonal to inter-annual time scale have been available.

The Past 6000 years

To study in how far abrupt changes in monsoon precipitation are associated with changes in active and break phases during the period from 6000 years BP until present, a transient fully-coupled AOGCM simulations is analysed (Fischer and Jungclaus, 2011). It is found that none of the abrupt changes in simulated AIMR is associated with changes in rainfall over CI and NEI with opposite trends. However, it might be possible that the coarse resolution of the AOGCM simulations is not sufficient to simulate intraseasonal features of the ISM. For the most striking abrupt change in precipitation found over India around 2ka BP in this simulation, two higher resolved 50 year AGCM simulations with a resolution of T63L31 are carried out. Differences in rainfall show no signs of a dipole-like structure, thus confirming the results obtained from the coarse resolved AOGCM simulations that these changes are not due to changes on the intraseasonal time scale.

Due to the short time period between dry and wet event, changes of orbital parameters cannot explain the abrupt change in ISM precipitation but rather changes of sea surface temperatures. SSTs differ significantly between both time periods for most of the ocean basins with the most dominant patterns being: 1) a tripole SST pattern over the North Atlantic Ocean, 2) a warm northern Arabian Sea and 3) a cooler western Pacific Ocean during 1.7ka BP compared to 2ka BP. AGCM sensitivity simulations are carried out with changed lower boundary conditions for only one ocean basin for each simulation to separate effects from the IO, PO and NA. It is found that most rainfall changes between 1.7ka BP and 2ka BP are caused by different ocean temperatures over the PO and IO. The tripole SST pattern in the North Atlantic Ocean has a small effect. Based on these experiments it is further found that the Pacific Ocean SST changes cause a anomalous shift of the Indo-Pacific Walker circulation, which is clearly indicated in upper and lower velocity potentials, which both are shifted westerly during the wet phase. In contrast, the warmer northern Arabian Sea acts more locally with enhanced evaporation over this region and an increased moisture flux into northwestern India.

It should be noted that all simulations carried out within this study are forced by transient SST and SIC conditions. This means that high SST gradients at the borders of the selected ocean basins partly occur in the sensitivity experiments. No smoothing is applied at these boundaries to limit the effect, however, the boundaries of the ocean basins have been chosen across as many land-points as possible, as temperatures over these land-points are calculated by the AGCM itself and thus weaken possible temperature gradients.

Overall, results suggest the effect of transient changing SSTs to be small compared to the overall changes in monsoonal circulation and associated rainfall during 1.7ka BP and 2ka BP. This is mainly based on the fact that all circulations changes in the AGCM sensitivity exper-

iments are found to be consistent with changes of ocean basin SSTs. However, a drawback of the method applied is the choice of the Pacific-Indian Ocean boundary, which somehow divides the IPWP into two parts. The inconsistencies by the transient SSTs imposed here might cause some circulation features in the sensitivity experiments, which are not in line with overall circulation changes. Further model experiments are thought to be useful to fully investigate the role of Indo-Pacific SSTs and how they affect rainfall over the Indian subcontinent. Another assumption is the linear impact of SST changes over different ocean basins on rainfall over India as it is tried to explain all precipitation change by linearly adding up contributions from each ocean basin (sensitivity experiment). Obviously, atmospheric processes are highly non-linear, which also leads to the fact that the entire rainfall anomaly cannot be explained by using the presented simulations. However, even though the design of the sensitivity simulations is kept simple, the simulations have proven useful to analyse and understand changes in rainfall during the dry and wet period.

Based on the coarse resolved AOGCM data, it is tested in how far changes in rainfall over India during the complete 6000 years can be attributed to changes of the position of the Indo-Pacific Warm Pool and changes of SSTs over the northern Arabian Sea. Results suggest that shifts of the Indo-Pacific Warm Pool in combination with changed SSTs over the NARAB region play a major role in shifting global monsoon circulation also on centennial time-scales. However, in general neither a shift of the warm pool nor changes over the northern Arabian Sea alone are sufficient to trigger most of the extreme phases of AIMR. This stays especially true for long-lasting dry periods. The importance of the IPWP in leading to dry conditions over India is also found in proxy archives. Prasad et al. (2014) analysed lake sediments from Lake Lonar, located in the core monsoon region of India. Their findings suggest that long-lasting dry events found in the proxy archives are associated with warmer SST conditions over the Indo-Pacific Warm Pool (their Figure 6). Results obtained in this study partly confirm these findings as the dry event around 2ka BP is associated with an eastward shift of the Indo-Pacific Warm Pool. The SST anomaly pattern shows cooler SSTs over the north-eastern Indian Ocean and warmer SSTs over the western Pacific Ocean during *EH5-2ka* compared to *EH5-1.7ka*. Generally, these results are also in line with those obtained by Polanski et al. (2014).

In how far changes of local conditions over the northern Arabian Sea were present during drought events found in proxy data is not discussed by Prasad et al. (2014). The importance of surface conditions over the Arabian Sea onto ISM variability is addressed in several studies (e.g., Ghosh et al. 1978; Levine and Turner 2012). Thus, colder SSTs over the Arabian Sea influence the ISM due to their impact on moisture availability (Levine and Turner, 2012). The results are consistent with those presented in Polanski et al. (2014), who showed the importance of northern Arabian Sea SST anomalies during the MCA compared to the LIA in two ECHAM AGCM simulations. In addition to these results, the analyses presented in this study also reveal certain circulation anomalies associated with changes over the Indo-Pacific Warm Pool region as well as the NARAB.

Future Changes of the ISM

In this chapter, the tempo-spatial variability of the ISM¹ as projected by COSMOS² simulations carried out within the CMIP3³ under future greenhouse gas conditions is analyzed. The reason for using CMIP3 instead of latest CMIP5⁴ is to study possible future changes using the same models (ECHAM5 and CLM⁵) as for recent and paleo climate conditions (Chapter 3 & Chapter 4). As ECHAM6 is used instead of ECHAM5 in CMIP5 and CLM simulations forced by ECHAM5 under different greenhouse gas emission scenarios (B2, A1B, A2) are already available for the Indian region (Dobler and Ahrens, 2011) results obtained here are based on simulations carried out using CMIP3 model simulations. In Chapter 3 it is shown that both models capture observed features of the ISM on the intraseasonal timescale, which is the basis for analyses carried out here.

This chapter aims to answer the third research question:

**ARE POSSIBLE FUTURE CHANGES OF THE ISM RELATED TO AN ANOMALOUS RAINFALL
DIPOLE PATTERN OVER CI⁶ AND NEI⁷ ASSOCIATED WITH CHANGES ON THE INTRASEASONAL
TIME SCALE?**

5.1 Introduction

Several studies address the variability of the ISM under changed greenhouse gas concentrations (e.g., Kripalani et al., 2007; Turner and Slingo, 2009a,b; May, 2011, 2004; Menon et al., 2013). In general, CMIP3 models suggest an increase in mean monsoon rainfall under future climate conditions together with a weakening of the monsoon circulation (Ueda et al., 2006). This paradox between increasing rainfall but reduced low-level winds can be explained by an enhanced moisture supply over the Indian Ocean under future climate

¹Indian Summer Monsoon

²Community Earth System Models

³Coupled Model Intercomparison Project 3

⁴Coupled Model Intercomparison Project 5

⁵COSMO-CLM

⁶Central India

⁷North-eastern India

conditions. Similar results are also found by Meehl and Arblaster (2003), who showed that the precipitation increase over South Asia under enhanced GHG⁸ concentrations is primarily due to the increased moisture supply over the warmer Indian Ocean. However, there is a large spread between the models projections for the South Asian region within CMIP3 (Christensen et al., 2007), with an improved agreement for projection of models within CMIP5 (Menon et al., 2013). Under future climate conditions an increase of the interannual variability of the ISM is found in model projections (Meehl and Arblaster, 2003; Menon et al., 2013). According to Meehl and Arblaster (2003) this is associated with changes in SST⁹s over the Pacific Ocean and their impacts on the ISM via the Walker circulation.

Despite GCM based studies, future changes of the ISM have been further analysed using higher resolved RCM¹⁰ simulations (Dobler and Ahrens, 2011; Hassan et al., 2015). Their results indicate partly different projected changes in terms of precipitation by the end of the century in the RCM and in the driving global climate model. Dobler and Ahrens (2011) carried out RCM simulations under B1, A1B and A2 scenario conditions using COSMO-CLM forced by ECHAM5/MPI-OM at its lateral boundaries (Dobler and Ahrens, 2011). Their findings illustrate that the increasing rainfall trend over India found in the driving model runs is not present in the RCM rainfall fields, which show a decreasing trend towards the end of the century. A large spread in projected changes of different RCMs driven by the same GCM¹¹ is also found by Niu et al. (2015).

Besides analyses focusing on mean changes of the ISM, several studies investigated projected changes of active and break phases and extreme rainfall events on intraseasonal time-scales. Turner and Slingo (2009a) showed an increase of heavy precipitation events under doubled CO₂ concentrations, which is strongly coupled to the increased specific humidity. Regarding active and break events they find an intensification of both, however, no changes regarding occurrence or duration of breaks are found. The uncertainty of projected changes in frequency and duration of active and break spells is also revealed by Mandke et al. (2007) using ten different GCMs. More coherent results regarding active and break spells are presented by Sharmila et al. (2015) using four different GCMs, who showed that both are likely to intensify under future climate conditions.

None of these studies focuses on the contribution of changes on the intraseasonal time scale onto longer, e.g. decadal fluctuations of the ISM. However, shift of the A-B¹² regime to a more dominate break or active regime on decades in future would have a huge impact on the agricultural sector and thus India's society.

⁸Greenhouse Gas Concentrations

⁹Sea Surface Temperatures

¹⁰Regional Climate Model

¹¹General Circulation Model

¹²active-break

5.2 Data & Methodology

In this chapter RCM (CLM) as well as GCM (ECHAM5) simulations under future climate conditions are analysed. Future emission scenarios analysed in this study are: 1) Commitment simulation (COM), 2) B1 simulation (B1), 3) A1B simulation (A1B) and 4) A2 simulation (A2). The GHG emissions linked to each of these scenarios are very different, with B1 being associated with the lowest emission by the end of the 21st century. followed by A1B and A2 (see Figure 5.1).

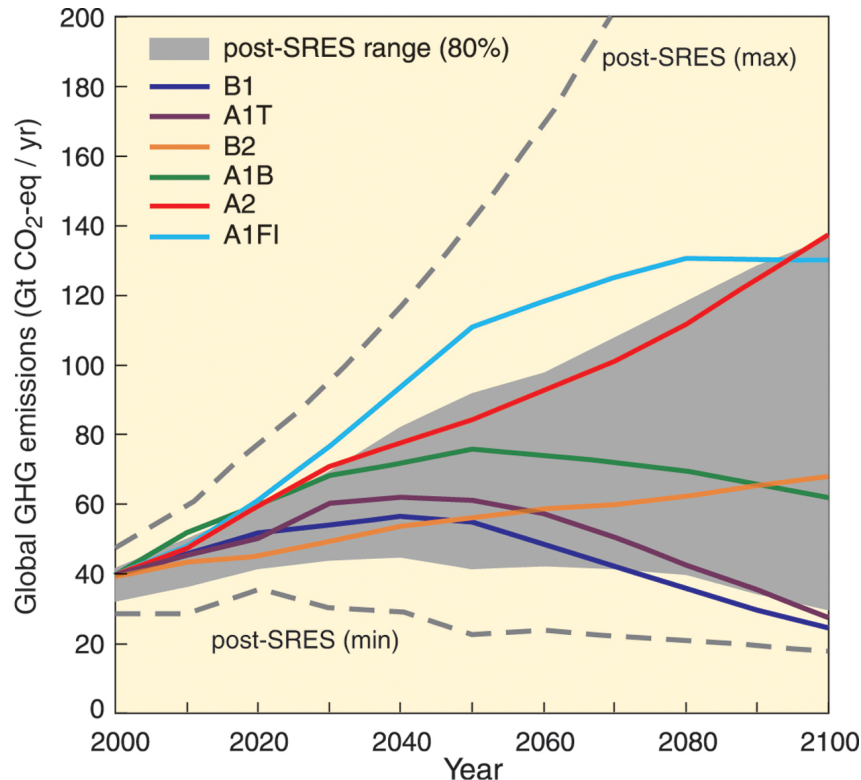


Figure 5.1: "Global GHG emissions (in GtCO₂-eq per year) in the absence of additional climate policies: six illustrative SRES marker scenarios (colored lines) and 80th percentile range of recent scenarios published since SRES (post-SRES) (gray shaded area). Dashed lines show the full range of post-SRES scenarios. The emissions include CO₂, CH₄, N₂O and F-gases." (IPCC Core Writing Team, 2007)

All CLM simulations are carried out using version 2.4.11 and share the same spatial resolution of 0.44° and 20 vertical levels (see Dobler and Ahrens 2011 for further information). The first ensemble member of the ECHAM5/MPIOM simulations carried out within the CMIP3 is used to force the CLM simulations at its lateral boundaries. Thus, only the first ensemble member of ECHAM5 is used to analyse future changes of the ISM. These ECHAM5 simulations have a horizontal resolution of T63 (≈ 200km) and 31 vertical levels. The time periods covered are 1960 until 2100 for the Commitment run (which is forced by observed GHG concentrations until the year 2000 and fixed concentrations afterwards), and 2001 until 2100 for B1, A1B and A2 simulations.

Seasonal rainfall amounts over India (AIMR¹³ region), as well as northeastern India (NEI) and Central India (CI) are used to investigate the influence of active and break spells on intraseasonal timescales on the ISM. As shown in Chapter, 4 seasonal rainfall timeseries over NEI and CI can be used as a proxy for the occurrence of active and break spells.

Timeseries are smoothed using a 21 year moving average filter to investigate long-term variability. The value of 21 years instead of 31 years (as used in Chapter 4) is chosen to make the results comparable to those published in Dobler and Ahrens (2011), who also used a 21 year running mean. Breakpoints in smoothed rainfall timeseries are calculated based on the method developed by Bai and Perron (2003), however, the minimum segment size is changed to 21 years according to the smoothing window size. All simulations analysed in this chapter are summarised in Table 5.1.

Identifier	Model-type	Time-period	Forcing Model
<i>COSMOS-COM (run1)</i>	AOGCM ¹⁴	1960 - 2100	N/A
<i>COSMOS-A1B (run1)</i>	AOGCM	2001 - 2100	N/A
<i>COSMOS-B1 (run1)</i>	AOGCM	2001 - 2100	N/A
<i>COSMOS-A2 (run1)</i>	AOGCM	2001 - 2100	N/A
<i>CLM-COM</i>	RCM	1960 - 2100	<i>COSMOS-COM (run1)</i>
<i>CLM-A1B</i>	RCM	2001 - 2100	<i>COSMOS-A1B (run1)</i>
<i>CLM-B1</i>	RCM	2001 - 2100	<i>COSMOS-B1 (run1)</i>
<i>CLM-A2</i>	RCM	2001 - 2100	<i>COSMOS-A2 (run1)</i>

Table 5.1: Overview to model simulations used in Chapter 5.

5.3 Future changes of Active and Break spells in CLM simulations

Firstly, seasonal rainfall amounts for all four CLM climate change scenarios (*CLM-COM*, *CLM-A1B*, *CLM-B1*, *CLM-A2*) are calculated over the Indian subcontinent (AIMR region). In accordance to Dobler and Ahrens (2011), all timeseries are smoothed using a 21-year running mean filter (Figure 5.2) to estimate future changes of mean ISM intensity.

In *CLM-COM*, AIMR decreases until around 2030 and increases afterwards. Under B1 conditions (*CLM-B1*) rainfall rates are rather stable until around 2060 with a increase from 2060 until 2080 and a drop in rainfall afterwards. ISM activity decreases throughout the 21st century under the A1B emission scenario (*CLM-A1B*) with an even more rapid decrease

¹³All-Indian Monsoon Rainfall

from around 2060 until 2090. Under A2 conditions (*CLM-A2*) a global maximum in AIMR is found around 2010 followed by a decreasing trend until 2100, which is very similar to the trend in A1B from around 2050. As described in Dobler and Ahrens (2011) the decreasing trend in AIMR, is found over most parts of India and the relative changes are most pronounced over northwestern India. In contrast, positive trends are found over southeastern India. However, trends over India (Dobler and Ahrens, 2011; their Figure 3) reveal no dipole like pattern as changes are comparably small over the eastern CMZ¹⁵ and especially NEI. This indicates that the linear trend in rainfall discussed in Dobler and Ahrens (2011) is not due to changes on the intraseasonal timescale, however, further analyses are necessary to prove this assumption. Besides, the long-term negative trend, decadal variations in AIMR are visible in all scenario simulations, with the strongest being the one found around 2010 in A2 and around 2080 in B1.

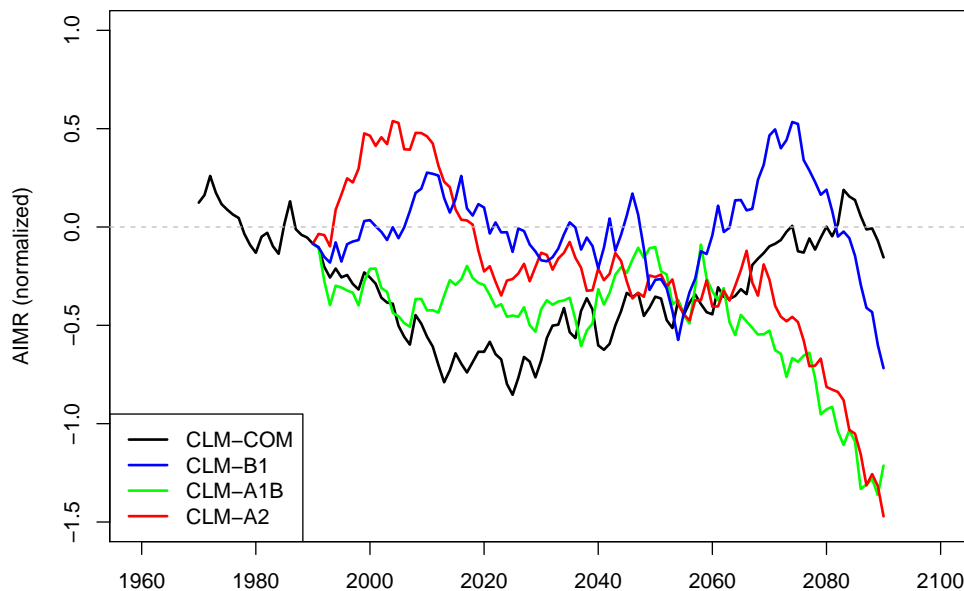


Figure 5.2: Rainfall timeseries over all-India (AIMR) smoothed with a 21 year running mean filter for four different COSMO-CLM climate change scenarios (COM, B1, A1B, A2) driven by ECHAM5 run1 simulations carried out within CMIP3.

Due to the long integration time of each scenario simulation of 100 years, breakpoints can be identified for CLM timeseries with the same method applied to paleo GCM data in Chapter 4 (Figure 5.3). The aim of this investigation is to analyse in how far the temporal variability of the ISM is related to changes in active and break spells.

In *CLM-COM*, four breakpoints are identified and linear regression models are fitted using the data for respective breakpoints. As expected, rainfall trends over CI share the same sign as rainfall trends over AIMR. In general, this is also true for rainfall trends at the breakpoints over NEI, meaning that changes in active and break spells are not driving the ISM

¹⁵Core Monsoon Region

variability. Only one breakpoint around the year 2011 is associated with a decreasing AIMR and CI rainfall trend and an increasing rainfall trend over NEI.

In *CLM-B1*, two breakpoints are identified, one around 2027 and the second around 2069. For both breakpoints indications of changes on the intraseasonal timescale are found, especially for the second breakpoint. AIMR and rainfall over CI decreases around 2027, whereas it increases over NEI, however, the trend is not significant. For the second breakpoint, AIMR and rainfall over CI increases, whereas the trend in rainfall over NEI is negative. It is worth mentioning that the decreasing trend in rainfall at the end of the 21st century in *CLM-B1* is also associated with a decreasing trend in rainfall over CI and an increasing trend in rainfall over NEI. These results suggest that the long-term variability of the ISM in *CLM-B1* is linked to changes on the intraseasonal timescale.

Under concentrations following the A1B scenario (*CLM-A1B*) two breakpoints are found. None of these breakpoints can be associated with changes of active and break phases, as rainfall trends share the same sign in all regions (AIMR, CI and NEI). For the simulation under A2 scenario conditions (*CLM-A2*), three breakpoints are identified. For the first two of them rainfall trends over all three regions share the same sign. However, the last breakpoint (around 2069) is linked with decreasing trends in rainfall over all-India and CI and an increasing trend over NEI.

Overall, results obtained from the RCM simulations are inconclusive. In total, 11 breakpoints could be identified in the four climate change scenario simulations, however, only 4 of them could be linked to changes on the intraseasonal timescale based on different trends in rainfall over central and northeastern India (3 of them with significant linear trends over central and northeastern India). This shows that other factors are more important in steering decadal-scale variability of the ISM.

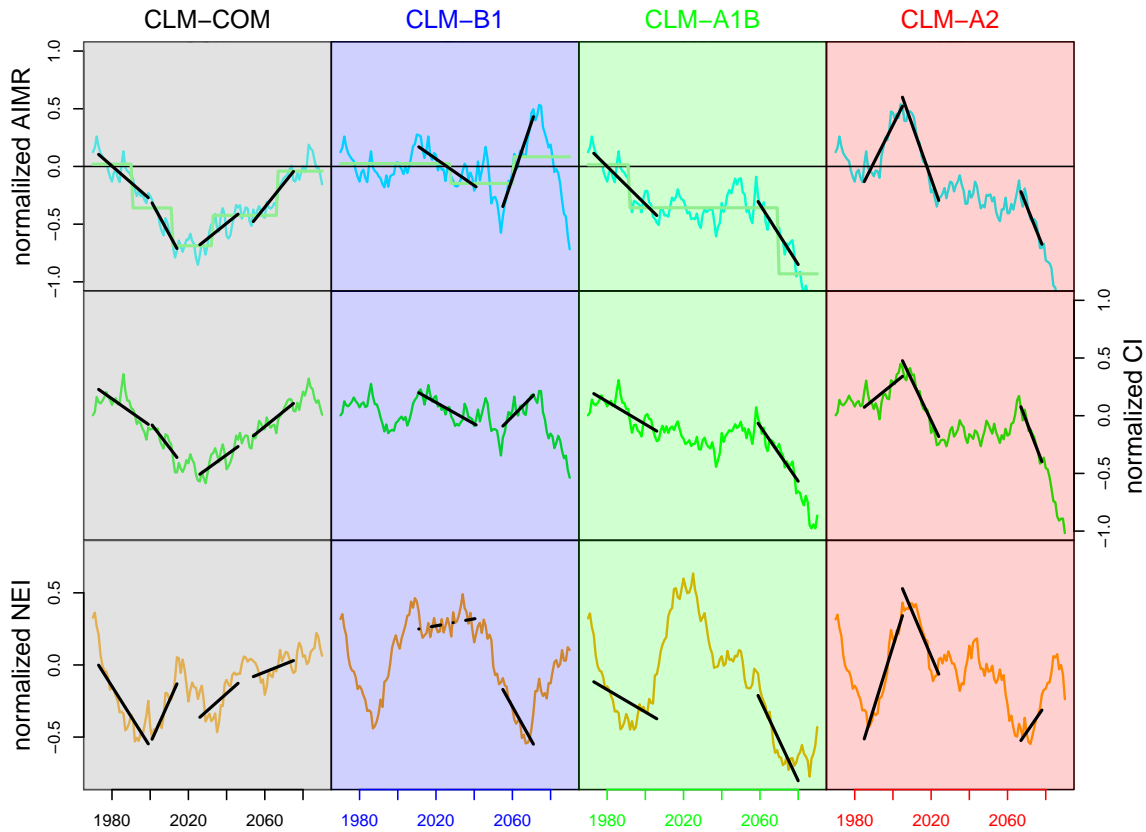


Figure 5.3: upper: Rainfall timeseries over all-India (AIMR) for four different CLM simulations under future emission scenarios (*CLM-COM*, *CLM-A1B*, *CLM-A2*, *CLM-B1*). Breakpoints are identified based on the method developed by Bai and Perron (2003) and to each breakpoint a linear regression model is fitted. middle: Rainfall timeseries over central India (CI) for four different climate change scenarios. For each breakpoint identified in AIMR timeseries a linear regression model is fitted to the corresponding CI rainfall. bottom: Rainfall timeseries over northeastern India (NEI) for four different climate change scenarios. For each breakpoint identified in AIMR timeseries a linear regression model is fitted to the corresponding NEI rainfall. All timeseries are normalised to the reference period from 1960 until 2000 and smoothed with a 21 year running mean filter. Significant linear regression models (p-level:5%) are indicated as solid and no-significant linear trends as dashed lines.

5.4 Future changes of Active and Break Spells in ECHAM5 simulations

In accordance with the previous section, ECHAM5 rainfall timeseries for *COSMOS-A1B (run1)*, *COSMOS-B1 (run1)*, *COSMOS-A2 (run1)* and *COSMOS-COM (run1)* simulation are analysed. All timeseries are smoothed using a 21 year running mean filter. As already pointed out by Dobler and Ahrens (2011) rainfall trends in ECHAM5 future scenario simulations do essentially differ compared to those found in the corresponding CLM simulations. A positive trend in AIMR is found for all future scenarios throughout the 21st century, however, large decadal-scale fluctuations are present, which is similar to the RCM results (Figure 5.4).

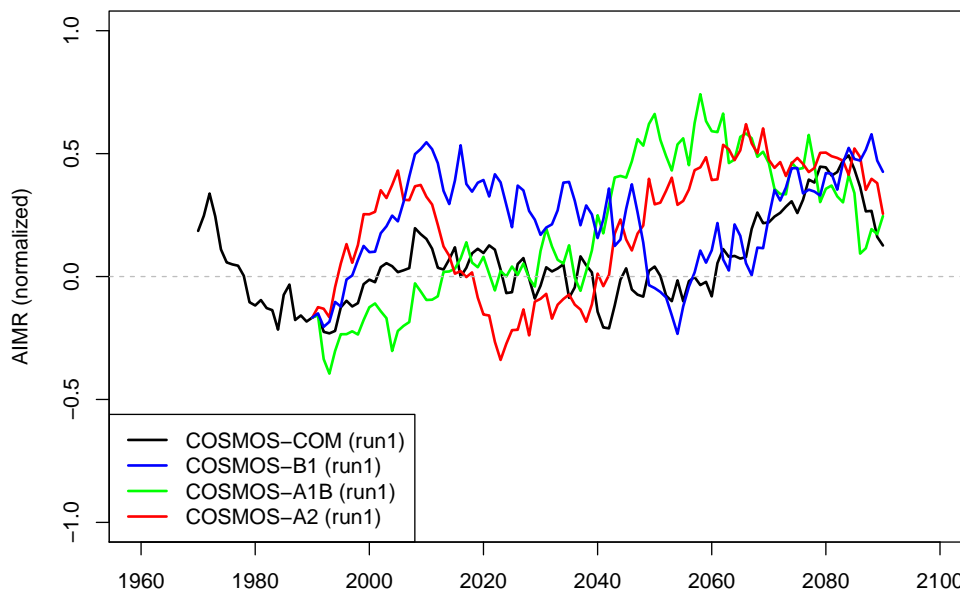


Figure 5.4: Rainfall timeseries over all-India (AIMR) smoothed with a 21 year running mean filter for four different ECHAM5 climate change scenarios (COM, B1, A1B, A2) carried out within CMIP3.

To answer the question in how far these changes on decadal time-scales are related to changes in active and break spells, timeseries for CI and NEI are computed (Figure 5.5). Again, changes in active and break spells are indicated by different signs of rainfall trends over central and northeastern India. Here, each scenario simulation is extended by the years 1960 until 2000 from the 20C (*COSMOS-COM (run1)*) simulation. This might lead to the identification of different breakpoints before 2000 in the scenario runs due to the window size of the moving average filter.

For *COSMOS-COM (run1)* three breakpoints are identified. None of them is suggested to be steered by changes in active and break spells, as rainfall trends over CI and NEI either share the same signs or the slope being not statistically different from zero (Figure 5.5).

In *COSMOS-B1 (run1)* four breakpoints are identified, but only one of them (the second one around 2023) can be attributed to changes in rainfall over CI and NEI with different signs (Figure 5.5).

Four breakpoints are also identified in the ECHAM5 simulation under A1B scenario concentrations (*COSMOS-A1B (run1)*). For three out of these four (around 1990, 2012, 2063) exists the tendency of changes on the intraseasonal timescale, however, only one breakpoint around 2012 is associated with significant linear trends in rainfall over CI and NEI with different signs (Figure 5.5).

Four breakpoints are also found for *COSMOS-A2 (run1)*, of which only the last one around 2063 can be associated to changes in active and break spells (Figure 5.5).

Overall, for a total of 15 breakpoints identified in smoothed AIMR rainfall only 5 can be associated with linear rainfall trends over CI and NEI with different trends (3 of them revealing significant trends over central and northeastern India). This is similar to results obtained for RCM simulations, which means that changes on the intraseasonal timescale are not the major factor influencing decadal-scale ISM variability in these AOGCM future climate projections.

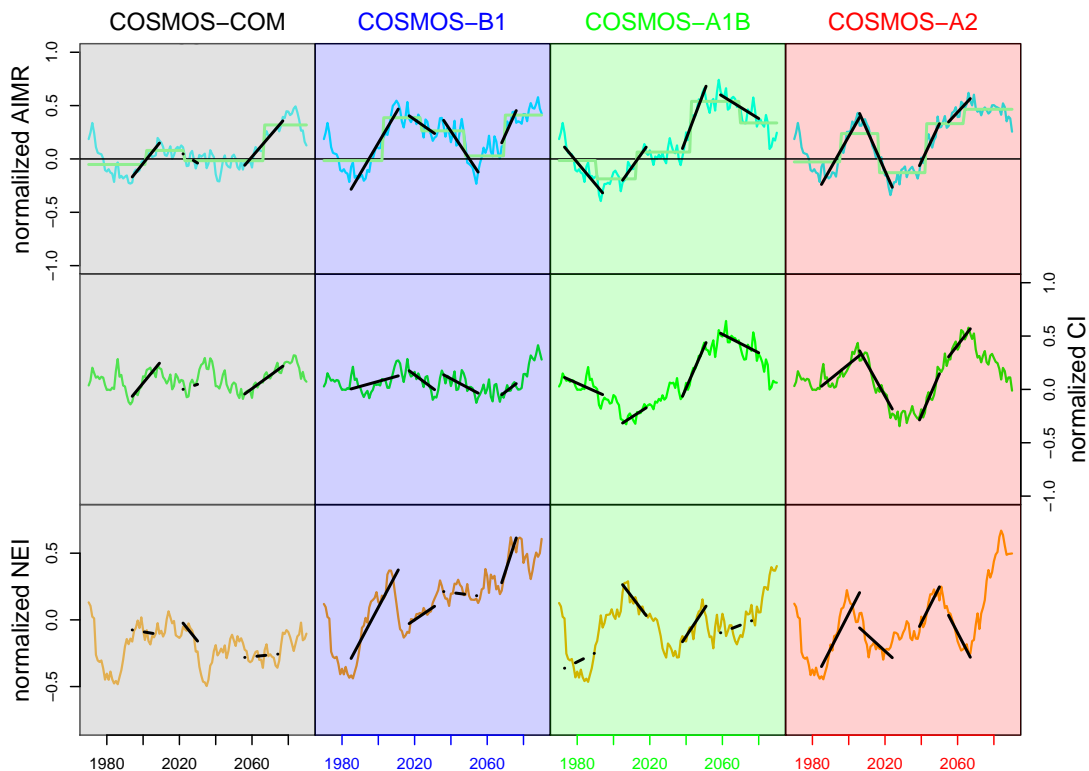


Figure 5.5: Identical to Figure 5.3, but for four different ECHAM5 simulations under future emission scenarios (*COSMOS-COM (run1)*, *COSMOS-A1B (run1)*, *COSMOS-A2 (run1)*, *COSMOS-B1 (run1)*). Breakpoints are identified based on the method developed by Bai and Perron (2003) and to each breakpoint a linear regression model is fitted.

5.5 Conclusion & Discussion

Results of this study reveal that linear long-term changes throughout the 21st century cannot be explained by changes on the intraseasonal timescale. This is shown by analyses of timeseries over all-India, central and northeastern India. This is also supported by linear rainfall trends over India (Dobler and Ahrens, 2011; their Figure 3) for which no prominent dipole patterns in monsoon rainfall are found. However, analyses of rainfall timeseries also show that projected linear trends during the 21st century are far smaller than decadal scale variability. Even though active and break spells are found not to be the major driver of decadal-scale ISM variability, it is shown that some changes in all-Indian monsoon rainfall (AIMR) can be associated with active and break spells. As changes in active and break spells would have a large impact on Indias society mainly due to impacts on the agricultural sector, decades with reduced active and an increased number of break spell days or vice versa could be devastating. For CLM B1 scenario simulations the highest rainfall over India is associated with changes in active and break spells (around 2070). This event together with the period around 2010 in the A2 scenario run shows the highest projected rainfall amount in all CLM scenario runs. Thus this event is an example for the impact of changes on intraseasonal timescales on long-term variability of the ISM in CLM data. This also supports results from Chapter 4, indicating that the strongest abrupt changes in rainfall over India are associated with changes on the intraseasonal time scale.

It is worth mentioning that results obtained here are not contradicting to other studies addressing active and break spells under future climate conditions, e.g. Sharmila et al. (2015) found changes in active and break spells with increased occurrence for both short breaks and short active phases in selected CMIP5 models. If similar changes of breaks and active spells would be present by the end of the century, no different trends in rainfall over northeastern and central India would be expected as the contribution of each cancels out the other. Results from this study indicate that asymmetric changes in breaks and active spells do not dominate long-term ISM variability. Thus, decadal scale ISM rainfall variability is mostly not associated with changes in the A-B regime in the future climate simulations discussed here.

Summary, Discussion & Outlook

6.1 Summary

In this thesis the spatial and temporal variability of the Indian Summer Monsoon under recent, paleo and future climate conditions is analyzed using well established global and regional climate models.

Findings from Sinha et al. (2011a) suggesting that abrupt changes of the ISM¹ during the past Millennium are associated with changes of active and break spells on the intraseasonal time scale revealed in proxy archives, motivated to test the following research question in this study:

TO WHICH EXTENT ARE ABRUPT CHANGES OF THE ISM UNDER PALEO AND FUTURE CLIMATE CONDITIONS RELATED TO CHANGES OF ACTIVE AND BREAK SPELLS ON THE INTRASEASONAL TIME SCALE?

To answer this question three main tasks are conducted:

Task 1 Validation	Are climate models (GCM/RCM) used in this study able to represent observed features of the intraseasonal variability of the ISM (active and break spells, northward propagation)?
Task 2 Paleoclimate	In how far are extreme phases of the ISM related to a dominant rainfall anomaly pattern during the Holocene. Is this associated with more active/break spells on the intraseasonal time scale?
Task 3 Future Climate	Are possible future changes of the ISM related to the same rainfall anomaly pattern and changes on the intraseasonal time scale?

¹Indian Summer Monsoon

A fixed AOGCM²-AGCM³-RCM⁴ model chain is used in this study. The advantage of using such a model chain is that long time periods are covered by the coarse resolved AOGCM, whereas interesting time periods can be simulated in a higher resolution using the AGCM or in an even higher resolution using the RCM. Thus, this approach takes into account that the representation of the Indian summer monsoon circulation and especially rainfall characteristics are depending on the model's resolution (Sperber et al., 1994; Abhik et al., 2014).

The AOGCM used in this study is COSMOS⁵, consisting of ECHAM5 for the atmosphere, MPI-OM for the ocean, JSBACH for vegetation and HAMOCC for ocean biochemistry (only used in some simulations). Consequently, AGCM simulations are carried out using ECHAM5 driven at its lower boundaries by ocean SST⁶s and SIC⁷s taken from the AOGCM simulations. Eventually, atmospheric fields from ECHAM5 are used to drive the RCM CLM⁸ at its lateral boundaries. AOGCM simulations with a resolution of T31L19 as well as AGCM simulations in T63L31 and RCM CLM simulations in a resolution of approximately 55 km are used. Due to computational costs the length of the simulations decrease with increasing resolution, meaning that AGCM simulations are limited to 200 years or less and CLM simulations to 30 years.

Task 1: Are climate models (GCM/RCM) used in this study able to represent observed features of the intraseasonal variability of the ISM (active and break spells, northward propagation)?

Chapter 3 addresses the first task about the validation of the models used in this study. Focus is put on the validation of the AGCM and RCM components used in this study as these are used to answer the main research question. Common features of the Indian summer monsoon on intraseasonal time scales include: active and break events and northward propagation of monsoon oscillations. It is shown that CLM is able to depict the seasonal cycle of rainfall over India but with a general underestimation of rainfall especially over northwestern India. The model shows positive skill in simulating dry and wet events on a weekly time scale as well as their spatio-temporal variability. Furthermore, it is shown that CLM is able to simulate the main observed circulation characteristics associated with dry and wet events (Befort et al., 2016). ECHAM5 has been extensively used to simulate the Indian summer monsoon under recent, paleo and future climate conditions and has already been positively evaluated with respect to several aspects (May, 2003; Polanski et al., 2014; Abhik et al., 2014). Thus, validation here is limited to the northward propagation of rainfall in

²Atmosphere-Ocean General Circulation Model

³Atmosphere-only General Circulation Model

⁴Regional Climate Model

⁵Community Earth System Models

⁶Sea Surface Temperatures

⁷Sea Ice Concentrations

⁸COSMO-CLM

the model, which is shown to be adequately simulated by ECHAM5 in T63L31, however, the northward propagation is limited to about 15° north. As all components of the model-chain can be positively validated, further analysis regarding changes on the intraseasonal time scale are meaningful. Coarse resolved AOGCM simulations are not analyzed with respect to northward propagation as these simulations are not to be expected to simulate this feature adequately, which has been the motivation to carry out higher resolved AGCM simulations.

Task 2: In how far are extreme phases of the ISM related to a dominant rainfall anomaly pattern during the Holocene. Is this associated with more active/break spells on the intraseasonal time scale?

Chapter 4 analyses in how far abrupt changes of the ISM during the Holocene can be attributed to changes in active and break spells on the intraseasonal time scale. This is motivated by results derived from proxy data from two locations, which show an abrupt shift at the same time but with opposite sign (Sinha et al., 2011a). One of these proxies is located over central India (CI), whereas the other one is located over northeastern India (NEI). Sinha et al. (2011a) hypothesizes that the opposite shifts in rainfall over NEI⁹ and CI¹⁰ suggest a rainfall dipole structure, which is well known to be associated with active and break phases of the monsoon on intraseasonal timescales.

To test in how far this hypothesis holds true for model data, an adapted algorithm based on a widely used method developed by Rajeevan et al. (2010) is used to identify active and break spells in global and regional model data. However, it is shown that this method is not suitable to detect years characterized by a dipole-like rainfall pattern over northeastern and central India. Thus, a different approach based on seasonal rainfall time series over NEI and CI is developed, where the choice of the regions is motivated by proxy locations used in Sinha et al. (2011a). It is shown that using both time series a rainfall dipole pattern on seasonal timescales is found, which is in turn associated with changes in active and break spells on the intraseasonal time scale for RCM and AGCM data.

Last Millennium

Based on 200 year AGCM simulations for the MCA¹¹, LIA¹² and REC¹³ the hypothesis is tested for the last Millennium. These simulations have been carried out within the HIMPAC project (Polanski et al., 2014) and are forced by SSTs and SICs from a fully-coupled AOGCM simulation covering the complete Millennium in a resolution of T31L19 (Jungclauss et al., 2010). The comparison of simulated rainfall with proxy data from the Indian subcontinent shows higher skill for the AGCM simulations in T63L31 compared to the coarser AOGCM simulation (Polanski et al., 2014). Unfortunately, the temporal resolution of the new proxy

⁹North-eastern India

¹⁰Central India

¹¹Medieval Climate Anomaly

¹²Little Ice Age

¹³Recent Climate

data generated within HIMPAC¹⁴ is too coarse to compare with results from the RCM simulations.

By analyzing rainfall rates over the Indian subcontinent, it is shown that about 50% of all abrupt changes identified in these AGCM simulations are associated with rainfall trends over CI and NEI with opposite signs. Thus, the hypothesis can be partly confirmed. Even though not all abrupt changes in ISM precipitation could be associated with changes on the intraseasonal time scale, results are encouraging. It should be mentioned that most changes in rainfall over India during the AGCM simulations are comparably small and changes are partly not significant, but the largest changes in AIMR¹⁵ can be related to changes in active and break spells.

Results obtained from AGCM simulations are further confirmed by CLM simulations. For each 200 year ECHAM5 time slice one dry and one wet period with a length of 30 years is selected and dynamically downscaled. As expected, abrupt changes associated with opposite rainfall trends over CI and NEI in ECHAM5 are also associated with a dominant rainfall dipole pattern in CLM.

Past 6000 years

To test the main hypothesis for the time period from the mid-Holocene until present a transient fully-coupled AOGCM simulation covering the past 6000 years in a resolution of T31L19 is analyzed (Fischer and Jungclaus, 2011). Here, abrupt changes of the ISM are not related to changes in rainfall over CI and NEI with opposite signs. This suggests that the mechanism from Sinha et al. (2011a) hypothesized for the last Millennium cannot be applied to the mid- to late Holocene climate. However, this could be also related to the coarse resolution of the AOGCM (see discussion in Section 6.2). Unfortunately, this could not be tested for this dataset as no daily data is available. The approach used here based on a model chain tries to overcome these issues by using higher resolved AGCM simulations (the general approach of using a GCM¹⁶ - RCM model chain is discussed in Section 6.2). Two higher resolved AGCM simulations for one abrupt change of AIMR in this dataset are carried out. However, they also do not reveal any dipole-like rainfall anomaly pattern similar to the results obtained for the fully-coupled AOGCM simulations. These AGCM simulations confirm that changes on the intraseasonal time scale play a minor role in determining this abrupt change and suggest that it might not be caused by the coarse resolution of the AOGCM.

As the main hypothesis could not be confirmed for abrupt changes found between 6000 years BP¹⁷ and present in this dataset, the two higher-resolved AGCM time slices for the dry event around 2ka BP and the wet event around 1.7ka BP are analyzed to find reasons for this abrupt change in monsoon precipitation over India. As changes in orbital parameters and

¹⁴HIMPAC - Himalaya: Modern and Past Climates

¹⁵All-Indian Monsoon Rainfall

¹⁶General Circulation Model

¹⁷Before Present

thus changes in incoming solar radiation are small between both time periods, the shift in precipitation over India is probably associated with changes in SSTs. Significant differences in SSTs are found over most ocean basins, including the North Atlantic, Pacific and Indian Ocean. Based on the 50 year simulations for 1.7ka BP and 2ka BP only, it is impossible to disentangle the effects of each ocean basin. Thus, sensitivity studies with different SSTs over different oceans are carried out to separate the effects of different lower boundary conditions over these regions on the Indian monsoon. It is found that changes over the North Atlantic Ocean have only minor influence, whereas a vast impact is revealed for different SSTs over the Pacific and Indian Ocean. Findings suggest that the position of the IPWP¹⁸ and the SSTs over the NARAB¹⁹ play a vital role in determining the abrupt change in ISM rainfall during this period. It could be shown that a shift of the position of the IPWP leads to a shift of the global monsoon circulation, with a westerly shift associated with a monsoon intensification. The SSTs over the northern Arabian sea influences the evaporation and thus moisture supply over this region. An enhanced atmospheric moisture content leads to an increased advection into the Indian subcontinent and thus rainfall over this region. Overall, it is found that especially dry conditions over India during the past 6000 years in the fully-coupled AOGCM simulation are associated with an simultaneous eastward shift of the IPWP and colder SSTs over the northern Arabian Sea. The potential impact of these findings on future model and proxy-based studies including favorable proxy locations is discussed in Section 6.3.

Task 3: Are possible future changes of the ISM related to the same rainfall anomaly pattern and changes on the intraseasonal time scale?

Projected future changes of the ISM are investigated under four different emission scenarios (Commitment, A1B, B1, A2). The respective CMIP3²⁰ COSMOS simulations as well as CLM simulations (Dobler and Ahrens, 2011) are analyzed. These CLM simulations are driven by the respective COSMOS simulation at its lateral boundaries. As all CLM simulations are forced by the first ensemble member of COSMOS, further analyses using COSMOS data are undertaken using the first ensemble member only.

Rainfall time series over all India (AIMR), CI and NEI are used to investigate in how far decadal fluctuations under increased GHG²¹ concentrations are related to changes in active and break spells. Similar to results obtained for the last Millennium, it is found that changes in active and break spells are not the major driver of ISM variability on decadal to multi-decadal time scales. However, some long-term variability could be associated with different trends in rainfall over central and northeastern India, which would have vast impact on India's society as especially agricultural products would be affected by an active-break regime shift.

¹⁸Indo-Pacific Warm Pool

¹⁹Northern Arabian Sea

²⁰Coupled Model Intercomparison Project 3

²¹Greenhouse Gas Concentrations

6.2 Discussion

Discussion of main Results

Results obtained in this study support the recent understanding of the Indian summer monsoon system, but give new insights into long-term variability, which should be taken into account for future paleoclimate studies from a model as well as proxy-based perspective.

To analyze in how far changes of the ISM can be investigated on the intraseasonal timescale using the regional climate model COSMO-CLM, a detailed validation of rainfall on subseasonal timescales has been carried out. It is found that mean climate rainfall characteristics are similar to those presented in Dobler and Ahrens (2010). A good agreement between observed and modeled active and break phases is found, which suggests that dry and wet conditions affecting India might be caused by large-scale circulation anomalies imposed by the driving model at the lateral boundaries. This confirms results from other RCM based studies analyzing the Indian summer monsoon intraseasonal variability (Bhaskaran et al., 1996, 1998). Bhaskaran et al. (1998) analyzed the ISV²² by applying an EOF²³ analysis on 850 hPa vorticity anomaly fields. The results suggest a strong relation between the PC²⁴s of the leading EOFs from the GCM and RCM, which they assume to be linked to the eastward propagating oscillation in the GCM. However, they also show that ISO²⁵s in the RCM are not always associated with those in the GCM. This is in line with results presented in this study showing some deviations between dry and wet phases in COSMO-CLM and ERA-Interim. The general agreement in simulating the rainfall pattern associated with ISOs between COSMO-CLM and its driving model has been also shown in case of ECHAM5 (see Figure 3.13 on page 58).

The advantage of using an RCM is based on its higher ability to simulate the spatial structures of rainfall (e.g. Bhaskaran et al. 1998). In this study it has been shown that COSMO-CLM is able to represent the main observed rainfall variability patterns (see Figure 3.7 on page 45). Another study using WRF model to analyze the ISV of ISM suggests reasonable agreement of the modeled and observed BSISO²⁶ (Kolusu et al., 2014). However, the simulation of the observed northward propagation is limited, which they link to the NCEP-II reanalysis used to drive WRF at its lateral boundaries (Kolusu et al., 2014). This again demonstrates that regional ISOs in the RCM are linked to its driving model. In this study, a general good agreement between observed and modeled ISOs is found which is, however, also limited in its northward propagation. The better agreement of the northward propagation to observations in this study compared to Kolusu et al. (2014) might also be associated with the good representation of ISOs in ERA-Interim.

²²intraseasonal variability

²³Empirical Orthogonal Function

²⁴Principal Component

²⁵intra-seasonal oscillation

²⁶Boreal Summer Intraseasonal Oscillations

The results for ECHAM5 suggest a good agreement in terms of northward propagation of ISOs in the model, the northward propagation is however limited, which is in line with other studies (Abhik et al., 2014). Overall, results support other studies showing that ECHAM5 is able to represent observed intraseasonal features of the ISM w.r.t. northward propagation (Sperber and Annamalai, 2008).

As presented in this study, some abrupt changes in ECHAM5 model data could be linked to different trends in rainfall over central and northeastern India and also the CLM simulations confirm a dipole-like rainfall pattern in some cases. As the dipole rainfall pattern on seasonal time-scales is linked to the occurrence in active and break spells, it could be concluded that changes on the intraseasonal time-scale cause shifts on multi-decadal timescales. This, to some extent, challenges the current understanding of the impact of ISV onto longer time-scales (Krishnamurthy and Shukla, 2000; Sperber et al., 2000; Krishnamurthy and Shukla, 2007).

Krishnamurthy and Shukla (2000) show in their study that seasonal mean rainfall anomalies are dominated by long-lasting seasonal patterns. The results are based on the fact that correlations between daily rainfall anomalies (after removing seasonal means) and seasonal mean rainfall anomalies are generally small, whereas the correlation between daily rainfall anomalies (including the seasonal mean) and seasonal mean rainfall anomalies is generally high. This indicates the existence of rainfall anomaly patterns, which persist throughout the season. There are some shortcomings using their method, as e.g. the seasonal mean rainfall pattern within a year with a high occurrence of breaks might be heavily influenced by these breaks. However, when computing daily rainfall anomalies by subtracting seasonal mean anomalies this "break pattern" will be automatically removed. Similar concerns regarding this method are raised by Goswami et al. (2006b). In a different study, Rajeevan et al. (2010) show that interannual variation is not mainly steered by interannual variations on the intraseasonal time-scale and Goswami and Mohan (2001) showed that seasonal rainfall is influenced by a shift in the occurrence of active and break phases. As stated above these different results with respect to the influence of ISOs on seasonal mean rainfall can be explained by the different methods used to separate the ISOs. Results presented in this thesis are based on seasonal mean rainfall anomalies over two different regions, however, it is shown that they are linked to shifts in active and break phases, which are defined by using the SPI²⁷. This means that the climatological seasonal cycle is removed but the seasonal mean anomalies are still included in the SPI time series. This could be a reason that results obtained here show an influence on the longer-term monsoon variability in contrast to some studies, e.g. Krishnamurthy and Shukla (2000) showing that the influence of changes in the ISV is small on interannual time-scales as the latter study also removed seasonal mean anomalies.

²⁷Standardized Precipitation Index

It is also important to note that in this thesis the impact of changes in the ISV onto multi-decadal to centennial time-scales has been investigated, rather than the relation to interannual variability. Thus, the hypothesis that abrupt changes on centennial time-scales (Sinha et al., 2011a) is steered by changes on the intraseasonal time-scale is not per se contradicting to the results from e.g. Krishnamurthy and Shukla (2000) showing that the influence of changes in the ISV is small on interannual time-scales. On interdecadal time-scales ENSO²⁸ is thought to play a major role (see Goswami (2006) and references therein), however, also intraseasonal oscillations are known to undergo inter-decadal changes in observations (Goswami, 2006). Goswami (2006) show that the amplitude of intraseasonal variability corresponds to the interdecadal variability of ENSO. This can be explained as there is a in phase relationship between ENSO and SSTs over the Indian Ocean on interdecadal time-scales (Goswami, 2006; their Figure 7.10a). The warmer SSTs over the equatorial Indian Ocean lead to enhanced convection over the tropical Indian Ocean and in turn to a suppression of convection over the Indian subcontinent with a decrease in ISO activity (Goswami, 2006). Similar results are also found by Zveryaev (2002), showing that the 30-60 day ISO are stronger over parts of the Indian Ocean due to increased SSTs over the Indian Ocean and weaker over the Indian subcontinent.

Overall, results presented in this thesis are valuable as it is the first time (up to the authors knowledge) that the hypothesis from Sinha et al. (2011a) has been tested using climate model data. Thus, this thesis might build the basis for a more in depth analysis of the impact on subseasonal time-scales on multi-decadal variability using e.g. recently developed reanalysis products covering the past century (see Section 6.3).

Results for centennial scale variability in an AOGCM simulation covering the past 6000 years suggest that abrupt changes in this model simulation are not linked to a dipole-like rainfall pattern over India. In other words the mechanism from Sinha et al. (2011a) hypothesised for the last Millennium is not valid for the mid- to late Holocene in this model simulation. This could potentially be related to the coarse resolution (horizontal & vertical) of the AOGCM, which might be not suitable to simulate intraseasonal features of the ISM. Abhik et al. (2014) support this hypothesis in their study about the sensitivity of the representation of the northward propagation of BSISO to the vertical resolution in ECHAM5. They showed that the models ability to simulate this feature is reduced if using 19 levels compared to using 31 levels. Thus, this might affect the coarse resolved AOGCM simulations analysed here as they do provide a resolution of T31L19. Furthermore, other studies have shown that finer spatial resolutions lead to an enhanced representation of spatial and temporal characteristics of the Indian summer monsoon (Sperber et al., 1994; Lal et al., 1997).

The approach used here based on a model chain tries to overcome these issue of resolution by using higher resolved AGCM simulations. Two higher resolved AGCM simulations

²⁸El Niño Southern Oscillation

are carried out for one abrupt change of AIMR in this dataset. Nevertheless, they do not reveal any dipole-like rainfall anomaly pattern similar to the results obtained from the fully-coupled AOGCM simulations. The AGCM simulations confirm that changes on the intraseasonal time scale play a minor role in determining this abrupt change in precipitation and suggest that it might not be caused by the coarse resolution of the AOGCM. However, it is worth mentioning that air-sea interactions are important for the representation of BSISO in climate models (Sharmila et al., 2013), which are not included in the AGCM simulations. A possibility to overcome the issue of carrying out long climate simulations in high resolution including air-sea interactions with limited computational costs is discussed in Section 6.3.

Further analyses focusing on potential mechanisms steering the long-term ISM variability in this model simulation, show that sea surface temperatures over the Arabian Sea as well as over the IPWP region have an impact on rainfall over India. These results support findings from Polanski et al. (2014) who found differences in SSTs over this region between the Medieval Climate Anomaly and the LIA. The results presented here go a step further compared to those shown in Polanski et al. (2014) by addressing the impact of changed sea surface temperatures over the Indian Ocean using model sensitivity experiments. The impact of Arabian Sea SSTs on the ISM rainfall has been already investigated by Ghosh et al. (1978); Levine and Turner (2012). Levine and Turner (2012) carried out idealised model simulation to analyse the impact of changed SST conditions over the Arabian Sea using the HadGEM3 model. Their findings that colder SSTs over this region lead to a reduction in rainfall over India are supported by sensitivity climate model simulation results presented in this thesis. The influence of the IPWP on rainfall over India is also pointed out by Annamalai et al. (2013). In their study, the decreasing rainfall trend over India during the recent decades is analysed and linked to increasing temperatures over the Indo-Pacific Warm Pool region. The results presented here are consistent with those from Annamalai et al. (2013) regarding the impact of the western Pacific SSTs. Annamalai et al. (2013) show that the warming trend over the IPWP region is associated with an east-west shift in precipitation with lower rainfall rates over India and wetter conditions over the western Pacific Ocean. This east-west shift in precipitation is also found in the model simulations here (see Figure 4.16 & Figure 4.15). Also an anomalous moisture transport from northerly direction into south east Asia is found in the dry compared to the wet phase (Figure 4.17), which seems in line with increased advection of dry into the south Asian monsoon as shown by Annamalai et al. (2013) (their Figure 4b). However, there are some substantial differences to the results presented in Annamalai et al. (2013) as SSTs are higher over the eastern Indian Ocean during the wet period, whereas trends in temperatures over the Indian Ocean and IPWP are in phase as shown in Annamalai et al. (2013). Furthermore, warmer SSTs over the equatorial Indian Ocean are thought to decrease ISO activity over India (see discussion above & Goswami 2006) and therefore decrease rainfall is expected, whereas an increase is

found in the analysed model simulations. This might be explained as the effect of the warm northern Arabian Sea outperforms the impact from the warmer SSTs over the Indian Ocean. Furthermore, Meehl and Arblaster (2002) showed that the impact of changed SSTs over the Indian Ocean is sensitive to the area where these anomalies are present. Anomalous conditions over the entire Indian Ocean north of 10° south more rainfall are linked with enhanced rainfall over India, whereas less rainfall is found if anomalies are only present close to the equator (Meehl and Arblaster, 2002). Thus, results presented in this thesis are in line with those from Meehl and Arblaster (2002) as SST differences between the dry and wet period are found also north of 10° north (Figure 4.14). An open question also remains about the cause of the changed SST conditions over the IPWP for a long time period. Annamalai et al. (2013) explain the observed trend in SST over the IPWP by increased GHG concentrations, but this cannot explain results shown in this thesis as GHG concentrations are fixed in the model simulation.

Besides these climate model based studies, the impact of sea surface temperatures is also pointed out in proxy-based studies. Prasad et al. (2014) found a relation between SSTs over the IPWP and rainfall over India in proxy data, with higher SSTs over the IPWP linked to drier conditions over the Indian subcontinent. This is basically in line with the results presented here, for which the dry phase of the Indian monsoon is linked with warmer SSTs around Papua New Guinea but colder conditions north of Indonesia. Another study analysing a marine proxy in the IPWP region during the past 70.000 years shows that salinity in this region is related to Dansgaard/Oeschger cycles over Greenland (Stott et al., 2002). This is accompanied by eastward and westward shifts of the atmospheric convection on millennial time-scales.

Based on the results obtained in this thesis, it is hypothesised that long-lasting dry and wet epochs over India are associated with a simultaneous shift of the IPWP and changed SSTs over the northern Arabian Sea. The reasons for changed rainfall rates over India are two-fold: firstly caused by an east-west shift of the monsoon circulation (anomalous Walker circulation) and secondly due to increased/decreased moisture supply over the Northern Arabian Sea, which is further advected into the Indian subcontinent leading to increased/decreased rainfall rates. The anomalous easterly moisture transport from the Pacific Ocean into the Bay of Bengal is thought to prevent moisture to be transported from the Bay of Bengal into the Pacific Ocean, leading to an enhanced moisture supply over the Bay of Bengal. The hypothesis by Annamalai et al. (2013) that the Rossby wave response due to enhanced convection over the IPWP caused advection of dry/cold air into the monsoon region and thus affecting rainfall over India can be partly confirmed. Impacts of changes in the local Hadley-Cell circulation seem to be only of secondary order (at least in this model simulation), as increased SSTs over the equatorial Indian Ocean are thought to lead to decreased rainfall amounts (see discussion above).

Methodology – AOGCM-AGCM-RCM Model Chain

It cannot be ruled out completely that long-lasting dry and wet periods are not steered by changes on the intraseasonal time-scale, even though no indications could be found in the climate model simulation covering the past 6000 years. Several studies show that the model resolution impacts the northward propagation in climate models (Sperber et al., 1994; Abhik et al., 2014). However, due to computational costs it hasn't been possible to carry out higher resolved coupled climate model simulations for the past 6000 years. It is tried to overcome this by running a higher resolved AGCM forced by SSTs and SICs from the coupled run for time periods selected from the coarse resolution run. However, results are similar w.r.t. the intraseasonal variability as no dominant dipole rainfall pattern could be found. It might be argued that this approach is not justified as the coupling between atmosphere and ocean is important for the representation and development of ISOs, which has been pointed out by several studies (Wang et al., 2009; Sharmila et al., 2013). Wang et al. (2009) showed that the inclusion of an interactive ocean model improves the representation of BSISOs over the Indian region. These findings are further supported by Sharmila et al. (2013). Thus, higher-resolved coupled climate model simulations for selected time-periods might be superior to analyse changes on intraseasonal timescales. However, this means that the climate evolution in these coupled-simulations are probably different to those in the coarse resolved model used to select time-periods if not externally driven by e.g. solar insolation changes. Similar limitations as discussed for the AGCM simulations apply for the regional climate model runs as an atmosphere-only model is used as well. Furthermore, the RCM results suggest similar findings to those obtained from the driving GCM. That means RCM simulations do not provide additional information if one is interested in analysing long-term changes of the Indian summer monsoon affecting the whole Indian subcontinent. However, if one is interested in local-scale changes RCMs are an important tool due to their higher resolution. A discussion about a refined methodology to tackle the question about changes of the ISM on intraseasonal time-scales during the Holocene is given in Section 6.3.

6.3 Outlook

It must be mentioned that an easy-to-apply proxy for the variability of active and break spells, based on time series of seasonal rainfall amounts over central India (CI) and north-eastern India (NEI) is used in this study. The advantage of this approach is the applicability to a huge range of model data, as usually sub-monthly rainfall amounts are not available for long model integrations, e.g. paleo simulations covering the past 6000 years or more. The reason for not using such an index is due to data availability, but also due to the hypothesis from Sinha et al. (2011a) which is based on regional rainfall time series. However, a method based on sub-monthly timescales including other variables describing, e.g. atmospheric circulation during active and break spells to detect a pure active/break signal in longer-term variability would be useful.

Next steps should include analyses aiming to understand what drives ISM shifts to a more active or break regime-type. This includes the investigations of impacts of SST anomalies on intraseasonal timescales, as done by e.g. Krishnan et al. (2006). Here, the method based on rainfall time series over CI and NEI could be valuable to further detect such intraseasonally driven ISM regime shifts.

As discussed in Section 6.2 the AOGCM - AGCM - RCM model chain is designed to overcome shortcomings in fully coupled model simulations due to their coarse resolution. However, air-sea interactions are important to represent intraseasonal features of the ISM. As it is not possible to carry out long simulations covering several thousands of years using a fully-coupled model in a high resolution the idea of simulating selected time-periods with a higher resolved model is appealing. A possible solution to obtain model simulations with high resolution and include air-sea interactions might be the usage of a model as described in Hirons et al. (2015). Hirons et al. (2015) present an atmosphere-only GCM, which is coupled to a mixed layer-thermodynamic ocean model for which salinity and temperature corrections must be prescribed. This means that variability modes as e.g. ENSO or AMO²⁹ cannot be represented as these rely on dynamical ocean processes. This might be even beneficial, if using the model within a model-chain, as the simulations could be constrained to a desired ocean state. Thus, it would be possible to select interesting time-periods based on a coarse resolved fully-coupled AOGCM and then simulate these periods in a higher resolution including air-sea interactions with state of the ocean being constrained, which cannot be warranted for a fully-coupled simulation.

Despite these potential shortcomings in the methodology, some part of decadal-scale ISM variability could be attributed to changes on the intraseasonal time-scale in paleo climate simulations as well as future climate projections. However, these results are based on model simulations only, which have their known deficits due to parameterizations and model resolutions. Decadal variability of the ISM is also found in observational datasets (Figure 1.5)

²⁹Atlantic Multi-decadal Oscillation

and it would be interesting to investigate in how far the observed variability is related to changes in active and break spells expressed in a prominent dipole rainfall pattern.

Whereas rainfall over India from 1871 is available from the IITM³⁰, common reanalysis data allowing to analyse changes in atmospheric circulation are only available since around 1950. Here, the recently developed 20th century reanalysis datasets from NOAA and ECMWF, namely NOAA-20CR (Compo et al., 2011) and ERA-20C (Poli et al., 2016), are helpful to analyse atmospheric changes associated with decadal fluctuations of ISM variability. If decadal-scale variability of the ISM is partly related to changes in active and break spells, it would have a huge impact on the Indian society. The distinct break/active spell rainfall anomaly pattern (dipole structure) would lead to regionally different impacts in terms of rainfall, e.g. persisting flood conditions over central India and drought conditions over northeastern India and vice versa over several decades. Considering this fact it is crucial to investigate mechanisms controlling the frequency and intensity of active and break spells from a seasonal to decadal perspective. In context of recent efforts of decadal prediction systems (<http://www.fona-miklip.de/>, Müller et al., 2012), an adequate representation of steering mechanisms in such a decadal prediction system could have a huge impact on mitigation and adaptation strategies over India.

CMIP5³¹ model simulations are available to analyse projected future changes of ISM variability and their relation to active and break spells. As shown by Menon et al. (2013), the response to increased CO_2 concentrations on the Indian monsoon rainfall is much more consistent in CMIP5 models compared to CMIP3 models, which increases our confidence in the reliability of results. As discussed, the model's ability to represent intraseasonal features of the ISM is crucial to obtain reliable results answering the question in how far changes on intraseasonal timescales affect long-term fluctuations. Here, the newest model generation (CMIP5) shows improved skill compared to older model versions (Sperber et al., 2013). Thus, expanding the analysis by further model simulations, especially carried out using the newest model generation would be necessary to achieve more reliable conclusions.

The findings of this thesis should be taken into account for further studies focusing on the ISM variability using both, model simulations as well as proxy archives. For the climate model scientific community it extends our knowledge about potential driver of longer-term Indian monsoon variability including the role of intraseasonal oscillations, surface conditions over the Indo-Pacific Warm Pool as well as the Arabian Sea. The proxy-archive scientific community could use the findings to select suitable regions for new proxy-archives. As intraseasonal variability is connected with a dipole pattern over northeastern and central India, a combination of proxies from both location might be useful to obtain robust signals of ISM variability (as done by Sinha et al., 2011a). Furthermore, combining marine proxies from the IPWP region, the Arabian Sea and terrestrial proxies from India is thought to be useful due to their teleconnections via a shift in the atmospheric circulation and its impact on rainfall over India.

³⁰Indian Institute of Tropical Meteorology

³¹Coupled Model Intercomparison Project 5

Bibliography

- Abhik, S., Mukhopadhyay, P., and Goswami, B. N. (2014). Evaluation of mean and intraseasonal variability of Indian summer monsoon simulation in ECHAM5: identification of possible source of bias. *Climate Dynamics*, 43(1):389–406. (Cited on pages 57, 59, 87, 120, 125, 126, and 129.)
- Ajayamohan, R. S. (2007). Simulation of South-Asian Summer Monsoon in a GCM. *Pure and Applied Geophysics*, 164(10):2117–2140. (Cited on page 32.)
- Annamalai, H., Hafner, J., Sooraj, K. P., and Pillai, P. (2013). Global Warming Shifts the Monsoon Circulation, Drying South Asia. *Journal of Climate*, 26(9):2701–2718. (Cited on pages 127 and 128.)
- Asharaf, S. and Ahrens, B. (2013). Soil-moisture memory in the regional climate model COSMO-CLM during the Indian summer monsoon season. *Journal of Geophysical Research-Atmospheres*, 118(12):6144–6151. (Cited on page 32.)
- Asharaf, S., Dobler, A., and Ahrens, B. (2012). Soil Moisture-Precipitation Feedback Processes in the Indian Summer Monsoon Season. *Journal of Hydrometeorology*, 13(5):1461–1474. (Cited on pages 32 and 33.)
- Ashok, K., Guan, Z. Y., and Yamagata, T. (2001). Impact of the Indian Ocean Dipole on the relationship between the Indian monsoon rainfall and ENSO. *Geophysical Research Letters*, 28(23):4499–4502. (Cited on pages 17, 18, 32, and 89.)
- Bai, J. and Perron, P. (2003). Computation and Analysis of Multiple Structural Change Models. *Journal of Applied Econometrics*, 18(1):1–22. (Cited on pages 66, 74, 78, 79, 106, 112, 115, 117, 154, and 157.)
- Basu, B. K. (2007). Diurnal variation in precipitation over India during the summer monsoon season: Observed and model predicted. *Monthly Weather Review*, 135(6):2155–2167. (Cited on pages 13 and 32.)
- Befort, D. J., Leckebusch, G. C., and Cubasch, U. (2016). Intraseasonal variability of the Indian summer monsoon: wet and dry events in COSMO-CLM. *Climate Dynamics*, pages 1–17. (Cited on pages 27, 29, and 120.)

- Berger, A. and Loutre, M. F. (1991). Insolation values for the climate of the last 10 million years. *Quaternary Science Reviews*, 10(4):297 – 317. (Cited on pages 28, 83, 84, 85, 154, and 155.)
- Berger, A. L. (1978). Long-Term Variations of Daily Insolation and Quaternary Climatic Changes. *Journal of the Atmospheric Sciences*, 35(12):2362–2367. (Cited on page 83.)
- Bhaskaran, B., Jones, R. G., Murphy, J. M., and Noguer, M. (1996). Simulations of the Indian summer monsoon using a nested regional climate model: Domain size experiments. *Climate Dynamics*, 12(9):573–587. (Cited on page 124.)
- Bhaskaran, B., Murphy, J. M., and Jones, R. G. (1998). Intraseasonal Oscillation in the Indian Summer Monsoon Simulated by Global and Nested Regional Climate Models. *Monthly Weather Review*, 126(12):3124–3134. (Cited on page 124.)
- Bhat, G. S. (2006). The Indian drought of 2002 - a sub-seasonal phenomenon? *Quarterly Journal of the Royal Meteorological Society*, 132(621):2583–2602. (Cited on pages 15 and 33.)
- Blanford, H. F. (1886). Rainfall of India. *Mem. India Meteorol. Dep.*, 2. (Cited on page 15.)
- Böhm, U., Kücken, M., Ahrens, W., Block, A., Hauffe, D., Keuler, K., Rockel, B., and Will, A. (2006). CLM - the climate version of LM: Brief description and long-term applications. *COSMO Newsletter*, 6:225–235. (Cited on page 35.)
- Braconnot, P., Loutre, M.-F., Dong, B., Joussaume, S., and Valdes, P. (2002). How the simulated change in monsoon at 6 ka BP is related to the simulation of the modern climate: results from the Paleoclimate Modeling Intercomparison Project. *Climate Dynamics*, 19(2):107–121. (Cited on page 63.)
- Braconnot, P., Otto-Bliesner, B., Harrison, S., Joussaume, S., Peterchmitt, J.-Y., Abe-Ouchi, A., Crucifix, M., Driesschaert, E., Fichefet, T., Hewitt, C. D., Kageyama, M., Kitoh, A., Laîné, A., Loutre, M.-F., Marti, O., Merkel, U., Ramstein, G., Valdes, P., Weber, S. L., Yu, Y., and Zhao, Y. (2007). Results of PMIP2 coupled simulations of the Mid-Holocene and Last Glacial Maximum - Part 1: experiments and large-scale features. *Climate of the Past*, 3(2):261–277. (Cited on page 62.)
- Cai, Y., Zhang, H., Cheng, H., An, Z., Edwards, R. L., Wang, X., Tan, L., Liang, F., Wang, J., and Kelly, M. (2012). The Holocene Indian monsoon variability over the southern Tibetan Plateau and its teleconnections. *Earth and Planetary Science Letters*, 335–336:135 – 144. (Cited on page 63.)

- Chabangborn, A., Brandefelt, J., and Wohlfarth, B. (2014). Asian monsoon climate during the Last Glacial Maximum: palaeo-data-model comparisons. *Boreas*, 43(1):220–242. (Cited on page 62.)
- Chen, G.-S., Liu, Z., and Kutzbach, J. E. (2014). Reexamining the barrier effect of the Tibetan Plateau on the South Asian summer monsoon. *Climate of the Past*, 10(3):1269–1275. (Cited on page 14.)
- Cheng, H., Fleitmann, D., Edwards, R. L., Wang, X., Cruz, F. W., Auler, A. S., Mangini, A., Wang, Y., Kong, X., Burns, S. J., and Matter, A. (2009). Timing and structure of the 8.2 kyr B.P. event inferred from $\delta^{18}\text{O}$ records of stalagmites from China, Oman, and Brazil. *Geology*, 37(11):1007–1010. (Cited on page 62.)
- Chokngamwong, R. and Chiu, L. S. (2008). Thailand daily rainfall and comparison with TRMM products. *Journal of Hydrometeorology*, 9(2):256–266. (Cited on pages 38 and 42.)
- Christensen, J. H., Hewitson, B., Busuioc, A., Chen, A., Gao, X., Held, I., Jones, R., Kolli, R. K., Kwon, W.-T., Laprise, R., Magaña Rueda, V., Mearns, L., Menéndez, C. G., Räisänen, J., Rinke, A., Sarr, A., and Whetton, P. (2007). *Climate Change 2007: The Physical Science Basis. Contribution of Working Group I to the Fourth Assessment Report of the Intergovernmental Panel on Climate Change*, chapter 11 Regional Climate Projections. Cambridge University Press, Cambridge, United Kingdom and New York, NY, USA. (Cited on page 110.)
- Clivar (2016). <http://www.clivar.org/asian-australian-monsoon>. accessed March 2016. (Cited on pages 14 and 151.)
- Compo, G. P., Whitaker, J. S., Sardeshmukh, P. D., Matsui, N., Allan, R. J., Yin, X., Gleason, B. E., Vose, R. S., Rutledge, G., Bessemoulin, P., Brönnimann, S., Brunet, M., Crouthamel, R. I., Grant, A. N., Groisman, P. Y., Jones, P. D., Kruk, M. C., Kruger, A. C., Marshall, G. J., Mauder, M., Mok, H. Y., Nordli, Ø., Ross, T. F., Trigo, R. M., Wang, X. L., Woodruff, S. D., and Worley, S. J. (2011). The Twentieth Century Reanalysis Project. *Quarterly Journal of the Royal Meteorological Society*, 137(654):1–28. (Cited on page 131.)
- Dallmeyer, A., Claussen, M., Fischer, N., Haberkorn, K., Wagner, S., Pfeiffer, M., Jin, L., Khon, V., Wang, Y., and Herzschuh, U. (2015). The evolution of sub-monsoon systems in the Afro-Asian monsoon region during the Holocene - comparison of different transient climate model simulations. *Climate of the Past*, 11(2):305–326. (Cited on pages 19 and 63.)
- Dallmeyer, A., Claussen, M., and Otto, J. (2010). Contribution of oceanic and vegetation feedbacks to Holocene climate change in monsoonal Asia. *Climate of the Past*, 6(2):195–218. (Cited on page 32.)

- Dash, S. K., Shekhar, M. S., and Singh, G. P. (2006). Simulation of Indian summer monsoon circulation and rainfall using RegCM3. *Theoretical and Applied Climatology*, 86(1):161–172. (Cited on page 33.)
- Dee, D. P., Uppala, S. M., Simmons, A. J., Berrisford, P., Poli, P., Kobayashi, S., Andrae, U., Balmaseda, M. A., Balsamo, G., Bauer, P., Bechtold, P., Beljaars, A. C. M., van de Berg, L., Bidlot, J., Bormann, N., Delsol, C., Dragani, R., Fuentes, M., Geer, A. J., Haimberger, L., Healy, S. B., Hersbach, H., Hólm, E. V., Isaksen, I., Kållberg, P., Köhler, M., Matricardi, M., McNally, A. P., Monge-Sanz, B. M., Morcrette, J. J., Park, B. K., Peubey, C., de Rosnay, P., Tavolato, C., Thépaut, J. N., and Vitart, F. (2011). The ERA-Interim reanalysis: configuration and performance of the data assimilation system. *Quarterly Journal of the Royal Meteorological Society*, 137(656, A):553–597. (Cited on pages 34 and 35.)
- Ding, Q. and Wang, B. (2005). Circumglobal Teleconnection in the Northern Hemisphere Summer. *Journal of Climate*, 18(17):3483–3505. (Cited on page 17.)
- Ding, Q. and Wang, B. (2007). Intraseasonal Teleconnection between the Summer Eurasian Wave Train and the Indian Monsoon. *Journal of Climate*, 20(15):3751–3767. (Cited on page 16.)
- Dixit, Y., Hodell, D. A., and Petrie, C. A. (2014a). Abrupt weakening of the summer monsoon in northwest India ~4100 yr ago. *Geology*, 42(4):339–342. (Cited on pages 7 and 9.)
- Dixit, Y., Hodell, D. A., Sinha, R., and Petrie, C. A. (2014b). Abrupt weakening of the Indian summer monsoon at 8.2 kyr B.P. *Earth and Planetary Science Letters*, 391:16 – 23. (Cited on page 62.)
- Dobler, A. and Ahrens, B. (2010). Analysis of the Indian summer monsoon system in the regional climate model COSMO-CLM. *Journal of Geophysical Research-Atmospheres*, 115:D16101. (Cited on pages 26, 32, 33, 53, and 124.)
- Dobler, A. and Ahrens, B. (2011). Four climate change scenarios for the Indian summer monsoon by the regional climate model COSMO-CLM. *Journal of Geophysical Research-Atmospheres*, 116:D24104. (Cited on pages 28, 29, 31, 32, 55, 109, 110, 111, 112, 113, 116, 118, and 123.)
- Feng, S. and Hu, Q. (2008). How the North Atlantic Multidecadal Oscillation may have influenced the Indian summer monsoon during the past two millennia. *Geophysical Research Letters*, 35(1):L01707. (Cited on page 89.)
- Fischer, N. and Jungclauss, J. H. (2011). Evolution of the seasonal temperature cycle in a transient Holocene simulation: orbital forcing and sea-ice. *Climate of the Past*, 7(4):1139–1148. (Cited on pages 28, 29, 82, 83, 89, 101, 107, 122, and 156.)

- Fleitmann, D., Burns, S. J., Mangini, A., Mudelsee, M., Kramers, J., Villa, I., Neff, U., Al-Subbary, A. A., Buettner, A., Hippler, D., and Matter, A. (2007). Holocene ITCZ and Indian monsoon dynamics recorded in stalagmites from Oman and Yemen (Socotra). *Quaternary Science Reviews*, 26:170 – 188. (Cited on page 63.)
- Fleitmann, D., Burns, S. J., Mudelsee, M., Neff, U., Kramers, J., Mangini, A., and Matter, A. (2003). Holocene Forcing of the Indian Monsoon Recorded in a Stalagmite from Southern Oman. *Science*, 300(5626):1737–1739. (Cited on pages 19 and 63.)
- Gadgil, S. (1995). Climate change and agriculture - An Indian perspective. *Current Science*, 69(8):649–659. (Cited on page 16.)
- Gadgil, S. (2003). The Indian Monsoon and Its Variability. *Annual Review of Earth and Planetary Sciences*, 31:429–467. (Cited on pages 15, 16, and 33.)
- Gadgil, S. and Sajani, S. (1998). Monsoon precipitation in the AMIP runs. *Climate Dynamics*, 14(9):659–689. (Cited on page 32.)
- Gerrity, J. P. (1992). A Note On Gandin and Murphy's Equitable Skill Score. *Monthly Weather Review*, 120(11):2709–2712. (Cited on page 36.)
- Ghosh, S. K., Pant, M. C., and Dewan, B. N. (1978). Influence of the Arabian Sea on the Indian summer monsoon. *Tellus*, 30(2):117–125. (Cited on pages 15, 108, and 127.)
- Gopinathan, C. K. and Sastry, J. S. (1990). Relationship between Indian summer monsoon rainfall and the position of Pacific Ocean Warm pool. *Indian Journal of Marine Sciences*, 19(4):246–250. (Cited on pages 64 and 90.)
- Goswami, B. N. (2005). *Intraseasonal Variability in the Atmosphere–Ocean Climate System*, chapter 2 South Asian monsoon. Springer-Verlag Berlin Heidelberg. (Cited on page 15.)
- Goswami, B. N. (2006). *The Asian Monsoon*, chapter 7 The Asian monsoon: Interdecadal variability, pages 295–328. Springer, Berlin Heidelberg. (Cited on pages 126 and 127.)
- Goswami, B. N., Ajayamohan, R. S., Xavier, P. K., and Sengupta, D. (2003). Clustering of synoptic activity by Indian summer monsoon intraseasonal oscillations. *Geophysical Research Letters*, 30(8). (Cited on page 15.)
- Goswami, B. N., Madhusoodanan, M. S., Neema, C. P., and Sengupta, D. (2006a). A physical mechanism for North Atlantic SST influence on the Indian summer monsoon. *Geophysical Research Letters*, 33(2). (Cited on pages 62 and 89.)
- Goswami, B. N. and Mohan, R. S. A. (2001). Intraseasonal Oscillations and Interannual Variability of the Indian Summer Monsoon. *Journal of Climate*, 14(6):1180–1198. (Cited on pages 20, 33, and 125.)

- Goswami, B. N., Wu, G., and Yasunari, T. (2006b). The Annual Cycle, Intraseasonal Oscillations, and Roadblock to Seasonal Predictability of the Asian Summer Monsoon. *Journal of Climate*, 19(20):5078–5099. (Cited on pages 20 and 125.)
- Graham, N. E., Ammann, C. M., Fleitmann, D., Cobb, K. M., and Luterbacher, J. (2011). Support for global climate reorganization during the "Medieval Climate Anomaly". *Climate Dynamics*, 37(5):1217–1245. (Cited on page 64.)
- Gupta, A. K., Anderson, D. M., and Overpeck, J. T. (2003). Abrupt changes in the Asian southwest monsoon during the Holocene and their links to the North Atlantic Ocean. *Nature*, 421:354–357. (Cited on pages 62 and 63.)
- Gupta, A. K., Das, M., and Anderson, D. M. (2005). Solar influence on the Indian summer monsoon during the Holocene. *Geophysical Research Letters*, 32(17):L17703. (Cited on page 63.)
- Hahn, D. G. and Manabe, S. (1975). The Role of Mountains in the South Asian Monsoon Circulation. *Journal of the Atmospheric Sciences*, 32(8):1515–1541. (Cited on page 14.)
- Hahn, D. G. and Shukla, J. (1976). Apparent Relationship Between Eurasian Snow Cover and Indian Monsoon Rainfall. *Journal of the Atmospheric Sciences*, 33(12):2461–2462. (Cited on page 32.)
- Hassan, M., Du, P., Jia, S., Iqbal, W., Mahmood, R., and Ba, W. (2015). An Assessment of the South Asian Summer Monsoon Variability for Present and Future Climatologies Using a High Resolution Regional Climate Model (RegCM4.3) under the AR5 Scenarios. *Atmosphere*, 6(11):1833–1857. (Cited on page 110.)
- Haywood, A. M., Ramstein, G., and Abe-Ouchi, A. (2011). Comparing structurally different climate models in a paleoenvironmental context. *Eos Trans. AGU*, 92(21):180–180. (Cited on page 62.)
- Hirons, L. C., Klingaman, N. P., and Woolnough, S. J. (2015). MetUM-GOML1: a near-globally coupled atmosphere–ocean–mixed-layer model. *Geoscientific Model Development*, 8(2):363–379. (Cited on page 130.)
- Huffman, G. J., Adler, R. F., Bolvin, D. T., Gu, G., Nelkin, E. J., Bowman, K. P., Hong, Y., Stocker, E. F., and Wolff, D. B. (2007). The TRMM Multisatellite Precipitation Analysis (TMPA): Quasi-Global, Multiyear, Combined-Sensor Precipitation Estimates at Fine Scales. *Journal of Hydrometeorology*, 8(1):38–55. (Cited on page 34.)
- Huffman, G. J., Adler, R. F., Morrissey, M. M., Bolvin, D. T., Curtis, S., Joyce, R., McGavock, B., and Susskind, J. (2001). Global Precipitation at One-Degree Daily Resolution from Multisatellite Observations. *Journal of Hydrometeorology*, 2(1):36–50. (Cited on page 34.)

- IITM (2016). <http://www.tropmet.res.in/~kolli/MOL/Monsoon/Historical/air.html>. accessed July 2016. (Cited on pages 17, 18, and 151.)
- IPCC Core Writing Team (2007). Climate Change: synthesis report. In Pachauri, RK and Reisinger, A, editor, *Contribution of Working Groups I, II and III to the Fourth Assessment Report of the Intergovernmental Panel on Climate Change*. IPCC, Geneva. (Cited on pages 111 and 156.)
- Jaeger, E. B., Stöckli, R., and Seneviratne, S. I. (2009). Analysis of planetary boundary layer fluxes and land-atmosphere coupling in the regional climate model CLM. *Journal of Geophysical Research-Atmospheres*, 114:D17106. (Cited on page 35.)
- Joussaume, S. and Taylor, K. (2000). The paleoclimate modeling intercomparison project. In Braconnot, P, editor, *The paleoclimate modeling intercomparison project (PMIP)*, Proceedings of the third PMIP workshop, pages 9–24, Canada, La Huardière. (Cited on page 62.)
- Joussaume, S., Taylor, K. E., Braconnot, P., Mitchell, J. F. B., Kutzbach, J. E., Harrison, S. P., Prentice, I. C., Broccoli, A. J., Abe-Ouchi, A., Bartlein, P. J., Bonfils, C., Dong, B., Guiot, J., Herterich, K., Hewitt, C. D., Jolly, D., Kim, J. W., Kislov, A., Kitoh, A., Loutre, M. F., Masson, V., McAvaney, B., McFarlane, N., de Noblet, N., Peltier, W. R., Peterschmitt, J. Y., Pollard, D., Rind, D., Royer, J. F., Schlesinger, M. E., Syktus, J., Thompson, S., Valdes, P., Vettoretti, G., Webb, R. S., and Wyputta, U. (1999). Monsoon changes for 6000 years ago: Results of 18 simulations from the Paleoclimate Modeling Intercomparison Project (PMIP). *Geophysical Research Letters*, 26(7):859–862. (Cited on pages 62 and 63.)
- Jungclaus, J. H., Lorenz, S. J., Timmreck, C., Reick, C. H., Brovkin, V., Six, K., Segschneider, J., Giorgetta, M. A., Crowley, T. J., Pongratz, J., Krivova, N. A., Vieira, L. E., Solanki, S. K., Klocke, D., Botzet, M., Esch, M., Gayler, V., Haak, H., Raddatz, T. J., Roeckner, E., Schnur, R., Widmann, H., Claussen, M., Stevens, B., and Marotzke, J. (2010). Climate and carbon-cycle variability over the last millennium. *Climate of the Past*, 6(5):723–737. (Cited on pages 27, 29, 65, 66, 105, and 121.)
- Kageyama, M., Merkel, U., Otto-Bliesner, B., Prange, M., Abe-Ouchi, A., Lohmann, G., Ohgaito, R., Roche, D. M., Singarayer, J., Swingedouw, D., and Zhang, X. (2013). Climatic impacts of fresh water hosing under Last Glacial Maximum conditions: a multi-model study. *Climate of the Past*, 9(2):935–953. (Cited on page 62.)
- Kessler, E. (1969). On the Distribution and Continuity of Water Substance in Atmospheric Circulation. *Meteor. Monogr.*, 10:88pp. (Cited on pages 26 and 35.)
- Kim, S. T., Yu, J.-Y., and Lu, M.-M. (2012). The distinct behaviors of Pacific and Indian Ocean warm pool properties on seasonal and interannual time scales. *Journal of Geophysical Research-Atmospheres*, 117:D05128. (Cited on pages 64 and 99.)

- Kolusu, S. R., Prasanna, V., and Preethi, B. (2014). Simulation of Indian Summer Monsoon Intra-seasonal Oscillations Using WRF Regional Atmospheric Model. *International Journal of Earth and Atmospheric Science*, 1(1):35–53. (Cited on page 124.)
- Kripalani, H. R., Oh, H. J., Kulkarni, A., Sabade, S. S., and Chaudhari, S. H. (2007). South Asian summer monsoon precipitation variability: Coupled climate model simulations and projections under IPCC AR4. *Theoretical and Applied Climatology*, 90(3):133–159. (Cited on page 109.)
- Kripalani, R. H. and Kumar, P. (2004). Northeast monsoon rainfall variability over south peninsular India vis-à-vis the Indian Ocean dipole mode. *International Journal of Climatology*, 24(10):1267–1282. (Cited on page 13.)
- Krishnamurthy, L. and Krishnamurthy, V. (2014). Decadal scale oscillations and trend in the Indian monsoon rainfall. *Climate Dynamics*, 43(1):319–331. (Cited on page 90.)
- Krishnamurthy, L. and Krishnamurthy, V. (2016). Teleconnections of Indian monsoon rainfall with AMO and Atlantic tripole. *Climate Dynamics*, 46(7):2269–2285. (Cited on page 89.)
- Krishnamurthy, V. and Goswami, B. N. (2000). Indian Monsoon-ENSO Relationship on Interdecadal Timescale. *Journal of Climate*, 13(3):579–595. (Cited on page 18.)
- Krishnamurthy, V. and Shukla, J. (2000). Intraseasonal and Interannual Variability of Rainfall over India. *Journal of Climate*, 13(24):4366–4377. (Cited on pages 20, 21, 44, 105, 125, 126, and 151.)
- Krishnamurthy, V. and Shukla, J. (2007). Intraseasonal and Seasonally Persisting Patterns of Indian Monsoon Rainfall. *Journal of Climate*, 20(1):3–20. (Cited on pages 20, 71, 105, and 125.)
- Krishnamurthy, V. and Shukla, J. (2008). Seasonal persistence and propagation of intraseasonal patterns over the Indian monsoon region. *Climate Dynamics*, 30(4):353–369. (Cited on page 20.)
- Krishnamurti, T. N. and Bhalme, H. N. (1976). Oscillations of a Monsoon System. Part I. Observational Aspects. *Journal of the Atmospheric Sciences*, 33(10):1937–1954. (Cited on page 15.)
- Krishnan, R., Kumar, V., Sugi, M., and Yoshimura, J. (2009). Internal Feedbacks from Monsoon-Midlatitude Interactions during Droughts in the Indian Summer Monsoon. *Journal of the Atmospheric Sciences*, 66(3):553–578. (Cited on pages 16, 32, 46, 47, and 51.)
- Krishnan, R., Ramesh, K. V., Samala, B. K., Meyers, G., Slingo, J. M., and Fennessy, M. J. (2006). Indian Ocean-monsoon coupled interactions and impending monsoon droughts. *Geophysical Research Letters*, 33(8). (Cited on page 130.)

- Krishnan, R. and Sugi, M. (2003). Pacific decadal oscillation and variability of the Indian summer monsoon rainfall. *Climate Dynamics*, 21(3):233–242. (Cited on page 90.)
- Krishnan, R., Zhang, C., and Sugi, M. (2000). Dynamics of Breaks in the Indian Summer Monsoon. *Journal of the Atmospheric Sciences*, 57(9):1354–1372. (Cited on page 16.)
- Kulkarni, A., Sabade, S. S., and Kripalani, R. H. (2009). Spatial variability of intra-seasonal oscillations during extreme Indian monsoons. *International Journal of Climatology*, 29(13):1945–1955. (Cited on page 15.)
- Kumar, K. K., Rajagopalan, B., and Cane, M. A. (1999). On the weakening relationship between the Indian monsoon and ENSO. *Science*, 284(5423):2156–2159. (Cited on page 18.)
- Kumar, K. K., Rajagopalan, B., Hoerling, M., Bates, G., and Cane, M. (2006). Unraveling the Mystery of Indian Monsoon Failure During El Niño. *Science*, 314:115–119. (Cited on page 18.)
- Kutzbach, J. E. and Otto-Bliesner, B. L. (1982). The sensitivity of the African-Asian Monsoonal Climate to Orbital Parameter Changes for 9000 Years B.P in a Low-Resolution General Circulation Model. *Journal of the Atmospheric Sciences*, 39(6):1177–1188. (Cited on page 63.)
- Laing, A. and Evans, J. L. (2011). Introduction to Tropical Meteorology. http://www.goes-r.gov/users/comet/tropical/textbook_2nd_edition/index.htm. (accessed July 2016). (Cited on page 95.)
- Lal, M., Cubasch, U., Perlwitz, J., and Waszkewitz, J. (1997). Simulation of the Indian Monsoon Climatology in ECHAM3 Climate Model: Sensitivity to Horizontal Resolution. *International Journal of Climatology*, 17(8):847–858. (Cited on page 126.)
- Levine, R. C. and Turner, A. G. (2012). Dependence of Indian monsoon rainfall on moisture fluxes across the Arabian Sea and the impact of coupled model sea surface temperature biases. *Climate Dynamics*, 38(11):2167–2190. (Cited on pages 15, 98, 108, and 127.)
- Liu, Y.-H., Henderson, G. M., Hu, C.-Y., Mason, A. J., Charnley, N., Johnson, K. R., and Xie, S.-C. (2013). Links between the East Asian monsoon and North Atlantic climate during the 8,200 year event. *Nature Geoscience*, 6(2):117–120. (Cited on page 62.)
- Lloyd-Hughes, B. and Saunders, M. A. (2002). A drought climatology for Europe. *International Journal of Climatology*, 22(13):1571–1592. (Cited on page 36.)
- Loschnigg, J. and Webster, P. J. (2000). A Coupled Ocean–Atmosphere System of SST Modulation for the Indian Ocean. *Journal of Climate*, 13(19):3342–3360. (Cited on pages 13 and 151.)

- Lucas-Picher, P., Christensen, J. H., Saeed, F., Kumar, P., Asharaf, S., Ahrens, B., Wiltshire, A. J., Jacob, D., and Hagemann, S. (2011). Can Regional Climate Models Represent the Indian Monsoon? *Journal of Hydrometeorology*, 12(5):849–868. (Cited on pages 32 and 33.)
- Mandke, S. K., Sahai, A. K., Shinde, M. A., Joseph, S., and Chattopadhyay, R. (2007). Simulated changes in active/break spells during the Indian summer monsoon due to enhanced CO₂ concentrations: assessment from selected coupled atmosphere-ocean global climate models. *International Journal of Climatology*, 27(7):837–859. (Cited on page 110.)
- Marsland, S. J., Haak, H., Jungclaus, J. H., Latif, M., and Röske, F. (2003). The Max-Planck-Institute global ocean/sea ice model with orthogonal curvilinear coordinates. *Ocean Modelling*, 5(2):91 – 127. (Cited on page 25.)
- Marzin, C., Kallel, N., Kageyama, M., Duplessy, J.-C., and Braconnot, P. (2013). Glacial fluctuations of the Indian monsoon and their relationship with North Atlantic climate: new data and modelling experiments. *Climate of the Past*, 9(5):2135–2151. (Cited on page 62.)
- Masumoto, Y. and Yamagata, T. (1991). On the Origin of a Model ENSO in the Western Pacific. *Journal of the Meteorological Society of Japan. Ser. II*, 69(2):197–207. (Cited on page 18.)
- May, W. (2004). Simulation of the variability and extremes of daily rainfall during the Indian summer monsoon for present and future times in a global time-slice experiment. *Climate Dynamics*, 22(2):183–204. (Cited on pages 32 and 109.)
- May, W. (2011). The sensitivity of the Indian summer monsoon to a global warming of 2°C with respect to pre-industrial times. *Climate Dynamics*, 37(9):1843–1868. (Cited on pages 32 and 109.)
- May, W. H. (2003). The Indian Summer Monsoon and its Sensitivity to the Mean SSTs: Simulations with the ECHAM4 AGCM at T106 Horizontal Resolution. *Journal of the Meteorological Society of Japan*, 81(1):57–83. (Cited on pages 32 and 120.)
- Meehl, G. A. (1997). The South Asian Monsoon and the Tropospheric Biennial Oscillation. *Journal of Climate*, 10(8):1921–1943. (Cited on page 17.)
- Meehl, G. A. and Arblaster, J. M. (2002). Indian Monsoon GCM Sensitivity Experiments Testing Tropospheric Biennial Oscillation Transition Conditions. *Journal of Climate*, 15(9):923–944. (Cited on pages 64 and 128.)
- Meehl, G. A. and Arblaster, J. M. (2003). Mechanisms for projected future changes in south Asian monsoon precipitation. *Climate Dynamics*, 21(7):659–675. (Cited on page 110.)

- Menon, A., Levermann, A., Schewe, J., Lehmann, J., and Frieler, K. (2013). Consistent increase in Indian monsoon rainfall and its variability across CMIP-5 models. *Earth System Dynamics*, 4(2):287–300. (Cited on pages 109, 110, and 131.)
- Mooley, D. A. and Parthasarathy, B. (1984). Fluctuations in All-India summer monsoon rainfall during 1871–1978. *Climatic Change*, 6(3):287–301. (Cited on page 17.)
- Müller, W. A., Baehr, J., Haak, H., Jungclaus, J. H., Kröger, J., Matei, D., Notz, D., Pohlmann, H., von Storch, J. S., and Marotzke, J. (2012). Forecast skill of multi-year seasonal means in the decadal prediction system of the Max Planck Institute for Meteorology. *Geophysical Research Letters*, 39(22). (Cited on page 131.)
- Nakicenovic, N., Alcamo, J., Davis, G., de Vries, B., Fenhann, J., Gaffin, S., Gregory, K., Grübler, A., Jung, T. Y., Kram, T., La Rovere, E. L., Michaelis, L., Mori, S., Morita, T., Pepper, W., Pitcher, H., Price, L., Riahi, K., Roehrl, A., Rogner, H.-H., Sankovski, A., Schlesinger, M., Shukla, P., Smith, S., Swart, R., van Rooijen, S., Victor, N., and Dadi, Z. (2000). *Special Report on Emissions Scenarios*. Cambridge University Press. (Cited on page 28.)
- Nguyen, K. C. and McGregor, J. L. (2009). Modelling the Asian summer monsoon using CCAM. *Climate Dynamics*, 32(2):219–236. (Cited on page 32.)
- Niu, X., Wang, S., Tang, J., Lee, D.-K., Gutowski, W., Dairaku, K., McGregor, J., Katzfey, J., Gao, X., Wu, J., Hong, S., Wang, Y., and Sasaki, H. (2015). Projection of Indian summer monsoon climate in 2041-2060 by multiregional and global climate models. *Journal of Geophysical Research-Atmospheres*, 120(5):1776–1793. (Cited on page 110.)
- Overpeck, J., Anderson, D., Trumbore, S., and Prell, W. (1996). The southwest Indian Monsoon over the last 18 000 years. *Climate Dynamics*, 12(3):213–225. (Cited on pages 62 and 63.)
- Parthasarathy, B., Munot, A. A., and Kothawale, D. R. (1994). All-India monthly and seasonal rainfall series: 1871–1993. *Theoretical and Applied Climatology*, 49(4):217–224. (Cited on page 18.)
- Polanski, S., Fallah, B., Befort, D. J., Prasad, S., and Cubasch, U. (2014). Regional moisture change over India during the past Millennium: A comparison of multi-proxy reconstructions and climate model simulations. *Global and Planetary Change*, (122):176–185. (Cited on pages 15, 27, 29, 65, 66, 105, 106, 108, 120, 121, and 127.)
- Polanski, S., Rinke, A., Dethloff, K., Lorenz, S., Wang, Y., and Herzsuh, U. (2012). Simulation and Comparison Between Mid-Holocene and Preindustrial Indian Summer Monsoon Circulation Using a Regional Climate Model. *The Open Atmospheric Science Journal*, 6(1):42–48. (Cited on page 63.)

- Poli, P., Hersbach, H., Dee, D. P., Berrisford, P., Simmons, A. J., Vitart, F., Laloyaux, P., Tan, D. G. H., Peubey, C., Thépaut, J.-N., Trémolet, Y., Hólm, E. V., Bonavita, M., Isaksen, L., and Fisher, M. (2016). ERA-20C: An Atmospheric Reanalysis of the Twentieth Century. *Journal of Climate*, 29(11):4083–4097. (Cited on page 131.)
- Prasad, S., Anoop, A., Riedel, N., Sarkar, S., Menzel, P., Basavaiah, N., Krishnan, R., Fuller, D., Plessen, B., Gaye, B., Röhl, U., Wilkes, H., Sachse, D., Sawant, R., Wiesner, M. G., and Stebich, M. (2014). Prolonged monsoon droughts and links to Indo-Pacific warm pool: A Holocene record from Lonar Lake, central India. *Earth and Planetary Science Letters*, 391:171 – 182. (Cited on pages 19, 63, 64, 108, and 128.)
- Prasad, S. and Enzel, Y. (2006). Holocene paleoclimates of India. *Quaternary Research*, 66(3):442 – 453. (Cited on page 62.)
- Prömmel, K., Cubasch, U., and Kaspar, F. (2013). A regional climate model study of the impact of tectonic and orbital forcing on African precipitation and vegetation. *Palaeogeography, Palaeoclimatology, Palaeoecology*, 369:154 – 162. (Cited on page 26.)
- Raddatz, T. J., Reick, C. H., Knorr, W., Kattge, J., Roeckner, E., Schnur, R., Schnitzler, K.-G., Wetzell, P., and Jungclaus, J. (2007). Will the tropical land biosphere dominate the climate–carbon cycle feedback during the twenty-first century? *Climate Dynamics*, 29(6):565–574. (Cited on page 25.)
- Rajeevan, M., Gadgil, S., and Bhate, J. (2010). Active and break spells of the Indian summer monsoon. *Journal of Earth System Science*, 119(3):229–247. (Cited on pages 15, 16, 66, 67, 71, 74, 76, 78, 79, 105, 121, 125, and 151.)
- Ramaswamy, C. (1962). Breaks in the Indian summer monsoon as a phenomenon of interaction between the easterly and the sub-tropical westerly jet streams. *Tellus*, 14(3):337–349. (Cited on page 16.)
- Ramesh, R. (2001). High resolution Holocene monsoon records from different proxies: An assessment of their consistency. *Current Science*, 81(11):1432–1436. (Cited on page 64.)
- Rao, G. S. L. H. V. P. (2008). *Agricultural meteorology*. PHI Learning, Dehli. ISBN-978-81-203-3338-3. (Cited on pages 13 and 15.)
- Rehfeld, K., Marwan, N., Breitenbach, S. F. M., and Kurths, J. (2013). Late Holocene Asian summer monsoon dynamics from small but complex networks of paleoclimate data. *Climate Dynamics*, 41(1):3–19. (Cited on page 63.)
- Ritter, B. and Geleyn, J.-F. (1992). A Comprehensive Radiation Scheme For Numerical Weather Prediction Models With Potential Applications In Climate Simulations. *Monthly Weather Review*, 120(2):303–325. (Cited on pages 26 and 35.)

- Roeckner, E., Bäuml, G., Bonaventura, L., Brokopf, R., Esch, M., Giorgetta, M., Hagemann, S., Kirchner, I., Kornblueh, L., Manzini, E., Rhodin, A., Schlese, U., Schulzweida, U., and Tompkins, A. (2003). The atmospheric general circulation model ECHAM 5. PART I: Model description. Report No 349, Max Planck Institute for Meteorology. (Cited on page 25.)
- Roeckner, E., Lautenschlager, M., and Schneider, H. (2006a). IPCC-AR4 MPI-ECHAM5_T63L31 MPI-OM_GR1.5L40 20C3M run no.1: atmosphere 6 HOUR values MPImet/MaD Germany. (Cited on page 29.)
- Roeckner, E., Lautenschlager, M., and Schneider, H. (2006b). IPCC-AR4 MPI-ECHAM5_T63L31 MPI-OM_GR1.5L40 SRESA1B run no.1: atmosphere 6 HOUR values MPImet/MaD Germany. (Cited on page 29.)
- Roeckner, E., Lautenschlager, M., and Schneider, H. (2006c). IPCC-AR4 MPI-ECHAM5_T63L31 MPI-OM_GR1.5L40 SRESA2 run no.1: atmosphere 6 HOUR values MPImet/MaD Germany. (Cited on page 29.)
- Roeckner, E., Lautenschlager, M., and Schneider, H. (2006d). IPCC-AR4 MPI-ECHAM5_T63L31 MPI-OM_GR1.5L40 SRESB1 run no.1: atmosphere 6 HOUR values MPImet/MaD Germany. (Cited on page 29.)
- Saeed, F., Hagemann, S., and Jacob, D. (2009). Impact of irrigation on the South Asian summer monsoon. *Geophysical Research Letters*, 36(20):L20711. (Cited on page 33.)
- Schneider, T., Bischoff, T., and Haug, G. H. (2014). Migrations and dynamics of the intertropical convergence zone. *Nature*, 513(7516):45–53. (Cited on pages 19 and 151.)
- Sharmila, S., Joseph, S., Sahai, A. K., Abhilash, S., and Chattopadhyay, R. (2015). Future projection of Indian summer monsoon variability under climate change scenario: An assessment from CMIP5 climate models. *Global and Planetary Change*, 124:62 – 78. (Cited on pages 110 and 118.)
- Sharmila, S., Pillai, P. A., Joseph, S., Roxy, M., Krishna, R. P. M., Chattopadhyay, R., Abhilash, S., Sahai, A. K., and Goswami, B. N. (2013). Role of ocean–atmosphere interaction on northward propagation of Indian summer monsoon intra-seasonal oscillations (MISO). *Climate Dynamics*, 41(5):1651–1669. (Cited on pages 127 and 129.)
- Shukla, J. and Paolino, D. A. (1983). The Southern Oscillation and Long-Range Forecasting of the Summer Monsoon Rainfall over India. *Monthly Weather Review*, 111(9):1830–1837. (Cited on page 17.)

- Sijikumar, S., John, L., and Manjusha, K. (2013). Sensitivity study on the role of Western Ghats in simulating the Asian summer monsoon characteristics. *Meteorology and Atmospheric Physics*, 120(1):53–60. (Cited on page 14.)
- Sinha, A., Berkelhammer, M., Stott, L., Mudelsee, M., Cheng, H., and Biswas, J. (2011a). The leading mode of Indian Summer Monsoon precipitation variability during the last millennium. *Geophysical Research Letters*, 38(15):L15703. (Cited on pages 7, 9, 19, 20, 21, 64, 66, 69, 71, 73, 74, 76, 78, 80, 87, 105, 106, 119, 121, 122, 126, 130, 131, 151, and 154.)
- Sinha, A., Stott, L., Berkelhammer, M., Cheng, H., Edwards, R. L., Buckley, B., Aldenderfer, M., and Mudelsee, M. (2011b). A global context for megadroughts in monsoon Asia during the past millennium. *Quaternary Science Reviews*, 30(1–2):47 – 62. (Cited on pages 63 and 64.)
- Slingo, J. and Annamalai, H. (2000). 1997: The El Niño of the century and the response of the Indian summer monsoon. *Monthly Weather Review*, 128(6):1778–1797. (Cited on page 17.)
- Sontakke, N. A. and Singh, N. (1996). Longest instrumental regional and all-India summer monsoon rainfall series using optimum observations: reconstruction and update. *Holocene*, 6(3):315–331. (Cited on page 44.)
- Sperber, K. R. and Annamalai, H. (2008). Coupled model simulations of boreal summer intraseasonal (30–50) day variability, Part 1: Systematic errors and caution on use of metrics. *Climate Dynamics*, 31(2):345–372. (Cited on pages 20, 59, and 125.)
- Sperber, K. R., Annamalai, H., Kang, I.-S., Kitoh, A., Moise, A., Turner, A., Wang, B., and Zhou, T. (2013). The Asian summer monsoon: an intercomparison of CMIP5 vs. CMIP3 simulations of the late 20th century. *Climate Dynamics*, 41(9):2711–2744. (Cited on pages 20 and 131.)
- Sperber, K. R., Hameed, S., Potter, G. L., and Boyle, J. S. (1994). Simulation of the Northern Summer Monsoon in the ECMWF Model: Sensitivity to Horizontal Resolution. *Monthly Weather Review*, 122(11):2461–2481. (Cited on pages 120, 126, and 129.)
- Sperber, K. R., Slingo, J. M., and Annamalai, H. (2000). Predictability and the relationship between subseasonal and interannual variability during the Asian summer monsoon. *Quarterly Journal of the Royal Meteorological Society*, 126(568):2545–2574. (Cited on pages 33 and 125.)

- Srinivas, C. V., Hariprasad, D., Bhaskar Rao, D. V., Anjaneyulu, Y., Baskaran, R., and Venkaraman, B. (2013). Simulation of the Indian summer monsoon regional climate using advanced research WRF model. *International Journal of Climatology*, 33(5):1195–1210. (Cited on pages 32, 33, and 54.)
- Stott, L., Poulsen, C., Lund, S., and Thunell, R. (2002). Super ENSO and Global Climate Oscillations at Millennial Time Scales. *Science*, 297(5579):222–226. (Cited on page 128.)
- Suhas, E., Neena, J. M., and Goswami, B. N. (2013). An Indian monsoon intraseasonal oscillations (MISO) index for real time monitoring and forecast verification. *Climate Dynamics*, 40(11-12):2605–2616. (Cited on pages 15, 33, 36, 39, 40, 53, and 56.)
- Thamban, M., Kawahata, H., and Rao, V. P. (2007). Indian summer monsoon variability during the holocene as recorded in sediments of the Arabian Sea: Timing and implications. *Journal of Oceanography*, 63(6):1009–1020. (Cited on page 63.)
- Thomas, B., Kasture, S. V., and Satyan, V. (2000). Sensitivity of Asian summer monsoon and tropical circulations to 1987 and 1988 sea surface temperature anomalies. *Atmósfera*, 13(3):147–166. (Cited on page 95.)
- Tian, S.-F. and Yasunari, T. (1992). Time and Space Structure of Interannual Variations in Summer Rainfall over China. *Journal of the Meteorological Society of Japan*, 70(1B):585–596. (Cited on page 17.)
- Tiedtke, M. (1989). A Comprehensive Mass Flux Scheme For Cumulus Parameterization In Large-scale Models. *Monthly Weather Review*, 117(8):1779–1800. (Cited on pages 26 and 35.)
- Turner, A. G. and Slingo, J. M. (2009a). Subseasonal extremes of precipitation and active-break cycles of the Indian summer monsoon in a climate-change scenario. *Quarterly Journal of the Royal Meteorological Society*, 135(640):549–567. (Cited on pages 36, 53, 109, and 110.)
- Turner, A. G. and Slingo, J. M. (2009b). Uncertainties in future projections of extreme precipitation in the Indian monsoon region. *Atmospheric Science Letters*, 10(3):152–158. (Cited on page 109.)
- Ueda, H., Iwai, A., Kuwako, K., and Hori, M. E. (2006). Impact of anthropogenic forcing on the Asian summer monsoon as simulated by eight GCMs. *Geophysical Research Letters*, 33(6):L06703. (Cited on page 109.)
- United Nations (2015). *World population prospects: The 2015 revision, key findings and advance tables*. Department of Economic and Social Affairs, Population Division, United Nations, New York, USA. (Cited on pages 7 and 9.)

- Uppala, S. M., Kållberg, P. W., Simmons, A. J., Andrae, U., Da Costa Bechtold, V., Fiorino, M., Gibson, J. K., Haseler, J., Hernandez, A., Kelly, G. A., Li, X., Onogi, K., Saarinen, S., Sokka, N., Allan, R. P., Andersson, E., Arpe, K., Balmaseda, M. A., Beljaars, A. C. M., Van De Berg, L., Bidlot, J., Bormann, N., Caires, S., Chevallier, F., Dethof, A., Dragosavac, M., Fisher, M., Fuentes, M., Hagemann, S., Hólm, E., Hoskins, B. J., Isaksen, L., Janssen, P. A. E. M., Jenne, R., McNally, A. P., Mahfouf, J.-F., Morcrette, J.-J., Rayner, N. A., Saunders, R. W., Simon, P., Sterl, A., Trenberth, K. E., Untch, A., Vasiljevic, D., Viterbo, P., and Woollen, J. (2005). The ERA-40 re-analysis. *Quarterly Journal of the Royal Meteorological Society*, 131(612):2961–3012. (Cited on page 32.)
- Valcke, S. (2013). The OASIS3 coupler: a European climate modelling community software. *Geoscientific Model Development*, 6(2):373–388. (Cited on page 25.)
- Wang, B. (2006). *The Asian Monsoon*. Springer, Berlin Heidelberg. (Cited on page 32.)
- Wang, B., Kang, I. S., and Lee, J. Y. (2004). Ensemble Simulations of Asian-Australian Monsoon Variability by 11 AGCMs. *Journal of Climate*, 17(4):803–818. (Cited on page 32.)
- Wang, B., Wu, R. G., and Li, T. (2003). Atmosphere-Warm Ocean Interaction and Its Impacts on Asian-Australian Monsoon Variation. *Journal of Climate*, 16(8):1195–1211. (Cited on page 32.)
- Wang, W., Chen, M., and Kumar, A. (2009). Impacts of Ocean Surface on the Northward Propagation of the Boreal Summer Intraseasonal Oscillation in the NCEP Climate Forecast System. *Journal of Climate*, 22(24):6561–6576. (Cited on page 129.)
- Webster, P. J., Magaña, V. O., Palmer, T. N., Shukla, J., Tomas, R. A., Yanai, M., and Yasunari, T. (1998). Monsoons: Processes, predictability, and the prospects for prediction. *Journal of Geophysical Research*, 103(C7):14451–14510. (Cited on pages 17 and 90.)
- Wetzel, P., Maier-Reimer, E., Botzet, M., Jungclaus, J., Keenlyside, N., and Latif, M. (2006). Effects of Ocean Biology on the Penetrative Radiation in a Coupled Climate Model. *Journal of Climate*, 19(16):3973–3987. (Cited on page 25.)
- Wu, H., Svoboda, M. D., Hayes, M. J., Wilhite, D. A., and Wen, F. (2007). Appropriate application of the Standardized Precipitation Index in arid locations and dry seasons. *International Journal of Climatology*, 27(1):65–79. (Cited on page 44.)
- Yasunari, T. (1990). Impact of Indian monsoon on the coupled atmosphere/ocean system in the tropical pacific. *Meteorology and Atmospheric Physics*, 44(1):29–41. (Cited on pages 17 and 18.)

- Yatagai, A., Kamiguchi, K., Arakawa, O., Hamada, A., Yasutomi, N., and Kitoh, A. (2012). APHRODITE: Constructing a Long-Term Daily Gridded Precipitation Dataset for Asia Based on a Dense Network of Rain Gauges. *Bulletin of the American Meteorological Society*, 93(9):1401–1415. (Cited on page 34.)
- Zheng, Y., Singarayer, J. S., Cheng, P., Yu, X., Liu, Z., Valdes, P. J., and Pancost, R. D. (2014). Holocene variations in peatland methane cycling associated with the Asian summer monsoon system. *Nature Communications*, 5. (Cited on page 63.)
- Zveryaev, I. I. (2002). Interdecadal changes in the zonal wind and the intensity of intraseasonal oscillations during boreal summer Asian monsoon. *Tellus A*, 54(3):288–298. (Cited on page 126.)

List of Figures

1.1	Schematic model of the a) boreal summer and b) winter monsoon system and mean surface winds (black arrows) and their associated Ekman transports (gray arrow). (taken from Loschnigg and Webster (2000), their Figure 13)	13
1.2	Mean summer circulation and its associated atmospheric flow (taken from Clivar, 2016)	14
1.3	Rainfall composite anomaly (mm) during dry spells (left panel) and wet spells (right panel). Figures are taken and adapted from Rajeevan et al. (2010).	16
1.4	All-India Summer Monsoon (June-September) Rainfall (AISMR) Anomalies during 1871-2015. Rainfall anomalies are given relative to its long-term mean (taken from IITM, 2016).	17
1.5	All-India Summer Monsoon (June-September) Rainfall (AISMR) Anomalies during 1871-2015 smoothed using a 31 year running mean (taken from IITM, 2016).	18
1.6	Temporal evolution of the temperature contrast between the extra-tropics of the Northern and Southern hemispheres (black lines) a proxy for runoff into Cariaco (red line) and a proxy of Indian monsoon rainfall (blue line) (adapted from Schneider et al. (2014)). For further information about the proxies and derived indices please refer to Schneider et al. (2014).	19
1.7	$\delta^{18}O$ timeseries for proxy located in northeastern India (blue), proxy located in central India (green) and in the Arabian Sea (orange) (Figure from Sinha et al. (2011a), their Figure 3). For further information about proxy locations and methods used please refer to Sinha et al. (2011a).	21
1.8	"EOF 1 of (a) standardised daily anomalies (5-day running means) and (b) standardised seasonal anomalies of rainfall for JJAS of the 1901–70 period. Positive contours are shaded." (Krishnamurthy and Shukla, 2000; their Figure 6)	21
1.9	Schematic overview of model chain used in this study.	23

2.1	Domain of COSMO-CLM simulations used in this study + height of topography (shaded). Red line indicates boundaries of AIMR ³² region.	26
3.1	Mean rainfall during JJAS [mm/d] (1979-2007) for a) Aphrodite, b) COSMO-CLM and c) difference between COSMO-CLM and Aphrodite.	34
3.2	Climatological daily precipitation (1979-2009) over India (AIMR) for Aphrodite, ERA-Interim reanalysis data as well as COSMO-CLM simulation data. Rainfall amounts are smoothed with a 10-day running mean filter.	38
3.3	Taylor diagram for precipitation anomalies for: COSMO-CLM, ERA-Interim, TRMM and GPCP. Analysis are performed for AIMR for 1979 until 2007 (ERA-Interim and COSMO-CLM only) as well as 1998 until 2007 (all datasets) with Aphrodite as reference dataset. The filled dot gives the results for precipitation over whole India (AIMR)	39
3.4	Cross-Correlation of zonally average precipitation (for longitudinal section between 70°-100°) against a reference point near 85° east and 12.5° north for a) GPCP, b) ERA-Interim and c) COSMO-CLM.	40
3.5	Summer season 2002 LMISO phase diagram for a) GPCP, b) ERA-Interim and c) COSMO-CLM.	41
3.6	Summer season 2005 LMISO phase diagram for a) GPCP, b) ERA-Interim and c) COSMO-CLM.	41
3.7	SPI EOF loading patterns, based on weekly JJAS precipitation amount from 1979 until 2009, derived for Aphrodite, ERA-Interim and COSMO-CLM. The values within the square brackets represent the explained variance of each loading pattern.	45
3.8	Anomaly composites of vorticity (shaded) + wind field (arrows) in 850 hPa for COSMO-CLM (a & c) and ERA-Interim data (b & d). a) & b): dry events simulated by COSMO-CLM; c) & d): dry event not simulated by COSMO-CLM; e) & f): dry events simulated by COSMO-CLM only. Shaded areas are significant with an p-value of 5% (t-test).	48
3.9	Anomaly composites of vorticity (shaded) + wind field (arrows) in 500 hPa for COSMO-CLM (a & c) and ERA-Interim data (b & d). a) & b): dry events simulated by COSMO-CLM; c) & d): dry event not simulated by COSMO-CLM; e) & f): dry events simulated by COSMO-CLM only. Shaded areas are significant with an p-value of 5% (t-test).	49

³²All-Indian Monsoon Rainfall

3.10	Anomaly composites of vorticity (shaded) + wind field (arrows) in 200 hPa for COSMO-CLM (a & c) and ERA-Interim data (b & d). a) & b): dry events simulated by COSMO-CLM; c) & d): dry event not simulated by COSMO-CLM; e) & f): dry events simulated by COSMO-CLM only. Shaded areas are significant with an p-value of 5% (t-test).	50
3.11	Anomaly composites of vorticity (shaded) + wind field (arrows) in 850 hPa for COSMO-CLM (a & c) and ERA-Interim data (b & d). a) & b): wet events simulated by COSMO-CLM; c) & d): wet event not simulated by COSMO-CLM; e) & f): wet events simulated by COSMO-CLM only. Shaded areas are significant with an p-value of 5% (t-test)	52
3.12	Cross-Correlation of zonally average precipitation (for longitudinal section between 70°-100°) against a reference point near 85° east and 12.5° north for GPCP (topleft), <i>EH5-REC</i> (topright), <i>CCLM-REC-wet</i> (bottomleft) and <i>CLM-COM</i> (bottomright).	56
3.13	Composites anomalies [mm/d] for the eight MISO phases for left column: GPCP, 2nd left column: ECHAM5 REC, 3rd left column: CCLM-REC-wet and right: CLM-20C.	58
4.1	All Indian Monsoon Rainfall (AIMR) for all three ECHAM5 simulations during the last Millennium: MCA ³³ (900-1100, green), LIA ³⁴ (1515-1715, blue) and REC ³⁵ (1800-2000, red). Indicated in cyan and orange are the selected wet & dry time periods, respectively (each 31 years), which are downscaled using CLM ³⁶	67
4.2	Mean rainfall difference [mm/d] between COSMO-CLM simulations for wet and dry periods selected from ECHAM5. Significant (p-value<0.05) rainfall anomalies are dotted.	70
4.3	Composite anomaly for years with (a) high/low rainfall anomalies over central India and northeastern India. The green box indicates the region used as central India, and the red box the region used as northeastern India. (b) increased number of active/ decreased number of break days and vice versa. (c) high and low rainfall anomalies over the AIMR region, including all India. Areas for which rainfall between both composites differs significantly using a t-test with an error probability of 1% are dotted.	72

³³Medieval Climate Anomaly

³⁴Little Ice Age

³⁵Recent Climate

³⁶COSMO-CLM

- 4.4 Relative occurrence of active days (a) and break days (b) for all years, years with anomalous wet conditions over CI and dry conditions over NEI as well as years with anomalous dry conditions over CI and wet conditions over NEI in COSMO-CLM. 74
- 4.5 (top) 31 year running mean of normalised AIMR time series for MCA, LIA and REC.
 (middle) 31 year running mean of normalised number of active spell days
 (bottom) 31 year running mean of normalised number of break spell days . . . 75
- 4.6 (a) Rainfall composite anomaly [mm/d] for years with high/low rainfall anomalies over central India and northeastern India. The green box indicates the region used as central India, and the red box the region used as northeastern India.
 (b) Rainfall composite anomaly [mm/d] for years with high/low number of active spell days and low/high number of break spell days. Areas for which rainfall between both composites differs significantly using a t-test with an error probability of 1% are dotted. 77
- 4.7 Relative occurrence of active days (a) and break days (b) for all years, years with anomalous wet conditions over CI and dry conditions over NEI as well as years with anomalous dry conditions over CI and wet conditions over NEI in ECHAM5. 77
- 4.8 Standardised rainfall timeseries, smoothed by a 31 year running mean, for precipitation over all India (AIMR; top panel), over the core monsoon region (CI; middle panel) and over northeastern India (NEI; lower panel). Breakpoints (green lines in upper panel) are calculated following Bai and Perron (2003). A linear regression model is fitted to each breakpoint (black lines) for all rainfall time series. Significant slopes different to zero are marked as solid, not significant ($p.\text{level} > 0.01$) are marked as dashed-dotted lines. All timeseries are firstly normalised and then smoothed by a 31 year running mean. 79
- 4.9 Difference in smoothed & standardised AIMR rainfall before and after each respective breakpoint for all 10 breakpoints found in ECHAM5 simulations for MCA, LIA and REC. Breakpoints, which could be linked to changes in active and break spells as hypothesised by Sinha et al. (2011a) are indicated as filled points. 80
- 4.10 top: Precipitation over the All-Indian subcontinent (AIMR) smoothed by a 201 year running mean (black line) and solar insolation at 25°North during 15th of July calculated following Berger and Loutre (1991) (blue line).
 bottom: Normalised residuals of standardised precipitation minus regressed solar insolation onto precipitation over AIMR region. Phases, for which standardised precipitation exceeds +2/-2 are indicated in blue/red. 84

- 4.11 Pie diagrams indicating phases for which standardised rainfall exceeds +2 (indicated in blue) or -2 (indicated in red). Precipitation at each grid point has been detrended by regressing the insolation at 25° North calculated according to Berger and Loutre (1991). Black rectangles indicate grid points with positive correlations between original precipitation time series and insolation at 25° North, whereas grey rectangles indicate negative correlations between both time series. Numbers within the rectangles give the correlation coefficient. Dashed pie-segments in the pie-diagrams of each grid points indicate wet and dry phases calculated using All-Indian monsoon rainfall (left-bottom pie-diagram). 85
- 4.12 Standardised, linearly detrended rainfall time series over AIMR (top), CI (middle) and NEI (bottom). All time series are firstly smoothed by a 201 year running mean, detrended and eventually normal zed by its own standard deviation. Extreme dry and wet periods are indicated by red and blue bars. . . 86
- 4.13 Rainfall difference [mm/d] between a) *EH5-1.7ka* and *EH5-2ka* event derived from T31 AOGCM simulation (*COSMOS-Holocene*) and b) difference between *EH5-1.7ka* and *EH5-2ka* derived from T63L31 AGCM simulations (*EH5-2ka* & *EH5-1.7ka*). Regions with significant differences (plevel=0.1) are dotted in red (using a two-tailed t-test). 88
- 4.14 Sea surface temperature difference (June to September) between
left: *EH5-1.7ka* (50 years) and *EH5-2ka* (50 years) [K].
right: *EH5-1.7ka* (30 years) and *EH5-2ka* (30 years) [K]
Regions with significant changes (plevel=0.05) are dotted. Coloured lines display the boundaries of the regions used for sensitivity studies. 89
- 4.15 Rainfall difference [mm/d] between a) *EH5-1.7ka* and *EH5-2ka* (50 years),
b) *EH5-1.7ka* and *EH5-2ka* (30 years) 91
- 4.16 Rainfall difference [mm/d] between a) *EH5-1.7ka* and *EH5-2ka* event (30 years), b) *EH5-1.7ka-IO* and *EH5-2ka*, c) *EH5-1.7ka-PO* and *EH5-2ka* and d) *EH5-1.7ka-NA* and *EH5-2ka*. Regions with significant differences (plevel=0.1) are dotted in red (using a two-tailed t-test for a) and a paired t-test for b),c),d)). 92
- 4.17 Anomalous moisture transport in 850 hPa (contour & vector).
a) Averaged moisture transport derived from *EH5-1.7ka*; b) Difference between *EH5-1.7ka* and *EH5-2ka*, c) Difference between *EH5-1.7ka-IO* and *EH5-2ka*, d) Difference between *EH5-1.7ka-PO* and *EH5-2ka* and e) Difference between *EH5-1.7ka-NA* and *EH5-2ka*. Velocity potential is given in $m/s \cdot kg/kg$ 94

- 4.18 Velocity potential in 200 hPa (contour) and divergent winds (vector).
 a) Averaged velocity potential derived from *EH5-1.7ka*; b) Difference between *EH5-1.7ka* and *EH5-2ka*, c) Difference between *EH5-1.7ka-IO* and *EH5-2ka*, d) Difference between *EH5-1.7ka-PO* and *EH5-2ka* and e) Difference between *EH5-1.7ka-NA* and *EH5-2ka*. Velocity potential is given in $10^6 m^2/s$ 96
- 4.19 Velocity potential in 850 hPa (contour) and divergent winds (vector).
 a) Averaged velocity potential derived from *EH5-1.7ka*; b) Difference between *EH5-1.7ka* and *EH5-2ka*, c) Difference between *EH5-1.7ka-IO* and *EH5-2ka*, d) Difference between *EH5-1.7ka-PO* and *EH5-2ka* and e) Difference between *EH5-1.7ka-NA* and *EH5-2ka*. Velocity potential is given in $10^6 m^2/s$ 97
- 4.20 Difference in evaporation in mm/d between a) *EH5-1.7ka* and *EH5-2ka*, b) *EH5-1.7ka-IO* and *EH5-2ka*, c) *EH5-1.7ka-PO* and *EH5-2ka* and e) *EH5-1.7ka-NA* and *EH5-2ka*. Note that a downward evaporation flux is defined positively, thus condensation is defined positive and evaporation linked to negative values. 98
- 4.21 Difference in moisture advection [$m/s \cdot kg/kg$] between a) *EH5-1.7ka* and *EH5-2ka*, b) *EH5-1.7ka-IO* and *EH5-2ka*, c) *EH5-1.7ka-PO* and *EH5-2ka* and e) *EH5-1.7ka-NA* and *EH5-2ka*. Daily mean wind speeds and specific humidity values are used to derive moisture advection. 98
- 4.22 a) AIMR b) Position of IPWP c) SST over NARAB d) SST over NEIO e) SST over NINO1+2 region f) SST over NINO3 region g) SST over NINO3+4 region h) SST over NINO4 region. All time series are derived from T31L19 COSMOS AOGCM simulation (Fischer and Jungclaus, 2011) and smoothed using a 51 year running mean. 101
- 4.23 AOGCM time series for a) AIMR anomaly, b) anomalous position of IPWP and c) SST anomaly over NARAB region. Time-series are linearly detrended and smoothed using a 201-year running mean. Time periods for which the respective value exceeds the standard deviation are marked in blue if wetter conditions over India would be expected and brown if drier conditions over India would be expected. 103
- 5.1 "Global GHG emissions (in GtCO₂-eq per year) in the absence of additional climate policies: six illustrative SRES marker scenarios (colored lines) and 80th percentile range of recent scenarios published since SRES (post-SRES) (gray shaded area). Dashed lines show the full range of post-SRES scenarios. The emissions include CO₂, CH₄, N₂O and F-gases." (IPCC Core Writing Team, 2007) 111
- 5.2 Rainfall timeseries over all-India (AIMR) smoothed with a 21 year running mean filter for four different COSMO-CLM climate change scenarios (COM, B1, A1B, A2) driven by ECHAM5 run1 simulations carried out within CMIP3. 113

- 5.3 upper: Rainfall timeseries over all-India (AIMR) for four different CLM simulations under future emission scenarios (*CLM-COM*, *CLM-A1B*, *CLM-A2*, *CLM-B1*). Breakpoints are identified based on the method developed by Bai and Perron (2003) and to each breakpoint a linear regression model is fitted.
middle: Rainfall timeseries over central India (CI) for four different climate change scenarios. For each breakpoint identified in AIMR timeseries a linear regression model is fitted to the corresponding CI rainfall.
bottom: Rainfall timeseries over northeastern India (NEI) for four different climate change scenarios. For each breakpoint identified in AIMR timeseries a linear regression model is fitted to the corresponding NEI rainfall.
All timeseries are normalised to the reference period from 1960 until 2000 and smoothed with a 21 year running mean filter. Significant linear regression models (p-level:5%) are indicated as solid and no-significant linear trends as dashed lines. 115
- 5.4 Rainfall timeseries over all-India (AIMR) smoothed with a 21 year running mean filter for four different ECHAM5 climate change scenarios (COM, B1, A1B, A2) carried out within CMIP3. 116
- 5.5 Identical to Figure 5.3, but for four different ECHAM5 simulations under future emission scenarios (*COSMOS-COM (run1)*, *COSMOS-A1B (run1)*, *COSMOS-A2 (run1)*, *COSMOS-B1 (run1)*). Breakpoints are identified based on the method developed by Bai and Perron (2003) and to each breakpoint a linear regression model is fitted. 117

List of Tables

2.1	AOGCM, AGCM and RCM simulations used in this study. Experiments marked with * have been carried out within this thesis.	29
3.1	Datasets used in this study as well as the temporal coverage, horizontal resolution, temporal resolution and the database used to derive this product (only given for precipitation datasets). For some datasets other horizontal/temporal resolutions are available and the value given here indicates the resolution used within this study. The superscript indicates the parameter used in this study: 1) precipitation, 2) zonal + meridional wind speed components in 500hPa	35
3.2	Definition of SPI classes	37
3.3	Gerrity skill scores (GSS) for COSMO-CLM, ERA-Interim, TRMM and GPCP compared to Aphrodite observation dataset based on SPI values derived from weekly rainfall over AIMR region.	43
4.1	Overview to model simulations used in Chapter 4	66
4.2	Differences in mean rainfall over India (AIMR), the presence of a rainfall anomaly dipole pattern, differences in active as well as break spells for all 15 possible simulation pairs from CLM simulations for MCA,LIA and REC. Significant differences using a Kolmorow-Smirnow test with an error probability of 0.1 are marked in bold.	68
4.3	Overview to model simulations used in Chapter 4, Section 4.3	83
4.4	Regions used for the calculation of sea surface temperature based oceanic indices.	99
4.5	Correlation coefficients between oceanic index and rainfall over India (AIMR), based on yearly values (upper row) and after smoothing each time-series with a 51 year moving average (lower row).	100
5.1	Overview to model simulations used in Chapter 5.	112

Acronyms

A-B active-break

AMO Atlantic Multi-decadal Oscillation

AGCM Atmosphere-only General Circulation Model

AOGCM Atmosphere-Ocean General Circulation Model

AIMR All-Indian Monsoon Rainfall

AMOC Atlantic Meridional Overturning Circulation

BP Before Present

BSISO Boreal Summer Intraseasonal Oscillations

CI Central India

CGT circumglobal teleconnection

CLM COSMO-CLM

CMZ Core Monsoon Region

COSMOS Community Earth System Models

EEOF Extended Empirical Orthogonal Function

ENSO El Niño Southern Oscillation

EOF Empirical Orthogonal Function

GCM General Circulation Model

GHG Greenhouse Gas Concentrations

HIMPAC HIMPAC - Himalaya: Modern and Past Climates

IITM Indian Institute of Tropical Meteorology

- IO** Indian Ocean
- IOD** Indian Ocean Dipole
- IPWP** Indo-Pacific Warm Pool
- ISM** Indian Summer Monsoon
- ISO** intra-seasonal oscillation
- ISV** intraseasonal variability
- ITCZ** inter-tropical convergence zone
- JJAS** June-September
- LGM** Last Glacial Maximum
- LIA** Little Ice Age
- MCA** Medieval Climate Anomaly
- MISO** Monsoon Intra-seasonal Oscillations
- MPI-M** Max Planck Institute of Meteorology
- NEIO** North Eastern Indian Ocean
- NA** North Atlantic
- NARAB** Northern Arabian Sea
- NEI** North-eastern India
- PC** Principal Component
- PMIP** Paleoclimate Modelling Intercomparison Project
- PO** Pacific Ocean
- PDO** Pacific Decadal Oscillation
- RCM** Regional Climate Model
- REC** Recent Climate
- SOI** Southern Oscillation Index
- SPI** Standardized Precipitation Index

SST Sea Surface Temperatures

SIC Sea Ice Concentrations

TC Tropical Cyclone

TCZ Tropical Convergence Zone

TBO Tropical Biennial Oscillation

CMIP3 Coupled Model Intercomparison Project 3

CMIP5 Coupled Model Intercomparison Project 5

Danksagung

Dank gilt meinem Doktorvater Prof. Dr. Ulrich Cubasch für die Möglichkeit der Bearbeitung dieses Themas. Auch wenn die letzten Jahre teilweise mit Schwierigkeiten verbunden waren, haben die Diskussionen und seine Anregungen mein wissenschaftliches Denken gestärkt und so auch die Qualität dieser Arbeit gesteigert. Nicht weniger konstruktiven Einfluss hatte die Zusammenarbeit mit meinem Zweitgutachter Dr. Gregor Leckebusch. Die Möglichkeit, nach dem Ende meines Vertrages in Berlin nach Birmingham zu wechseln, hatte positiven Einfluss auf unsere Zusammenarbeit in dieser Arbeit. Gerade die zahlreichen Diskussionen haben maßgeblich zur finalen Version dieses Dokuments beigetragen. Besonders möchte ich mich für seine Unterstützung auf persönlicher Ebene bedanken. Zusätzlicher Dank gilt Dr. Ingo Kirchner und Dr. Henning Rust für ihre Unterstützung beim Modellieren bzw. bei jeglichen statistischen Fragen.

Bei einer Vielzahl von Mitgliedern der AG Klimamodellierung, AG Clidia und den Mitarbeitern weiterer Arbeitsgruppen möchte ich mich für die anregenden Diskussion bedanken. Hier denke ich besonders an Tobias Pardowitz, Christopher Kadow und natürlich meinen Zimmerkollegen Tim Kruschke, wobei unsere Diskussionen über Frischwassereinträge, WTRACK und auch Fußball wesentlich zu einer guten Arbeitsatmosphäre beigetragen haben.

Die Arbeit wäre ohne meine Familie nicht möglich gewesen; vielen Dank an meine Eltern, meinen Bruder und Schwester für den moralischen Beistand. Größter Dank gilt Katrin für ihre grenzenlose Unterstützung bei dieser Arbeit ohne die die Finalisierung nicht möglich gewesen wäre. Ihr danke ich für die unzähligen Stunden gefüllt mit Diskussionen sowie ihre schier unerschöpfliche Geduld!